Journal of Structural Geology 33 (2011) 758–818

Contents lists available at ScienceDirect

Journal of Structural Geology

journal homepage: www.elsevier.com/locate/jsg

Review

The thermodynamics of deformed metamorphic rocks: A review

Bruce E. Hobbs [a,b,*], Alison Ord [a], Klaus Regenauer-Lieb [a,b]

[a] School of Earth and Environment, The University of Western Australia, Perth 6009, Australia
[b] CSIRO, Western Australia, Perth 6102, Australia

ARTICLE INFO

Article history:
Received 7 September 2010
Received in revised form
22 January 2011
Accepted 27 January 2011
Available online 9 February 2011

This paper is dedicated to the memory and work of Bruno Sander whose classical paper *Uber Zusammenhange zwischen Teilbewegung und Gefuge in Gesteinen* was published 100 years ago. Sander's work, often forgotten and sometimes incorrectly maligned, stands today as a fundamental contribution to Structural Geology. His ideas on the control of rock fabric by the movement picture or kinematic history are reinforced by the thermodynamic approach to Structural Geology reviewed in this paper.

Keywords:
Generalised thermodynamics
Coupled processes
Reaction-diffusion
Folding
Boudinage
Metamorphic differentiation
Microstructure
Critical systems

ABSTRACT

The deformation of rocks is a disequilibrium and strongly non-linear phenomenon with a number of interacting chemical, thermal and microstructural processes operating simultaneously. We review progress in this area over the past 30 years. Deforming-chemically reacting systems are dissipative systems and hence are characterised by highly ordered structures that develop through cooperative processes once parameters such as critical strains, strain-rates, fluid infiltration rates, damage densities or temperatures are attained. Such criticality is the hallmark of deformed rocks at all length scales and is the basis for a diverse range of structures such as foliations and lineations produced by metamorphic differentiation, rotation recrystallisation, folding, boudinage and micro to regional scale fracture systems. Criticality is identified with classical criticality and not self-organised criticality. The first and second laws of thermodynamics are used to show that such structural diversity arises from reaction-diffusion-deformation equations. Criticality of the system is associated with the stored energy becoming non-convex and structures arise in order to minimise this non-convex energy. These structures are scale invariant and hence are characterised by fractal and minimal surface geometries. Thermodynamics is a powerful discipline to integrate seemingly unrelated processes in structural geology and produce an integrated approach to the subject that crosses all length scales.

Prologue

The last review of the application of thermodynamics to the deformation of rocks was the paper: *Non-hydrostatic Thermodynamics and Its Geologic Applications* by Paterson (1973) who emphasised that he was only considering systems at equilibrium. In order to appreciate developments since then one should understand the historical context in which that paper was written. The extension of thermodynamics to systems not at equilibrium had been considered by many before Paterson's paper and had been developed particularly by De Groot (1952) and Prigogine (1955) with specific application to chemical systems, including diffusion, and based largely on earlier work by Onsager (1931a,b). There was very little attention paid to deforming systems in that body of work although De Groot and Mazur (1962) had introduced the concept of internal variables to define the state of a deforming system. Landmark papers were published by Biot (1955, 1958), Coleman and Noll (1963), Coleman and Gurtin (1967) and Rice (1971, 1975). These papers were seminal in that they expressed the second law of thermodynamics in terms of entropy production rate and in a way that the evolution of a general system, not at equilibrium, could be tracked with time; they introduced and clarified the concept and use of *internal variables* rather than the classical *state variables* of equilibrium thermodynamics. Importantly, these papers addressed

* Corresponding author.
E-mail address: Bruce.Hobbs@csiro.au (B.E. Hobbs).

0191-8141/$ – see front matter © 2011 Elsevier Ltd. All rights reserved.
doi:10.1016/j.jsg.2011.01.013

the *mechanics* of deforming systems as well as chemical aspects. The publication of many of these papers and the works by Truesdell and Noll (1965) and Truesdell (1966, 1969) was met with some controversy largely because Truesdell in particular (and in a not very subtle manner) pointed to serious flaws in the works of De Groot and Prigogine. The situation was not helped by the emphasis of the Truesdell School on mathematical formalism and rigour. By the time Paterson's paper appeared a large amount of confusion existed in the non-equilibrium literature (and even in the equilibrium areas that Paterson chose to address) and to a large extent this confusion continues in the literature. The essential areas of contention were: (i) The "Curie Principle or Theorem" that claimed quantities of different tensorial character cannot interact. The claim involved restrictions placed on the entropy production rate for coupled processes arising from the "theorem". (ii) The claim that processes "close" to equilibrium are linear whereas those "far" from equilibrium are non-linear. (iii) The claim that systems evolve so that the entropy production rate is a minimum. It turns out in hindsight (and we address these issues in this paper) that all three claims are without merit but in 1973 (and even today in some minds) the controversy was rife. Paterson chose not to address these issues. Since then the work of many, including in particular Ziegler (1963, 1983), Lavenda (1978), Coussy (1995, 2004, 2010), Houlsby and Puzrin (2006a) and Ross (2008), has clarified points of contention to the extent that the application of thermodynamics to deforming systems is now routine in many disciplines and some progress can be made in applying the concepts of thermodynamics to deforming-chemically reacting geological systems. That is the subject of this paper.

1. Introduction

Over the past 30 years there have been dramatic developments in structural geology, metamorphic petrology, physical metallurgy, continuum mechanics, physical chemistry and thermodynamics that are relevant to processes that operate within the Earth but these developments have evolved largely independently of each other and many have not yet been incorporated into main-stream structural geology. On the other hand many contributions made within structural geology over the past 30 years take on new significance when viewed in the context of new knowledge. This paper attempts to integrate some of these developments into a common framework that couples together the various processes of interest to structural and metamorphic geologists. The emphasis is on reviewing work done over the past 30 years rather than introducing a number of new results. Our aim is to assemble and integrate the existing work into the framework which has come to be known as Generalised Thermodynamics. This framework is convenient for formulating relationships between coupled processes in a manner that is not *ad hoc*, in that it ensures compatibility with the laws of thermodynamics, and is applicable to systems at equilibrium as well as far from equilibrium. Moreover the framework is a means of integrating and synthesising apparently diverse subjects and approaches. Clearly, because of the immense volume of material available we have had to be highly selective and have chosen references that illustrate specific points rather than attempt to be inclusive. The paper is therefore more a review of the subject than of the associated literature. We make an effort where possible to highlight the main review articles and important books in various associated fields.

This review is concerned with processes that operate within the crust of the Earth, the ways in which they dissipate energy and the ways in which these processes are coupled in the upper parts of the Earth to produce the structures we see in deformed metamorphic rocks. These processes involve permanent deformation in environments that cover temperatures ranging from atmospheric temperature to the solidus of many rocks, pressures ranging from atmospheric to about two GPa, mass transport both in the solid state and in fluids such as aqueous fluids and melts, thermal transport, both by advection and conduction, and chemical reactions. A thermodynamic approach emphasises that such processes do not operate independently of each other but are strongly coupled through the second law of thermodynamics. Each process dissipates energy, that is, it produces entropy, and so the coupling is dictated by the ways in which the entropy production rate is partitioned between the processes. By entropy production rate we mean the amount of heat produced at each point in the system per unit time divided by the current temperature at that point (Truesdell, 1966). If $\dot{s}$ is the specific entropy production rate at a particular point then the specific total dissipation function is defined at that point as $\Phi = T\dot{s}$ where T is the absolute temperature; the dissipation function, Φ, is a scalar and has the units Joules per kilogram per second; the overdot represents differentiation with respect to time. The total dissipation rate at each point, Φ, is the sum of the individual dissipation rates arising from each dissipative process operating at that point. The dissipation rates that concern us are those arising from plastic deformation, $\Phi^{plastic}$, mass transfer (by diffusion or by advection in a moving fluid), $\Phi^{mass\ transfer}$, chemical reactions, $\Phi^{chemical}$, and thermal transport, $\Phi^{thermal\ transport}$, and so

$$\Phi = T\dot{s} = \Phi^{plastic} + \Phi^{mass\,transfer} + \Phi^{chemical} + \Phi^{thermal\,transport} \geq 0 \quad (1)$$

where the inequality is a direct expression of the second law of thermodynamics for a system not at equilibrium; the equality holds for equilibrium. Eq. (1) is the fundamental equation that enables various processes to be coupled in a thermodynamically admissible manner (such that the laws of thermodynamics are obeyed); when the individual dissipation functions are expressed in an explicit manner Eq. (1) is often called the Clausius–Duhem inequality (Truesdell and Noll, 1965). If necessary additional dissipation functions could be added to Eq. (1) to represent other dissipative processes such as fracturing, grain-size reduction or microstructural evolution. Eq. (1) is true independently of the material properties of the material; it is true for homogeneous and inhomogeneous materials and for isotropic and anisotropic materials. Complicated interactions can be incorporated into Eq. (1) by introducing relations (determined by experiments) between various dissipation functions. Thus chemical softening arising from the formation of weak mineral phases during a metamorphic reaction can be incorporated by writing relations between $\Phi^{plastic}$ and $\Phi^{chemical}$.

It turns out that the manner in which the partitioning expressed by Eq. (1) is achieved across the various processes is dependent on the length scale involved; this not only introduces some simplifying aspects but is also the basis of a general principle of scale invariance that emerges from such work: *different processes dominate in producing entropy at different scales but similar structures develop at each scale*. By similar here we mean that structures of identical geometrical appearance are developed at a range of scales. The overall outcome is that different processes have strong feedback influences on others at different scales leading to the scale invariance of structures and to the mineral assemblages that we observe in the crust of the Earth. The general system we consider in this paper is a deforming, chemically reactive system in which microstructural/mineralogical evolution and mass and thermal transport play significant roles. Some examples of the feedback relations that can exist in such systems are illustrated in Fig. 1.

While the various processes mentioned above are operating, the system dissipates energy and hence is not at equilibrium. Thus, the overarching concepts that unify these various processes are

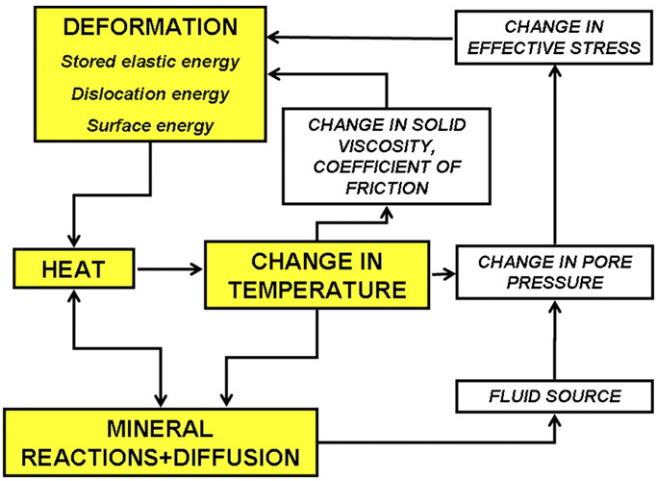

Fig. 1. Some possible feedback relations in a closed, deforming system with chemical reactions, fluid flow and thermal transport.

grounded in the thermodynamics of systems not at equilibrium. The traditional approach within geology as far as thermodynamics is concerned is strongly influenced by the work of Gibbs (1906) where, for the most part, equilibrium is assumed. The outcome is that non-equilibrium approaches have been largely neglected or even dismissed as irrelevant in the Earth Sciences, the argument being two-fold: (i) geological processes are so slow that equilibrium can be assumed and (ii) within a small enough region we can assume that equilibrium is attained (Thompson, 1959; Korzhinskii, 1959). Although both these points may be excellent approximations in some cases (see the treatment of Rice, 1975), the important point is that all of the processes mentioned above dissipate energy while they operate no matter how slow the process, or how small the system, and the resulting dissipation must be expressed in some manner. The subject that is now called *Generalised Thermodynamics* (Houlsby and Puzrin, 2006a) is concerned with the ways in which dissipated energy (entropy) is partitioned across the various processes operating in a deforming, chemically reacting system. However the system does not need to be far from equilibrium to be treated by Generalised Thermodynamics. In an adiabatic, homogeneously deforming elastic solid the deformation is reversible (McLellan, 1980); the entropy production rate is zero (the processes are isentropic) and the system is an equilibrium system. This is still part of Generalised Thermodynamics. In this particular case the stresses are non-hydrostatic but the system remains at equilibrium; non-hydrostatic thermodynamics is not synonymous with non-equilibrium thermodynamics. Discussions of equilibrium non-hydrostatic thermodynamics are given by Nye (1957), Paterson (1973) and McLellan (1980); we do not consider the subject further in this paper.

A deterrent to progress in applying non-equilibrium thermodynamics to deforming rocks is that developments in the subject have been dispersed across a large number of disciplines and languages, with conflicting or paradoxical propositions put forward, so that it has been difficult to produce a unified approach to the subject as far as geoscientists are concerned. An important example is the proposition that the entropy production rate (or the dissipation rate) is a minimum in non-equilibrium systems (Onsager, 1931a, b; Prigogine, 1955; Biot, 1955, 1958; Kondepudi and Prigogine, 1998). In an apparent paradox, others, in particular Ziegler (1963, 1983), have proposed exactly the opposite: that the entropy production rate is a maximum. We explore these and related concepts in Section 3.2. The outcome is that almost all of these apparently conflicting views turn out to be an expression of Ziegler's principle (Table 5). However, neither proposition is generally true (Ross, 2008) and only in special, but important, cases do such extremum principles exist. The thermodynamics of systems not at equilibrium is advancing at a rapid rate and much still needs to be established even at a very basic level.

In this review we first develop a ground-work in Generalised Thermodynamics and then move to apply these principles to rocks where deformation, thermal and fluid transport, chemical reactions, damage and microstructural evolution contribute to the evolution of the structure of rock masses. Our approach is to divide the subject into issues to do with length scales even though many basic results and principles hold at all scales. Thus we consider first the microscale ranging from microns to about a metre, then the intermediate scale ranging from about a metre to 100s of metres and then the regional scale measured in kilometres. We do this because as a general rule particular feedback mechanisms between coupled processes dominate at these characteristic length scales. Some, such as mineral reactions, have no characteristic length scale; we treat them initially as microscale phenomena but include them ultimately at all scales. Similarly, although damage is important at all scales, we elect to discuss this topic at the regional scale. Damage is a general term to describe any process that results in degradation of the strength of a material and includes fracturing, "void" or inclusion formation, grain-size reduction and chemical mechanisms of strength degradation such as stress corrosion. Most of the published results relevant to this paper are applicable at the microscale and so this review is clearly biased towards that scale. This is not to say that the intermediate and regional scales are not amenable to major advances in the future particularly with respect to understanding criticality (Sornette, 2000) at the large scale and its control on tectonic evolution.

It becomes clear that the principle of minimising the Helmholtz energy is an important principle at all scales. This principle is useful for both equilibrium and non-equilibrium systems and governs the formation of sub-domains within the system characterised by differing chemical compositions and/or fabric. Such sub-domains play the roles of energy minimisers and can take on fractal geometries in order to achieve overall compatibility with an imposed deformation. We treat this principle at the microscale but emphasise that it is fundamental at all scales.

2. Preliminaries

2.1. Notation

Symbols are defined in Table 1 and when first introduced in the text. Cartesian coordinates are used throughout. We use the convention that scalar quantities are represented in non-bold font: a, T, Ψ; vectors, tensors and matrices are represented by bold font: **J**, **A**, **σ**. Vector, tensor and matrix Cartesian components are represented using indices ranging from 1 to 3: J_i for vectors and σ_{ij} for second order tensors. The Einstein summation convention (Nye, 1957, p. 7) is used so that repeated indices mean summation on that index unless otherwise stated. The various tensor operations are as follows: (i) $\mathbf{a}\cdot\mathbf{b}$ is the scalar product of two vectors **a** and **b**; (ii) $\mathbf{a}\times\mathbf{b}$ is the vector product of two vectors **a** and **b**; (iii) **a:b** is the scalar product of two second order tensors a_{ij} and b_{ij} and is equivalent to $a_{ij}b_{ij}$; (iv) $\mathbf{a}\otimes\mathbf{b}$ is the tensor product of two vectors **a** and **b** so that

$$\mathbf{a}\otimes\mathbf{b} = \begin{bmatrix} a_1b_1 & a_1b_2 & a_1b_3 \\ a_2b_1 & a_2b_2 & a_2b_3 \\ a_3b_1 & a_3b_2 & a_3b_3 \end{bmatrix} \tag{2}$$

The tensor product of two vectors is also known as the dyadic product; the result of the $\otimes$ operation involving two vectors is

Table 1
Symbols used in the text with units.

Quantity	Description	Units, Typical Values
$\mathcal{A}$	Material constant	Pa s
A	Affinity; "driving force"	J kg^{-1}
Ar	Arrhenius Number	dimensionless
A, B, C, D, X, Y	Symbols representing chemical components	dimensionless
A ,B, C, D, X, Y	Concentrations of chemical components	Depends on context
a, b, c, d	Constants	Depends on context
$\mathcal{B}$	Constant	Pa s
B_{ij}	Generalised stress driving crystallographic preferred orientation development	Pa
a	Rate of generation of dislocations	s^{-1}
b	Burgers vector	m
c_i^{solid}, c_i^{fluid}	Concentrations of component i in the solid and fluid respectively	Dimensionless (volume or mass%)
c_p	Specific heat at constant pressure	J kg^{-1} K^{-1}
$\mathbb{C}$	Total chemical dissipation arising from all of the chemical reactions	J kg^{-1} s^{-1}
d	Grain-size	m
$\boldsymbol{D}$	Stretching tensor; deformation-rate tensor	s^{-1}
D^K	Diffusion coefficient for the Kth chemical component	m^2 s^{-1}
D_k	Diffusion coefficient for the kth population dislocation density	m^2 s^{-1}
f	Function	
$\mathbb{F}$	Function	
$\boldsymbol{F}$	Deformation gradient	dimensionless
F, G	Functions that express the rates of production of chemical components	
F^D, G^D	Functions that express the rates of production of chemical components in a deforming environment	
E, H	Non-linear functions of composition representing heterogeneous reaction sites	
Gr	Gruntfest Number	dimensionless
$\mathcal{G}$	Specific Gibbs energy	J kg^{-1}
$\mathcal{H}$	Specific enthalpy	J kg^{-1}
H	Mean curvature	m^{-1}
h	Thickness of shear zone	m
$\boldsymbol{I}$	Identity matrix	dimensionless
J_2	Second invariant of the stretching tensor	s^{-2}
$\boldsymbol{J}^K$	Flux of the Kth chemical component	m s^{-1}
$\boldsymbol{j}$	Darcy or infiltration flux	m s^{-1}
K	Gaussian curvature	m^{-2}
K^{fluid}	Fluid permeability	m^2
$K^{thermal}$	Thermal conductivity	W m^{-1} K^{-1}
k	Boltzmann's constant	J K^{-1}
k^{Turing}	Wave-number associated with a Turing instability	m^{-1}
$\boldsymbol{L}$	Velocity gradient	s^{-1}
L	Size of system	m
L^M	Rate of latent heat production from Mth reaction	J kg^{-1} s^{-1}
$l^{process}$	Length scale for a process over which feedback is important	m
l_m, l_{lm}	Mean free path of mobile and less mobile dislocations	m
m^K	Concentration of Kth reactant or product	kg m^{-3}
$\boldsymbol{m}^{\pm}$	Slip plane normals in a subgrain	dimensionless
N	Stress exponent in constitutive law	dimensionless
P, P^{fluid}	Pressure, fluid pressure	Pa
P_c	Critical buckling load	kg
$\boldsymbol{Q}$	Finite rotation matrix	dimensionless
$\mathcal{Q}$	Activation enthalpy	J kg^{-1}
R	Gas constant	J kg^{-1}
$\boldsymbol{R}^{\pm}$	Rotations in a subgrain	dimensionless
r	Radius	m
r^+; r^-	Forward and reverse reaction rates for a chemical reaction	s^{-1}
$\mathbf{s}$; $\boldsymbol{s}^{\pm}$	Slip direction vector; slip direction vectors in a subgrain	dimensionless
S_{ijkl}	Elastic compliance	Pa^{-1}
s	Specific entropy	J kg^{-1} K^{-1}
$\mathbf{T}$	Normal to slip plane - vector	dimensionless
T	Absolute temperature	K
t	Time	s
$\boldsymbol{U}$	Finite stretch tensor	dimensionless
U	Specific internal energy	J kg^{-1}
u,v	Concentration of chemical component	Depends on context
V_o, V_o^A	Specific volume of the material, specific volume of A	m^3 kg^{-1}
v; $\boldsymbol{v}$	Boundary velocity; Velocities of material points	m s^{-1}
$\mathbf{x}$, $\mathbf{X}$	Coordinates of a material point in the deformed, undeformed state	m
x_i, X_i	Cartesian coordinates of a material point in the deformed, undeformed state	m
Y_{ij}	Generalised damage stress	Pa
α_{ij}^Q	Internal variable for process Q	Depends on nature of Q
α, β	Constants	Depends on context
β_{ij}	Tensor measure of crystallographic preferred orientation	dimensionless
γ	Ratio of diffusivities	dimensionless
γ; $\gamma^{\pm}$	Shear strain; shear strains in a grain	dimensionless

(*continued on next page*)

Table 1 (*continued*)

Quantity	Description	Units, Typical Values
ε_{ij}, $\varepsilon_{ij}^{elastic}$, $\varepsilon_{ij}^{plastic}$	Small strain tensor, elastic strain, plastic strain	dimensionless
$\dot{\varepsilon}_{ij}$, $\dot{\varepsilon}_{ij}^{dissipative}$	Strain-rate, strain-rate arising from dissipative processes	s^{-1}
δ_{ij}	Kronecker delta	dimensionless
δ_{ij}	Tensor measure of damage	dimensionless
η, η^{A}	Viscosity, viscosity of A	Pa s
ξ	Extent of a mineral reaction	$0 \leq \xi \leq 1$;dimensionless
$\dot{\xi}$, $\dot{\xi}^{M}$	Rate of a mineral reaction, rate of the *M*th mineral reaction	s^{-1}
ξ_i	Perturbations	m
$\kappa^{thermal}$	Thermal diffusivity	$m^2\ s^{-1}$
$\kappa^{process}$	Diffusivity for a process	$m^2\ s^{-1}$
λ^{Turing}	Wavelength of the patterning associated with a Turing instability	m
μ^{K}	Chemical potential of the *K*th chemical component	$J\ kg^{-1}$
$\boldsymbol{\Omega}$	Spin tensor	dimensionless
v_m, v_{lm}	Velocity of mobile, less mobile dislocations	$m\ s^{-1}$
ω	Amplification factor	dimensionless
ϖ	Rate of interaction of dislocations	$m^4\ s^{-1}$
ρ, ρ_o	Density, initial density	$kg\ m^{-3}$
ρ_{lm}, ρ_m	Instantaneous densities of less mobile, mobile dislocations	$m\ m^{-3}$
ρ^{o}	Initial density of dislocations	$m\ m^{-3}$
σ_{ij}	Cauchy stress	Pa
τ	Characteristic time scale	s
τ	Shear stress	Pa
φ	Porosity	dimensionless
φ^{A}	Volume fraction of A	dimensionless
Φ	Dissipation function	$J\ kg^{-1}\ s^{-1}$
$\Phi^{mechanical}$	Contribution to the total dissipation from purely mechanical processes	$J\ kg^{-1}\ s^{-1}$
$\Phi^{diffusive}$	Contribution to the total dissipation from diffusive processes	$J\ kg^{-1}\ s^{-1}$
$\Phi^{chemical}$	Contribution to the total dissipation from chemical reactions	$J\ kg^{-1}\ s^{-1}$
$\Phi^{thermal}$	Contribution to the total dissipation from thermal diffusion	$J\ kg^{-1}\ s^{-1}$
χ	Taylor-Quinney coefficient	Assumed to be unity; dimensionless
χ^{A}, χ^{B}	Fractions of mechanical dissipation partitioned between reactions that produce A and B	dimensionless
χ_{ij}, χ_{ij}^{d}	Generalised stress associated with plastic strain, generalised stress associated with damage	Pa
Ψ	Specific Helmholtz energy	$J\ kg^{-1}$
ζ	Variation of fluid content	dimensionless

a rank-1 matrix that transforms as a second order tensor. This product is important in discussions of crystal plasticity and particularly in establishing compatibility of deformations between two adjacent domains deformed by single or multiple crystal slip (Section 4.11).

2.2. The "Curie principle"

The dissipation function, Φ, in Eq. (1) is a scalar quantity given by $\Phi = T\dot{s}$ but comprises the sum of other quantities that involve tensor quantities of higher order. Thus $\Phi^{plastic} = \sigma_{ij}\dot{\varepsilon}_{ij}^{plastic}$ and so involves the second order tensors, the Cauchy stress, σ_{ij}, and the plastic strain-rate, $\dot{\varepsilon}_{ij}^{plastic}$. Misconceptions concerning the veracity of coupling various processes through the use of Eq. (1) arise from the work of De Groot (1952) and Prigogine (1955) who proposed a "principle" which they labelled "The Curie principle or theorem" that says "*Quantities of different tensorial character cannot interact with each other*". Truesdell (1966, 1969) points out that there is nothing in the original works of Curie (1894, 1908) that resembles such a statement. Since a general tensor has no symmetry ascribed to it (other than the trivial property of symmetry or lack thereof about the leading diagonal) the De Groot "Curie principle or theorem" has nothing to do with symmetry. The so called "Curie principle" is nothing more nor less than a statement of the most elementary rule of (Cartesian) tensor algebra which says that: *tensors of the same order may be added to produce a tensor of the same order* (Eringen, 1962, p. 435). Otherwise an expression which adds Cartesian tensors of different orders makes no sense mathematically, physically or chemically. In Eq. (1) all of the terms such as $\Phi^{plastic} = \sigma_{ij}\dot{\varepsilon}_{ij}^{plastic}$ are scalars with units $J\ kg^{-1}\ s^{-1}$ as is the total dissipation. Unfortunately, the De Groot statement is commonly taken to mean: *processes involving quantities of different tensorial order cannot be coupled*. This is clearly wrong. Nye (1957, Chapter 10) gives many well established examples of the equilibrium properties of crystals where properties of different tensorial order are coupled or interact. Part of the misconception here seems to arise from the fact that many authors did not understand that quantities such as $\sigma_{ij}\dot{\varepsilon}_{ij}^{plastic}$ are scalars. After all, the quantity $\sigma_{ij}\dot{\varepsilon}_{ij}^{plastic}$ is, by definition, the *scalar* product of two second order tensors. All of the couplings described by Eq. (1) are scalars (see the set of Eqs. 23). The De Groot "Curie theorem" has been called the "non-existent theorem in algebra" by Truesdell (1966) since it is merely an expression of an elementary rule in tensor algebra and it certainly has no association with the Curie Principle as enunciated by Curie (1894, 1908).

2.3. Deformation, deformation-rate and constitutive relations

To be specific about the fundamental principles of Continuum Mechanics involved in this review and that underlie the thermodynamic formalism we include the following discussion. Different materials, when subjected to the same set of imposed movements or forces on their boundaries, behave in different manners and develop different internal stress states. In general, the stress state is a function of the kinematic history of the material and the way in which the stress state for a given material is related to the imposed kinematics is known as the *constitutive relation* for that material. We are interested only in the deformation of solids here (although the solid may contain some fluid), a solid being a material with at least one preferred stress free (or undeformed) state (Rajagopal and Srinivasa, 2004). Gases and liquids have no such state. A solid is elastic (or strictly, hyper-elastic, Fung, 1965) if the response to an imposed deformation is rate-independent, recoverable and the stress in the material can be derived from the Helmholtz energy, Ψ (Houlsby and Puzrin, 2006a). A solid is plastic if the response is rate-independent, non-recoverable and the stress in the material is governed by a yield

surface. Again, for hyper-plastic materials (the only materials we consider here) the stress can be derived from Ψ (Rice, 1975). A solid is viscous if the response is rate-dependent and non-recoverable. Again the stress can be derived from Ψ (Houlsby and Puzrin, 2006a). Most solids of interest in structural geology are elastic–plastic–viscous so that the shape and size of the yield surface is rate-dependent but the stress may always be derived from Ψ (Rice, 1975).

A deformation is defined by the set of equations

$$\mathbf{x} = f(\mathbf{X}) \tag{3}$$

where $\mathbf{x}$ and $\mathbf{X}$ are the coordinates of a material point in the deformed and undeformed states (Fig. 2) and f in general is a non-linear function. In general the deformation Eq. (3) consists, at each point, of a distortion, a rigid body rotation and a rigid body translation.

The deformation gradient is defined as

$$\boldsymbol{F} = \begin{bmatrix} \frac{\partial x_1}{\partial X_1} & \frac{\partial x_1}{\partial X_2} & \frac{\partial x_1}{\partial X_3} \\ \frac{\partial x_2}{\partial X_1} & \frac{\partial x_2}{\partial X_2} & \frac{\partial x_2}{\partial X_3} \\ \frac{\partial x_3}{\partial X_1} & \frac{\partial x_3}{\partial X_2} & \frac{\partial x_3}{\partial X_3} \end{bmatrix} \tag{4}$$

In Eqs. (3) and (4), x_1, x_2, x_3 are the Cartesian coordinates of a material point in the deformed state and X_1, X_2, X_3 are the coordinates of this same point in the undeformed state as shown in Fig. 2. Notice that for a general deformation the deformation gradient is not symmetric, so that $\frac{\partial x_i}{\partial X_j} \neq \frac{\partial x_j}{\partial X_i}$ and $\boldsymbol{F}$ has 9 independent components instead of the six independent components of the strain tensor. The volume change associated with the deformation is measured by J, the value of the determinant of $\boldsymbol{F}$; the deformation defined by Eq. (3) is constant-volume for $J = 1$. The significance of the deformation gradient is that it completely defines the deformation, including the stretch and rotation, of all line, surface and volume elements at each point within the body that it applies to (Bhattacharya, 2003) whereas various measures of the strain give a subset of this information. Specifically the deformation at a point $\mathbf{x}$ in the deformed body in terms of the deformation gradient is given by

$$\boldsymbol{x} = \boldsymbol{F}\boldsymbol{X} + \boldsymbol{c} \tag{5}$$

which says that each vector $\boldsymbol{X}$ in the undeformed state is distorted and rotated by the deformation gradient $\boldsymbol{F}$ and translated via a rigid motion by the vector $\boldsymbol{c}$ to become the vector $\boldsymbol{x}$. Both Eqs. (3) and (5) are referred to as a *deformation*. The finite stretch tensor, $\boldsymbol{U}$, and the finite rotation matrix, $\boldsymbol{Q}$, are given by (Bhattacharya, 2003):

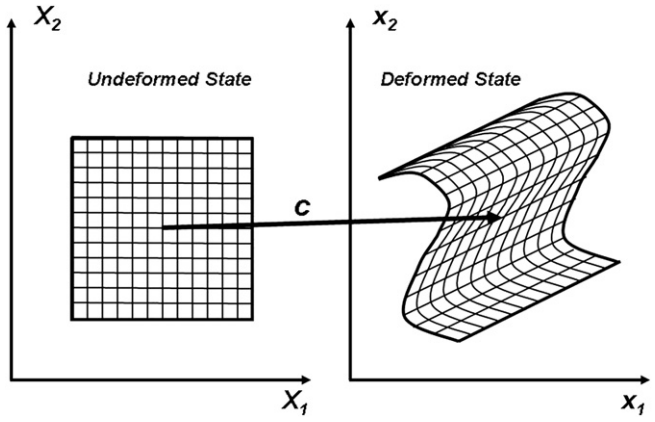

Fig. 2. The deformation expressed by Eqs. (3) and (5). The vector $\boldsymbol{c}$ is the rigid body translation in Eq. (5). (X_1, X_2) and (x_1, x_2) are the coordinates in the undeformed and deformed states respectively.

$$\boldsymbol{U} = \sqrt{\boldsymbol{F}^T\boldsymbol{F}} \text{ and } \boldsymbol{Q} = \boldsymbol{F}\boldsymbol{U}^{-1} \tag{6}$$

where the superscripts T,–1 stand for the transpose and the inverse of the relevant matrix. $\boldsymbol{U}$ has the same eigenvectors as $\boldsymbol{F}^T\boldsymbol{F}$ but the eigenvalues of $\boldsymbol{U}$ are the square roots of those of $\boldsymbol{F}^T\boldsymbol{F}$.

The above discussion concerns the geometry of the deformation and in particular the *results* of a deformation, namely, distortion as measured by the stretch, $\boldsymbol{U}$, and rotation as measured by $\boldsymbol{Q}$. In general the constitutive relation for a given material is a function of the kinematics of the deformation and not of the resulting geometry (and hence not of the strain). The kinematics (or *movement picture* of Sander, 1911) is measured by the spatial distribution of the velocities, $\boldsymbol{v}$, of material points and is expressed as the velocity gradient, $\boldsymbol{L}$:

$$\boldsymbol{L} = \begin{bmatrix} \frac{\partial v_1}{\partial X_1} & \frac{\partial v_1}{\partial X_2} & \frac{\partial v_1}{\partial X_3} \\ \frac{\partial v_2}{\partial X_1} & \frac{\partial v_2}{\partial X_2} & \frac{\partial v_2}{\partial X_3} \\ \frac{\partial v_3}{\partial X_1} & \frac{\partial v_3}{\partial X_2} & \frac{\partial v_3}{\partial X_3} \end{bmatrix} \tag{7}$$

In Eq. (7) the velocity gradient is expressed in terms of the undeformed coordinates; this is referred to as a Lagrangian formulation. If the X_i in Eq. (7) is replaced by the coordinates in the deformed state, x_i, then the formulation is Eulerian. The stretching tensor, $\boldsymbol{D}$, is given by $\boldsymbol{D} = \frac{1}{2}(\boldsymbol{L} + \boldsymbol{L}^T)$ and the spin tensor, $\boldsymbol{\Omega}$, is given by $\boldsymbol{\Omega} = \frac{1}{2}(\boldsymbol{L} - \boldsymbol{L}^T)$. $\boldsymbol{D}$ is also known as the deformation-rate tensor. It is a symmetrical second order tensor and so can be represented as an ellipsoid with principal axes equal to the principal deformation-rates. The stretching tensor and the Lagrangian strain-rate tensors are approximately equal for infinitesimal deformations. The Eulerian strain-rate tensor is approximately equal to the stretching tensor only for infinitesimal deformations with small spins (Eringen, 1962, p. 80). The principal axes of the Lagrangian strain-rate tensor are parallel to the principal axes of the stretching tensor (Eringen, 1962, p. 79). We use the convention that the termination *-ing* is used to denote a kinematic quantity. Thus *stretch* is a distortion and is a *geometric* term; *stretching* is the rate of distortion and is a *kinematic* term.

For the materials we are concerned with in structural geology the constitutive relation is expressed as

$$\sigma = \mathbb{F}(\boldsymbol{D}, T) \tag{8}$$

where $\mathbb{F}$ is a function that involves the history of the stretchings and temperatures that the material has experienced. In general $\mathbb{F}$ evolves as anisotropy, hardening and softening develop in the material as described by Houlsby and Puzrin (2006a). If softening or hardening arises from chemical reactions then the evolution of $\mathbb{F}$ has been described by Coussy and Ulm (1996). As $\mathbb{F}$ evolves to account for the development of anisotropy and hardening (softening) the stress continues to be defined by an evolved version of $\mathbb{F}$and the plastic part of the dissipation in (1) continues to be given by the current value of $\sigma_{ij}\dot{\epsilon}_{ij}^{plastic}$. The stress within a given material at a particular temperature is fixed by the nature of $\mathbb{F}$ and by the history of the movements that the material has experienced which in turn is governed by the history of the imposed velocity or force boundary conditions.

2.4. Overview of Section 2

The so called "Curie principle" of De Groot and Prigogine is sometimes raised as an assertion *that quantities of different tensorial character cannot interact* and hence that Eq. (1) cannot be used. The

statement in italics is simply a statement of the most elementary rule in tensor algebra that says *tensors of the same order may be added to produce a tensor of the same order* and has nothing to do with the Curie Principle proposed by Curie. All the quantities in Eq. (1) are scalars and hence Eq. (1) obeys this elementary rule. The "Curie principle" as proposed by De Groot and Prigogine places no restrictions on the partitioning of the rate of entropy production.

The constitutive laws of use in structural geology are those of a solid where the stress within the material is given by the history of the movements and temperatures that the material has experienced. These movements and temperatures are in turn dictated by the history of the boundary conditions. Thus the stress is controlled by the kinematics of deformation and not by the geometry (that is, the strain). For identical boundary conditions different solids (single crystal, polycrystalline or amorphous) have different stresses (and hence pressures) within them and evolve differently with time as the material hardens or softens or develops various forms of anisotropy. At each moment however during the deformation and temperature histories the plastic dissipation is given by the scalar quantity $\Phi^{plastic} = \sigma_{ij}\dot{\varepsilon}_{ij}^{plastic}$.

3. Principles of generalised thermodynamics

3.1. What is generalised thermodynamics?

Generalised Thermodynamics involves systems in which the classical state variables such as temperature and entropy are supplemented by other variables that define the state of a particular system when it is not in equilibrium. These variables are called *internal variables* (Kestin and Rice, 1970). All variables that define the state of the non-equilibrium system are functions of both space and time as opposed to Equilibrium Chemical Thermodynamics where the state variables are commonly taken as homogeneous in space at any particular time. For a system not at equilibrium, at any instant, the internal variables are a function of position and in most problems vary from point to point within the body. This means that the concept of an *extensive variable* or *extensive state function* proportional to the size of the body loses relevance. For this reason, where possible, the classical extensive variables and extensive state functions of Equilibrium Chemical Thermodynamics are replaced by *specific* quantities. Thus the entropy [J K^{-1}] and the Helmholtz energy [J] are replaced by the specific entropy [J K^{-1} kg^{-1}] and the specific Helmholtz energy [J kg^{-1}] and hence become intensive variables or intensive state functions. In some instances it may be convenient to use *molar* rather than *specific* quantities. This means that in general only intensive variables that have a value at each point in the body are considered in Generalised Thermodynamics.

Generalised Thermodynamics treats systems at equilibrium or far from equilibrium. In seeking a general term to describe this topic we borrow the term *Generalised Thermodynamics* from Houlsby and Puzrin (2006a). Generalised Thermodynamics is closely related to what Lavenda (1978) called *Continuum Thermodynamics*. Lavenda hoped that such a topic would ultimately become a "truly non-linear thermodynamic theory of continua" that would come about "through a synthesis of thermodynamic and kinetic concepts". In fact that synthesis is what we strive for here also although there is clearly still a long way to go. The term *non-equilibrium thermodynamics* is closely associated with the work of De Groot (1952) and Prigogine (1955). Although clearly many aspects of their approach contributed to modern thermodynamics, for reasons mentioned elsewhere some concepts within that body of work are not accepted here. Aspects of the De Groot–Prigogine approach have been thoroughly criticised by Truesdell (1966, 1969), Lavenda (1978) and Ross (2008).

The basic principle governing the description of equilibrium states is that for appropriate boundary conditions the Gibbs energy is a minimum; an equivalent statement is that the entropy is a maximum. This statement carries with it the connotation that, at equilibrium, the entropy production rate is zero. We use this statement that the entropy production rate is zero as a definition of an equilibrium state. The rate of entropy production plays a major role in the study of non-equilibrium systems and is commonly expressed as the Clausius–Duhem relation (Truesdell and Noll, 1965) which we explore in Section 3.3. Eq. (1) is a general statement of the Clausius–Duhem relation. For many systems (particularly many mechanical systems) the entropy production rate is a maximum (Ziegler, 1963) although there is considerable confusion and much discussion in the literature (Rajagopal and Srinivasa, 2004; Martyushev and Selezvev, 2006) concerning maximum and minimum entropy production rate principles. However, as discussed below, for some deforming systems, particularly those involving the development of multiple stationary states, and chemically reacting systems these principles do not hold (Ross and Vlad, 2005; Ross, 2008) and other means of exploring the evolution of such systems are necessary. This invariably involves a consideration of entropy production rates and hence some form of the Clausius–Duhem relation.

A recent approach (Ortiz and Repetto, 1999; Miehe and Lambrecht, 2003) in systems that dissipate energy is to track the evolution of the system by incrementally minimising the Helmholtz energy of the system. It is becoming apparent that criticality (Sornette, 2000) in deforming–reacting systems is a concept that needs considerable attention in structural geology. Systems become critical at a *critical point* where the Helmholtz energy as a function of some measure of the deformation ceases to be convex and becomes non-convex. This leads to the formation of subdomains within the system together with the dissipation of energy and hence these processes act as stored energy minimisers. Herein lies the origin of a large number of apparently unrelated fabrics such as microlithons, crenulation cleavages, metamorphic differentiation, recrystallisation by subgrain rotation and the crustal scale plumbing systems for melt migration. Notice that we specifically do not use the term "self-organised criticality" but prefer to resort to more classical concepts of criticality (Sornette, 2000; Ben-Zion, 2008).

Generalised Thermodynamics has now developed into a quite general science of the flux of energy through systems and supplements the classical approach to mechanics that involves only the continuity of mass and of momentum. Thermodynamics adds an extra dimension to the study of systems not at equilibrium in that it supplies rules by which the evolution of the system with time may be described. In principle a thermodynamic approach has the potential to integrate the complete range of processes of interest to structural geologists such as deformation (both rate-dependent and rate-independent deformations), heat flux, mineral reactions and mass transport, fluid flow, microstructural changes such as recrystallisation, grain-size reduction and fracturing, and crystallographic preferred orientation development. A formal framework for tackling non-equilibrium problems has evolved through the work of people such as Onsager (1931a, b); Biot (1955, 1958, 1978, 1984), Coleman and Gurtin (1967), Truesdell (1969), Rice (1971, 1975), Lavenda (1978), Ziegler (1963, 1983), Coussy (1995, 2004, 2010), Collins and Houlsby (1997), Maugin (1999), Ortiz and Repetto (1999); Collins and Hilder (2002), Rajagopal and Srinivasa (2004), Houlsby and Puzrin (2006a), Ross (2008) and Ross and Villaverde (2010); the framework developed here derives from that body of work. The list explicitly excludes contributions such as De Groot (1952) and Prigogine (1955); as indicated elsewhere that work contains a number of misconceptions including in particular

that systems "close" to equilibrium are linear whereas those "far" from equilibrium are non-linear; that "the Curie principle" as expressed by these authors is valid or even has meaning; that the evolution of chemical and thermal systems involves a principle called the "Principle of Minimum Entropy Production Rate"; and that only systems "far" from equilibrium can form "dissipative structures". Subsequent work (Ziegler, 1963; Truesdell 1966, 1969; Hunt et al. 1987, 1988; Ross and Vlad, 2005; Ross, 2008) has shown that all of these concepts are without merit.

Equilibrium Chemical Thermodynamics as developed by Gibbs (1906) depends on the construction of a function, the Gibbs energy, $\mathcal{G}$, which enables an equilibrium state for the system to be defined under the imposed conditions which in turn are defined by state variables such as pressure, P, and absolute temperature, T. The Gibbs energy is a function of these state variables: $\mathcal{G} = \mathcal{G}(P,T)$ and is given by $\mathcal{G} = \Psi + PV$ where P is the pressure and V the volume. Ψ is the Helmholtz energy given by $\Psi = U - Ts$ where U is the internal energy. A useful discussion of these quantities within both the context of equilibrium systems and solid/fluid systems not at equilibrium is given by Coussy (2010). If $\Delta\mathcal{G}$ is the Gibbs energy change associated with a chemical reaction then the condition for equilibrium is $\Delta\mathcal{G} = 0$ when

$$\frac{\mathrm{d}\Delta\mathcal{G}}{\mathrm{d}t} = 0 \tag{9}$$

and $\mathcal{G}$ is a minimum; t is time. We use the term equilibrium to mean a stationary state where all processes have ceased (zero entropy production rate). Steady state refers to a stationary state where processes still operate but the rates are independent of time (non-zero entropy production rate).

The state variables here are quantities that have unique non-zero values in the equilibrium state and these values must be independent of the path by which the equilibrium state was attained otherwise many different values of the state variables could define an equilibrium state. An outcome is that gradients in the state variables cannot exist at equilibrium for then $\mathcal{G}$ would have different values at different places in the system. Hence Equilibrium Chemical Thermodynamics considers systems where the temperature and pressure have the same values everywhere. Note however that the condition that T and P be the same everywhere is not a condition for the existence of the Gibbs energy. Despite claims to the contrary (McLellan, 1980, p. 193) the specific Gibbs energy is defined for a stressed system simply as the Legendre Transform of the Helmholtz energy (Rice, 1975; Biot, 1984; Houlsby and Puzrin, 2006a).

In Generalised Thermodynamics the specific Gibbs energy can have different values both in space and time within the system. However, as discussed below, the Gibbs energy is not useful in deforming systems unless the constitutive relation for the material and the deformation history is prescribed. The Helmholtz energy is the important quantity in deforming systems. The state and internal variables still define the state of the system but they too are functions of space and time so that gradients in these variables can exist and indeed these gradients can be internal variables in their own right (Kestin and Rice, 1970). Thus both ∇T and $\nabla \mu$ can be used as internal variables where ∇ is the gradient operator and μ is a chemical potential since both of these gradients reduce to zero at equilibrium. The only provisos on the internal variables in Generalised Thermodynamics are: (i) they are valid mathematical, physical and/or chemical quantities, (ii) they are objective in the sense that some measure of them is independent of the coordinate frame used, and (iii) they approach equilibrium values as equilibrium is approached. Some examples of internal variables used in the study of deforming metamorphic systems are given in Table 2.

In Table 2, the time derivatives of those quantities labelled *State or Internal Variables* are commonly referred to as "*thermodynamic fluxes*" whereas those labelled *Conjugate Variables* are commonly referred to as "*thermodynamic forces*" or as "*generalised stresses*". The terminology is unfortunate since in general neither the "fluxes" nor the "forces/stresses" have the indicated physical significance but the usage is firmly entrenched and useful. In Table 3 we list the thermodynamic fluxes and the conjugate thermodynamic forces for some processes of interest to structural geologists. A fundamental observation from Table 3 is that for processes such as thermal conduction, non-isothermal chemical diffusion and chemical reactions, the "fluxes" are never linear functions of the "forces". This observation is important when we come to consider extremum principles below. If the thermodynamic fluxes are proportional to the thermodynamic forces (as in many mechanical and fluid flow systems and in processes such as isothermal mass diffusion) the system is said to be "*thermodynamically linear*". Otherwise (and this includes non-isothermal mass diffusion, thermal conduction and all chemical reactions) the system is said to be "*thermodynamically non-linear*". Thus, even chemical systems are thermodynamically non-linear no matter if they be "close" or "far" from equilibrium (Hunt et al. 1987, 1988). The temperature times the entropy production rate for a particular process equals the thermodynamic flux multiplied by the thermodynamic force. In Table 3, $K^{thermal}$ is the thermal conductivity, K^{fluid} is the fluid permeability, D is the mass diffusivity or diffusion coefficient, k is Boltzman's constant, $\dot{\xi}$ is the chemical reaction rate, η is the viscosity and r^+, r^- are the forward and reverse reaction rates for a chemical reaction.

In applying the concepts of Equilibrium Chemical Thermodynamics for small strains to deforming-reactive solids, one replaces the mechanical role of the pressure, P, by the Cauchy stress tensor, σ_{ij}, and the mechanical role arising from small changes in the specific volume, V, by the small strain tensor, ε_{ij} (Houlsby and Puzrin, 2006a). The restriction to small strains is not an undue limitation since one is commonly concerned with developing incremental approaches that can be implemented in finite element or finite difference codes.

Table 2
State or internal variables and conjugate variables used in Generalised Thermodynamics relevant to Structural Geology.

State or Internal Variable	Conjugate Variable	Descriptions
$\varepsilon_{ij}^{elastic}$	σ_{ij}	Elastic strain; Stress
$\varepsilon_{ij}^{plastic}$	χ_{ij}	Plastic strain; Generalised stress (Houlsby and Puzrin, 2006a)
T	s	Absolute temperature; Entropy
ξ	A	Extent of chemical reaction; Affinity of chemical reaction (Kondepudi and Prigogine, 1998)
δ_{ij}	Y_{ij}	Tensor measure of damage; Generalised damage stress (Lyakhovsky et al., 1997; Karrech et al., 2011)
m^K	μ^K	Concentration of Kth chemical component; Chemical potential of Kth chemical component (Coussy, 1995, 2004)
d	χ_{ij}^d	Grain-size; Generalised stress associated with grain-size evolution
ζ	P^{fluid}	Variation of fluid content; Pore pressure of fluid (Detournay and Cheng, 1993; Coussy, 1995)
β_{ij}	B_{ij}	Tensor measure of crystallographic preferred orientation; Generalised stress driving crystallographic preferred orientation development. (Faria, 2006a, c, Faria et al., 2006b)

Table 3
Thermodynamic fluxes and forces for some common processes.

Process	Thermodynamic flux	Thermodynamic force
Deformation of Newtonian viscous material	Strain-rate, $\dot{\varepsilon}_{ij}$ $\dot{\varepsilon}_{ij} = \eta^{-1}\sigma_{ij}$	Cauchy stress, σ_{ij}
Deformation of Non-Newtonian viscous material	Strain-rate, $\dot{\varepsilon}_{ij}$ $\dot{\varepsilon}_{ij} = \mathcal{A}\sigma_{ij}(J_2)^{\frac{n-1}{2}}$	Cauchy stress, σ_{ij}
Thermal conduction	Thermal flux, $J^{thermal}$ $J^{thermal} = -K^{thermal}\nabla T$	∇T^{-1}
Chemical diffusion	Mass flux, J^{mass} $J^{mass} = -D\nabla\mu$	$\nabla\frac{\mu}{T}$
Fluid flow	Darcy velocity, u $u = -K^{fluid}\nabla P^{fluid}$	∇P^{fluid}
Chemical reaction	Reaction rate, $\dot{\xi}$ $\dot{\xi} = [r^+ - r^-]$	Affinity $kT\ln[\frac{r^+}{r^-}]$

Taking tensile stresses as positive, the pressure, P, and specific volume, V, are now given by:

$$P = -\frac{1}{3}\sigma_{kk} \quad \text{and} \quad V = V_0(1+\varepsilon_{kk}) = \frac{1}{\rho} \tag{10}$$

where V_0 is the initial specific volume and ρ is the current density. The initial density, ρ_0, is $1/V_0$. In a conceptual mapping of the quantities used in Equilibrium Chemical Thermodynamics, P is replaced by $-\sigma_{kk}$ and V by $V_0(\frac{1}{3}\delta_{ij}+\varepsilon_{ij})$ where δ_{ij} is the Kronecker delta. Thus PV is replaced by $-\sigma_{ij}V_0(\frac{1}{3}\delta_{ij}+\varepsilon_{ij}) = -V_0(\frac{1}{3}\sigma_{kk}+\sigma_{ij}\varepsilon_{ij})$ $= PV_0 - V_0\sigma_{ij}\varepsilon_{ij}$.

The expressions for the specific internal energy, U, the specific Helmholtz energy, Ψ, the specific enthalpy, $\mathcal{H}$, and the specific Gibbs energy, $\mathcal{G}$, are then given as in Table 4. Also given in Table 4 are expressions for the conjugate variables $\{\sigma_{ij}, \varepsilon_{ij}\}$ and $\{s, T\}$ in terms of U, Ψ, $\mathcal{H}$ and $\mathcal{G}$.

3.2. Extremum principles and system behaviour

The extremum principle universally used in Equilibrium Chemical Thermodynamics is that the Gibbs energy is a minimum at equilibrium. This principle has proved very powerful and has allowed exceptional progress in the construction of mineral phase equilibrium diagrams for quite complicated metamorphic reactions and bulk chemical compositions (Powell et al., 1998). However for systems not at equilibrium some other principle, or set of principles, would be useful in describing the evolution of the system as it proceeds towards equilibrium or is maintained far from equilibrium by fluxes of energy and/or mass. The extremum principles that have evolved over the past 30 years all involve a statement concerning the entropy production rate, the most general of which is the Clausius–Duhem relation.

A well known example in structural geology is represented by the Taylor (1938) and Bishop–Hill (Bishop and Hill, 1951) extremum principles used in calculating the evolution of crystallographic preferred orientations (Lister et al., 1978). The Taylor principle says: *In a deforming polycrystal, for a given imposed strain-increment, the energy dissipation by the shear strains on the slip systems (with specified critical resolved shear stresses) needed to accomplish that strain-increment is a minimum*. The Bishop–Hill principle is the linear programming dual of the Taylor principle and says that: *In a deforming polycrystal, for a given imposed strain-increment, the stress state that actually exists within the deforming crystal is that which maximises the energy dissipation*. We will see that the Bishop–Hill principle is equivalent to the Ziegler (1963, 1983) principle of maximum entropy production rate. The Bishop–Hill maximum work principle chooses that stress tensor in the deforming crystal which is as close as possible parallel to the imposed strain-rate tensor subject to the constraint that the imposed strain-increment must be achieved only by slip systems that define the yield surface.

Table 4
Thermodynamic quantities used in the small strain formulation of Generalised Thermodynamics (After Houlsby and Puzrin, 2006a).

Specific Internal Energy	Specific Helmholtz Energy	Specific Enthalpy	Specific Gibbs Energy
$U = U(\varepsilon_{ij}, s)$	$\Psi = \Psi(\varepsilon_{ij}, T)$ $\Psi = U - sT$	$\mathcal{H} = \mathcal{H}(\sigma_{ij}, s)$ $\mathcal{H} = U - V_o\sigma_{ij}\varepsilon_{ij}$	$\mathcal{G} = \mathcal{G}(\sigma_{ij}, T)$ $\mathcal{G} = \mathcal{H} - sT$ $\mathcal{G} = \Psi - V_o\sigma_{ij}\varepsilon_{ij}$
$V_o\sigma_{ij} = \frac{\partial U}{\partial \varepsilon_{ij}}$ $T = \frac{\partial U}{\partial s}$	$V_o\sigma_{ij} = \frac{\partial \Psi}{\partial \varepsilon_{ij}}$ $s = -\frac{\partial \Psi}{\partial T}$	$\varepsilon_{ij} = -\rho_0\frac{\partial \mathcal{H}}{\partial \sigma_{ij}}$ $T = \frac{\partial \mathcal{H}}{\partial s}$	$\varepsilon_{ij} = -\rho_o\frac{\partial \mathcal{G}}{\partial \sigma_{ij}}$ $s = -\frac{\partial \mathcal{G}}{\partial T}$

In order to proceed with the task of specifying principles that govern the evolution of non-equilibrium systems it is convenient to divide systems into those with single and multiple stationary states. A stationary state is one where the time rate of change of a particular variable is zero. A common example is a simple chemical system where one stationary state is an equilibrium state defined by the reaction rate being zero. Such a system has a single equilibrium stationary state (Hobbs and Ord, 2010a).

However even a simple chemical system such as

$$\mathrm{A} + \mathrm{B} \underset{k^-}{\overset{k^+}{\rightleftarrows}} \mathrm{C} + \mathrm{D} \tag{11}$$

has another stationary state where the rate of production of a chemical component is zero but the forward and/or reverse chemical reactions are still in progress Thus such reactions have at least two stationary states, one an equilibrium state and the other a steady non-equilibrium state given through the law of mass action by an equation of the form (Kondepudi and Prigogine, 1998):

$$\dot{\xi} = -\frac{\mathrm{d}A}{\mathrm{d}t} = k^+AB - k^-CD = 0 \tag{12}$$

where ξ is the extent of the reaction (Kondepudi and Prigogine, 1998), $\dot{\xi}$ is the reaction rate and A, B, C, D are written as the concentrations of the chemical components A, B, C, D. We use concentrations throughout this paper for simplicity although the discussion can be extended to use activities instead of concentrations (Ross, 2008, Chapter 9). k^+ and k^- are the rate constants for the forward and reverse reactions in Eq. (11).

Deforming non-linear elastic systems represent perhaps the simplest manifestation of systems with multiple stationary states and we include a brief description to highlight that even in such systems the evolution of the system can be complex, even chaotic. In linear elastic systems undergoing deformation it appears that only one equilibrium stationary state exists and that is the one that maximises the stored elastic energy (McLellan, 1980, pp. 313–314). This is the only stationary state that can exist for an adiabatically deforming linear elastic system. However for non-linear elastic systems where the non-linearity is introduced via a softening of the elastic modulus arising from some form of elastic damage or from geometrical softening arising from large rotations, multiple equilibrium stationary states commonly exist (Hunt and Wadee, 1991; Ericksen, 1998; Hunt et al., 1997a, b, 2000, 2001, 2006; Budd et al., 2001) and correspond to non-convex forms of the Helmholtz energy function. By non-convex here we mean that a plot of the Helmholtz energy against some measure of the deformation or deformation gradient has a number of "bumps" or discontinuities in it. This results in the development of kink, chevron and concentric folds in layered elastic materials (Section 5.3). The extremum principle involves the development of minima in the

stored elastic energy and corresponds to points where the stored elastic energy matches the energy required for slip on the layers. Such a principle corresponds to the Maxwell construction common in chemical systems involving two or more phases (Kondepudi and Prigogine, 1998) and represents a lower bound for the force required for the initiation of folding. However the first bifurcation in the system occurs *after* the peak stress is attained (Tvergaard and Needleman, 1980; Hunt and Wadee, 1991). Sequential bifurcations occur as the system jumps from one equilibrium stationary state to another although complexity can arise due to mode locking (Hunt and Everall, 1999; Everall and Hunt 1999). All such behaviour in an adiabatically deformed elastic system represents a progression through a series of equilibrium states and a full description of the system evolution relies on non-linear bifurcation theory (Guckenheimer and Holmes, 1986; Wiggins, 2003). In addition, softening behaviour can lead to localisation of fold packets in layered materials and a progression to chaos with fractal geometries (Hunt and Wadee, 1991). Multiple stationary states have also been described in deforming visco-elastic systems (Cheng and Zhang, 1999) and are well known in the study of martensitic transformations (Ericksen, 1998) and in the development of microstructure in anisotropic materials (Truskinovsky and Zanzotto, 1995, 1996). Examples of multiple stationary states arising from thermal–mechanical feedback in mantle deformations are discussed by Yuen and Schubert (1979). In chemical systems multiple stationary states are common (Epstein and Pojman, 1998; Ross, 2008) and are considered in detail in Section 4.1. The fundamental principle involved in understanding the evolution of these kinds of mechanical systems is that the Helmholtz energy is no longer convex and the system evolves to minimise the Helmholtz energy by forming a series of finer structures or chemical domains that lead to compatibility with the imposed deformation (Ball, 1977; Ball and James, 1987; Ortiz and Repetto, 1999). We explore such behaviour in detail in Sections 4.10 and 5.3. The transition from convex to non-convex Helmholtz energy functions is the hallmark of critical phenomena (Sornette, 2000; Ben-Zion, 2008) so that such behaviour seems to be a fundamental and universal aspect of deforming–reacting systems.

In systems with a single non-equilibrium stationary state, the commonly quoted extremum principle is that the entropy production is minimised (Prigogine, 1955; Biot, 1958). Examples of such systems that are widely quoted are steady heat conduction in a material with constant thermal conductivity (Kondepudi and Prigogine, 1998) and simple, uncoupled chemical reactions (Kondepudi and Prigogine, 1998). However Ross and Vlad (2005 and references therein) and Ross (2008, Chapter 12) show that, for these two classical systems, there is no extremum in the entropy production rate. It is only for systems where the relationship between thermodynamic fluxes and forces is linear that an extremum exists for the entropy production rate and this corresponds to a stationary state that is not an equilibrium state. If the relationship between thermodynamic fluxes and forces is non-linear then only one extremum in the entropy production rate exists and that is an equilibrium state. The linear situation is that commonly quoted and discussed by Prigogine (1955), Kondepudi and Prigogine (1998) and a host of others. However reference to Table 3 shows that at least for thermal conduction and chemical reactions the thermodynamic fluxes are not proportional to the thermodynamic forces. For mass diffusive processes the thermodynamic flux is proportional to the thermodynamic force only for isothermal situations. For further discussion and clarification of what is meant by "close" and "far" from equilibrium reference should be made to the interchange between Hunt, Hunt, Ross, Vlad and Kondepudi (Hunt et al. 1987, 1988; Kondepudi, 1988; Ross and Vlad, 2005; Ross, 2008).

For some systems (and this involves many mechanical systems; Houlsby and Puzrin, 2006a, b) the entropy production rate is maximised. Ziegler (1963 and references therein) seems to have been the first to propose this principle although we will see that the principle of maximum work proposed by Bishop and Hill (1951) is identical to that of Ziegler; Ziegler (1963) gives a good summary of other related principles. The Ziegler principle appears to hold, and is a powerful tool for defining the evolution of simple plastic deformations (Houlsby and Puzrin, 2006a, b). In order to understand Ziegler's arguments it is instructive to examine two ways in which the relationship between stress and dissipative strain-rate can be graphically represented. The first way, the yield surface, is well known and widely used. This surface was discussed in relation to localisation in rate-independent materials by Hobbs et al. (1990) and is shown in Fig. 3(a). The yield surface is drawn in stress space and stress states within the surface correspond to elastic deformations while stress states on the yield surface correspond to plastic deformations. If the yield surface corresponds to a function $f(\sigma_{ij})$ then the condition for plastic yield is $f = 0$ while $f < 0$ corresponds to elastic deformations. Stress states corresponding to $f > 0$ are physically unrealistic. If no volume change accompanies plastic deformation then the increment of plastic strain-rate, $\dot{\varepsilon}_{ij}^{dissipative}$ associated with the stress, σ_{ij}, is normal to the yield surface at the end point of the stress vector (Fig. 3a) and is given by $\dot{\varepsilon}_{ij} = \lambda \frac{\partial f}{\partial \sigma_{ij}}$ where λ is a constant known as a plastic multiplier. The dissipation is the scalar product of the stress and the incremental strain-rate: $T\dot{s} = \Phi = \sigma_{ij}\dot{\varepsilon}_{ij}^{dissipative}$. One can see from Fig. 3a that Φ is always positive in accordance with the second law of thermodynamics.

One can also plot another surface, the dissipation surface in strain-rate space (Fig. 3b) for a particular value of the dissipation function, $\Phi = \Phi_0$. Ziegler (1963, 1983) showed that for uncoupled deformations the stress corresponding to a particular strain-rate

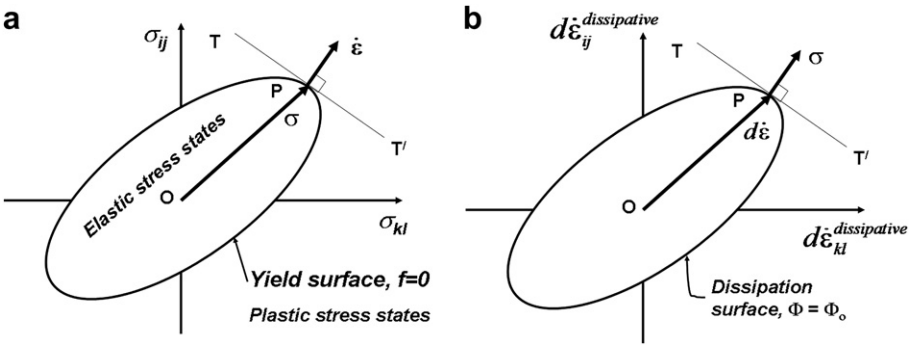

Fig. 3. Yield and dissipation surfaces. One is the Legendre transform of the other. Each diagram is a two dimensional section through six dimensions. (a) The yield surface. The coordinate axes are the components of the Cauchy stress, σ_{ij}. (b) The dissipation surface. The coordinate axes are the components of the incremental dissipative strain-rate tensor, $d\dot{\varepsilon}_{ij}^{dissipative}$.

increment is orthogonal to the dissipation surface at the end point of the strain-rate vector (Fig. 3b) and is given by $\sigma_{ij} = \nu \frac{\partial \Phi}{\partial \dot{\varepsilon}_{ij}^{dissipative}}$ where ν is a constant. Thus the yield surface and the dissipation surface are complementary to each other (Collins and Houlsby, 1997; Houlsby and Puzrin, 2006a) and in fact, just as the Gibbs energy can be obtained from the Helmholtz energy through a Legendre Transformation (Callen, 1960; Powell et al., 2005; Houlsby and Puzrin, 2006a) and *vice versa*, the yield surface can be obtained from the dissipation surface through a Legendre Transformation (Collins and Houlsby, 1997; Houlsby and Puzrin, 2006a) and *vice versa*.

As far as this review is concerned the importance of the *Ziegler orthogonality relation* is better seen by redrawing Fig. 3b as in Fig. 4 (a). In this figure the strain-rate vector touches the dissipation surface, $\Phi = \Phi_o$ at P where the tangent TPT′ is drawn. The Zeigler orthogonality relation says that the stress vector associated with the strain-rate is normal to this tangent. The dissipation (and hence the entropy production rate at a given temperature) is the scalar product of the strain-rate with the stress (or the projection of the strain-rate vector on to the stress vector). One can see from Fig. 4(a) that, because of the convexity of the dissipation surface, this scalar product is a maximum for the stress and strain that obey the orthogonality relation. For all other strain-rate vectors the scalar product with the stress is smaller. This is a graphical demonstration of the Ziegler principle of maximum entropy production rate which says that of all possible stress states the stress that is actually associated with a particular strain-rate produces a maximum in the entropy production rate. Although this argument depends on the convexity of the dissipation surface, Houlsby and Puzrin (1999) point out that the Ziegler principle holds also for weakly non-convex yield surfaces and for non associated flow (where the incremental strain-rate vector is not normal to the yield surface).

The Bishop–Hill theory of crystal plasticity is illustrated in Fig. 4 (b) where a section through the dissipation surface for a crystal undergoing deformation on multiple slip systems is shown. The same arguments as apply to Fig. 4(a) hold except now there is an ambiguity in the orientation of the tangent to the dissipation surface at a corner. Nevertheless the overall argument concerning entropy production rate holds as in Fig. 4(a).

3.2.1. Biot's thermodynamic approach

Biot developed a theory of quasi-static deformation (that is, inertia is neglected) based on a non-equilibrium thermodynamics approach derived from Onsager (1931a, b). This development is best presented in Biot (1955, 1958, 1978, 1984). The essential features are given below in a much abbreviated form. Consider a system displaced from equilibrium by perturbations ξ_i. At equilibrium, $\xi_i = 0$. These ξ_i represent one of the first references to internal variables and they define the thermodynamic state of a system not at equilibrium. They may be scalars such as temperature, the number of moles of chemical species or the variation in fluid content (Detournay and Cheng, 1993). Or they may be vectors or tensors such as displacement vectors or the elastic strain tensor. Then Biot proposed that the specific Helmholtz energy of the system, Ψ, may be written

$$\Psi = \frac{1}{2} a_{ij} \xi_i \xi_j \tag{13}$$

and the specific dissipation function, Φ, as

$$\Phi = \frac{1}{2} b_{ij} \dot{\xi}_i \dot{\xi}_j \tag{14}$$

The dot on $\dot{\xi}_i$ represents the material time derivative. a_{ij} and b_{ij} are tensors that relate the thermodynamic force to the conjugate variable in Eq. (13) or to the thermodynamic flux in Eq. (14).

Biot proceeds to show that the evolution of the system may be described by an expression which is now known in the literature as Biot's Equation for a standard dissipative system (Nguyen, 2000; Miehe and Lambrecht, 2003):

$$\frac{\partial \Psi}{\partial \xi_i} + \frac{\partial \Phi}{\partial \dot{\xi}_i} = 0 \tag{15}$$

Or, if the system is under the influence of external thermodynamic forces, Q_i, then

$$\frac{\partial \Psi}{\partial \xi_i} + \frac{\partial \Phi}{\partial \dot{\xi}_i} = Q_i \tag{16}$$

Biot discusses a layered system and explores solutions to Eq. (15) of the form

$$\xi = \xi_0 \exp[\omega t] \tag{17}$$

where ω is an amplification factor, and t is time. If ω is negative, the perturbations decay in amplitude with time and the system returns to equilibrium. However if ω is positive then the perturbations grow exponentially with time and some form of patterning develops. The point of this discussion is that Biot proposes that the stability and evolution of the system can be described with the use of just two functions, the Helmholtz energy and the dissipation function, an observation emphasised again much later by Houlsby and Puzrin (2006a, b) and which is the basis for Generalised Thermodynamics as described here.

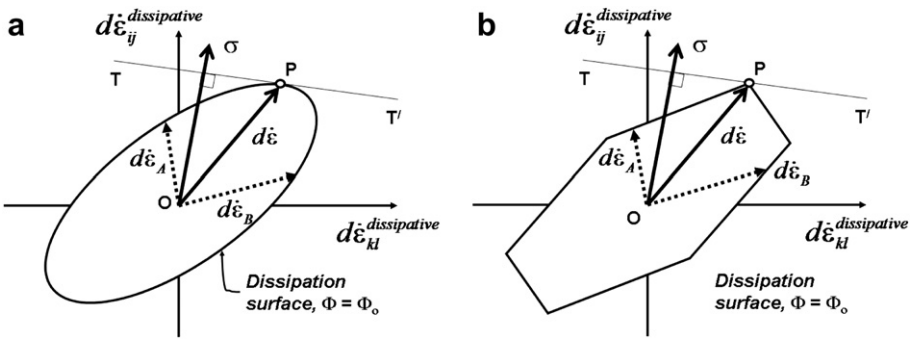

Fig. 4. Illustration of Ziegler's principle of maximum entropy production rate. The dissipation surface is drawn in incremental strain-rate space. (a) The stress associated with the imposed strain-rate is normal to the dissipation surface at P. Of all other possible strain-rate vectors, for example $d\dot{\varepsilon}_A$ and $d\dot{\varepsilon}_B$, the projection of the strain-rate vector on to the stress vector is smaller than the projection of the imposed strain-rate vector. This means that the dissipation arising from the stress and the imposed strain-rate is a maximum. The distance of the tangent plane TPT′ from the origin, O, is the work done by the stress during the imposed strain-rate increment. (b) The equivalent of (a) drawn for multiple slip single crystal plasticity. The argument for (a) follows even though there is ambiguity with respect to the orientation of the tangent at the corner of the yield surface.

Biot (1965, pp. 340–349) considers a thin rod of initial length, a deformed by a load, P parallel to the initial orientation of the rod, and constrained laterally by a viscous medium with viscosity, η. The possible sideways deflections of the rod, w, are expressed as a Fourier series:

$$w = \sum_{n=1}^{\infty} q_n \sin\left(n\pi\frac{x}{a}\right) \tag{18}$$

where q_n are amplitudes of the deflections, n is an integer, and x is the coordinate parallel to the initial orientation of the rod. Then Biot shows that the dissipation function and the Helmholtz energy of the system are related by Eq. (15) with a solution given by Eq. (17) and ω given by

$$\omega = \frac{\pi^2 n^2}{\eta a^2}\left(P - n^2 P_c\right) \tag{19}$$

where P_c is a critical buckling load. Thus, unstable modes grow if $P > n^2 P_c$ and ω is a maximum for a value of n representing the number of half-waves in which the rod buckles. This argument, together with the assumption that the deflections can be expressed in terms of a Fourier series, leads to the development of a strictly periodic result with the corresponding wavelength known as the *dominant wavelength*.

A summary of various extremum principles is given in Table 5. One can see that despite the various apparently conflicting formulations, all except the "minimum entropy production rate" principle of Prigogine and De Groot are equivalent and expressed by Ziegler's principle of maximum entropy production rate. One should be aware of the definitive discussions by Ziegler (1963), Hunt et al. (1987, 1988) and by Ross and Vlad (2005) before one embarks on the formidable and confusing task of reading the literature in this area.

3.3. Thermodynamic formulation

The above discussion has shown that in most non-linear systems there is no extremum entropy production theorem that enables us to explore the evolution of the system when not at equilibrium. Progress can be made however by deriving the general expression for entropy production rate in the system of interest and then making various simplifying assumptions such as constant temperature or no deformation. We show that this leads, at various scales, to systems of coupled reaction-diffusion equations (Cross and Hohenberg, 1993) or coupled reaction-diffusion-deformation equations (Ortoleva, 1989). These represent convenient and useful expressions of a combination of the first and second laws of thermodynamics.

We present below a brief summary of the thermodynamic framework used to couple various processes together so that the coupling is thermodynamically admissible, that is, the framework satisfies both the first and second laws of thermodynamics. The framework presented is very conservative. Far more intricate approaches are available such as the Extended Thermodynamics framework (Jou et al., 1993, 2001), the GENERIC framework (Ottinger, 2005), frameworks that involve the gradients of internal variables (Shizawa and Zbib, 1999; Shizawa et al. 2001; Voyiadjis and Dorgan, 2004) and approaches that involve finite deformations (Houlsby and Puzrin, 2006b). The framework we present is sufficient to illustrate the basic concepts. The interested reader is encouraged to explore the more advanced literature and we emphasise that the subject is advancing very rapidly. To a large extent our treatment follows that of Rice (1975), Coussy (1995, 2004) and Houlsby and Puzrin (2006a).

In Equilibrium Chemical Thermodynamics the state of a system is defined in terms of the Gibbs energy, $\mathcal{G} = \mathcal{G}(P,V)$ where P is obtained from an *equation of state* or is prescribed independently, usually as the lithostatic pressure. The equation of state is commonly that of an ideal or non-ideal gas, an inviscid fluid or an elastic solid (Stixrude and Lithgow-Bertelloni, 2005). Only in the case of an elastic solid is the stress specified. In Generalised Thermodynamics the stress is obtained from the constitutive relation Eq. (8) and the pressure is given by $P = -tr(\boldsymbol{\sigma})$. Thus the pressure is defined by the constitutive equation which is different for different materials. In other words *different materials subjected to identical boundary conditions will have different values for the pressure, P, within them*. We are interested in defining the state of systems independently of the constitutive equation (and hence does not involve the stress or the pressure) and in tracking the evolution of temperature in the system and so an energy function that involves some measure of the deformation and the temperature is useful. For this reason the Helmholtz energy rather than the Gibbs or internal energy is generally the function of use.

Table 5
A summary of various extremum principles proposed in non-equilibrium thermodynamics.

Extremum Principle	Statement of Principle	Status
Ziegler's principle of maximum entropy production rate (Ziegler, 1963)	If the stress is prescribed the actual strain-rate maximises the entropy production rate	True for many deforming systems; see Ziegler (1963, 1983) and Ross (2008)
Onsager's Reciprocity Relations and principle of least dissipation of energy (Onsager, 1931a,b)	Once the thermodynamic forces are fixed the actual thermodynamic fluxes maximise the dissipation. This is a consequence of the classical Onsager Reciprocity Relations. See Ziegler (1963)	Same as Ziegler's principle. Restricted to thermodynamically linear systems
Biot's principle of minimum entropy production rate (Biot, 1955)	If the stress and the rate of stress are prescribed the actual strain-rate minimises the dissipation function	Same as Ziegler's principle but was obtained from Onsager's principle
Prigogine's principle of minimum entropy production rate. (Prigogine, 1955)	If there are n thermodynamic forces and j of these are prescribed then the dissipation function is minimised by equating the k thermodynamic fluxes to zero for $k = j+1,\ldots,n$	Conceptually of completely different form to Ziegler's principle but follows from Ziegler's principle; relies on the imposition of constraints; see Ziegler (1963) and Ross (2008). For chemical and thermal conduction processes the minimum entropy production principle does not exist (Ross, 2008)
Taylor's minimum internal work principle (Taylor, 1938)	For a prescribed deformation increment imposed on a polycrystal and a given set of critical resolved shear stresses the shears on the operating slip systems minimise the work	Same as Ziegler's principle
Bishop–Hill maximum external work principle (Bishop and Hill, 1951)	For a prescribed deformation increment imposed on a polycrystalthe stress state that develops is such that the operating slip systems maximise the work. This is the linear programming dual of the Taylor principle	Same as Ziegler's principle

Following Biot (1955, 1958) and Rice (1975) we define the specific Helmholtz energy, Ψ, as

$$\Psi = U - Ts = \Psi\left(\varepsilon_{ij}^{elastic}, T, m^K, \xi^M, \alpha_{ij}^Q\right) \tag{20}$$

where U is the specific internal energy, T is the absolute temperature, s is the specific entropy, m^K is the concentration (kg m^{-3}) of the Kth chemical component, ξ^M is the extent of the Mth chemical reaction and α^Q is a parameter (scalar, vector or tensor) that describes the state of some variable, Q, of interest such as amount of damage, grain-size, degree of crystallographic preferred orientation and so on. If one wanted to incorporate the effects of changes in mineralogy or of fabric during deformation it would be done through the α_{ij}^Q term. Rice (1975) discusses the incorporation of dislocations, diffusion and micro-fracturing. Quantities that are conjugate to the internal variables expressed in Eq. (20) (following arguments presented by Coussy, 1995, 2004, and by Houlsby and Puzrin, 2006a; see also Tables 2 and 3) are

$$V_o\sigma_{ij} = \frac{\partial\Psi}{\partial\varepsilon_{ij}^{elastic}} \tag{21a}$$

$$s = -\frac{\partial\Psi}{\partial T} \tag{21b}$$

$$V_o\mu^K = -\frac{\partial\Psi}{\partial m^K} \tag{21c}$$

$$A^M = -\frac{\partial\Psi}{\partial\xi^M} \tag{21d}$$

$$V_oY_{ij}^Q = -\frac{\partial\Psi}{\partial\alpha_{ij}^Q} \tag{21e}$$

where σ_{ij} is the Cauchy stress, μ^K is the specific chemical potential of the Kth chemical component, A^M is the affinity of the Mth chemical reaction and Y^Q is known as the "generalised stress" associated with the Qth process and is the "driving force" for the Qth process.

We have seen that the second law of thermodynamics may be written:

$$T\dot{s} = \Phi = \Phi^{mechanical} + \Phi^{diffusive} + \Phi^{chemical} + \Phi^{thermal} \geq 0 \tag{22}$$

where Φ is the total dissipation function and $\Phi^{mechanical}$, $\Phi^{diffusive}$, $\Phi^{chemical}$ and $\Phi^{thermal}$ are the contributions to the total dissipation rate from mechanical, mass diffusive, chemical reaction and thermal transport processes respectively.

Specific statements of the dissipation functions associated with various processes are (see Coussy, 1995; 2004)

$$\Phi^{mechanical} = V_o\sigma_{ij}\dot{\varepsilon}_{ij}^{dissipative} + V_o\mu^K\dot{m}^K + s\dot{T} + V_oY_{ij}^Q\dot{\alpha}_{ij}^Q \tag{23a}$$

$$\Phi^{diffusive} = -V_o\mathbf{J}^K \bullet \left\{\nabla\mu^K - \frac{\partial\mu^K}{\partial T}\nabla T\right\} \tag{23b}$$

$$\Phi^{chemical} = A^M\dot{\xi}^M + \dot{L}^M \tag{23c}$$

$$\Phi^{thermal} = -c_p\kappa^{thermal}\nabla^2 T \tag{23d}$$

where summation on K, M or Q is intended and K, M and Q take on the values 1,…,ℵ ,1,…,ℜ and 1,….,ϒ respectively. In Eq. (23b), • represents the scalar product of vectors; in Eq. (23c) $\dot{L}^M$ is the rate of heat production from reaction M; in Eq. (23d) $\kappa^{thermal}$ is the thermal diffusivity and c_p is the specific heat at constant pressure.

If we consider isothermal systems, as is commonly done in metamorphic petrology, and neglect processes defined by Q in Eq. (20), then Eq. (22) reduces to

$$T\dot{s} = V_o\boldsymbol{\sigma}:\dot{\boldsymbol{\varepsilon}}^{dissipative} + V_o\mu^K\dot{m}^K - \mathbf{J}^K\cdot\nabla\mu^K - A^K\dot{\xi}^K - \dot{L}^K \geq 0 \tag{24}$$

where $\boldsymbol{\sigma}:\dot{\boldsymbol{\varepsilon}}$ is the scalar product of $\boldsymbol{\sigma}$ and $\dot{\boldsymbol{\varepsilon}}$. Eq. (24) is the Clausius–Duhem equation for an isothermal dissipative deforming system with coupled chemical reactions and diffusive mass transfer (Coussy, 1995, 2004). The importance of the equation is that it involves an equality on the left hand side that enables the entropy production rate to be completely specified.

For a non-isothermal system, if we assume that

$$\dot{\varepsilon}_{ij}^{total} = \dot{\varepsilon}_{ij}^{elastic} + \dot{\varepsilon}_{ij}^{dissipative} \tag{25}$$

Then, using Eqs. (20) and (21), we can eventually arrive at the Energy Equation (26) that expresses the change in temperature arising from all of the dissipative processes and does not include contributions from elastic deformations:

$$c_p\dot{T} = \chi V_o\sigma_{ij}\dot{\varepsilon}_{ij}^{dissipative} + V_o\mu^K\dot{m}^K - \sum_K \Phi_K^{diffusive} - \sum_K \Phi_K^{chemical} - \Phi^{thermal} \tag{26}$$

where χ is the Taylor-Quinney coefficient and represents the proportion of mechanical work arising from dissipative deformation that is available to increase the temperature or to drive diffusion, chemical reactions and structural adjustments such as fracturing or grain-size reduction. At high strains where the energy arising from deformation is stored in crystal defects, χ is generally in the range $0.85 \leq \chi \leq 1$ (Taylor and Quinney, 1934) and here we assume $\chi = 1$. The energy stored during deformation of calcite and released during recrystallisation was studied by Gross (1965). For a theoretical discussion of the amount of energy dissipated during deformation in various materials and comparisons with experiments see Stainier and Ortiz (2010).

For isothermal situations Eq. (26) reduces to a set of ℵ coupled reaction-diffusion-deformation equations (Section 3.4) of the form

$$V_o\mu^K\dot{m}^K = \mathbf{J}^K\cdot\nabla\mu^K + A^K\dot{\xi}^K + \dot{L}^K - V_o\chi^K\boldsymbol{\sigma}:\dot{\boldsymbol{\varepsilon}}^{dissipative} \tag{27}$$

where summation on K is not intended but K takes on the values 1,…,ℵ. χ^K is the proportion of energy dissipated by the deformation partitioned to the Kth reaction.

3.4. Link to reaction-diffusion equations

Reaction-diffusion equations describe the behaviour of many physical, biological and chemical systems and the behaviour of such equations has been intensively studied, especially for chemical systems, over the past 30 years. For an extensive review see Cross and Hohenberg (1993); the subject is developed in detail by Murray (1989). The general form of these equations for a two component homogeneous chemical system is

$$\begin{aligned}\frac{du_1}{dt} &= D_1\frac{\partial^2 u_1}{\partial x^2} + F(u_1,u_2)\\ \frac{du_2}{dt} &= D_2\frac{\partial^2 u_2}{\partial x^2} + G(u_1,u_2)\end{aligned} \tag{28}$$

where u_1 and u_2 are the concentrations of two chemical components, D_1 and D_2 are the diffusion coefficients for these two components, F and G generally are non-linear functions of composition.

If deformation is neglected in Eq. (27) these equations express relations of the form:

[Time rate of change of concentration of chemical component] = [Change in component due to diffusion] + [Rate of formation of component − Rate of consumption of component].

Or, taking the complete Eq. (27), we have

[Time rate of change of concentration of chemical component] = [Change in component due to diffusion] + [Rate of formation of component − Rate of consumption of component] − [Rate of change of component driven by deformation] (29)

The last term in square brackets in Eq. (29) represents processes such as dissolution or precipitation of the relevant chemical component driven by deformation. These processes feature prominently in the models presented by Ortoleva (1994); other approaches are given with examples by Ulm and Coussy (1995) and Coussy and Ulm (1996). Equations such as (29) are characterised by the development of instabilities if the system is driven from equilibrium by processes such as deformation, input of heat or a flux of chemical components. The instabilities commonly express themselves as some form of pattern formation in time, in the form of oscillations in some chemical parameter such as oxidation state, or in space in the form of patterns in chemical parameters. If the instabilities are solely temporal in nature they are called *waves* of which Hopf-instabilities are an example; if they are solely spatial in nature they are called Turing instabilities (Turing, 1952). In practice both forms of instabilities can form and compete with each other to develop a variety of spatial patterns (Turing, 1952; Murray, 1989; Epstein and Pojman, 1998, De Wit et al. 1996). Clearly, Turing instabilities or other forms of spatial patterning of mineral composition (Ortoleva, 1994) would be expressed in deformed metamorphic rocks as some form of metamorphic differentiation and we explore this in greater detail in Sections 4.2–4.5. Early work on this topic was presented by Ortoleva and co-workers (see Ortoleva, 1994 and references therein). The important point to note is that the general equation that results for isothermal situations (Eq. 27) has the same form as the reaction-diffusion-deformation equations. We will see that most of the coupling between processes of interest in structural geology at all scales is described by equations of this form.

We have shown that a combination of the first and second laws of thermodynamics says that the evolution of a quantity u within a deforming reacting body is given in a one dimensional spatial coordinate, x, by an equation of the form

$$\frac{\partial u}{\partial t} = q\frac{\partial^2 u}{\partial x^2} + F(u) \tag{30}$$

where F is commonly a non-linear function of u and q is a parameter with the dimensions of diffusivity. In many instances the evolution of a system requires N coupled equations of the form of Eq. (30) involving different quantities u_1, u_2,….., u_N. Eq. (30) is a standard reaction-diffusion equation that has been widely studied over the past 50 years (Cross and Hohenberg, 1993). A special form of Eq. (30) is the Swift–Hohenberg equation (Cross and Hohenberg, 1993, p. 873):

$$\frac{\partial u}{\partial t} = \frac{\partial^4 u}{\partial x^4} + q\frac{\partial^2 u}{\partial x^2} + F(u) \tag{31}$$

Both Eqs. (30) and (31) appear in various forms as the basis for describing many of the structures we observe in deforming metamorphic rocks. In particular, a stationary form of Eq. (31), that is, where $\frac{\partial u}{\partial t} = 0$, is

$$\frac{\partial^4 u}{\partial x^4} + q\frac{\partial^2 u}{\partial x^2} + F(u) = 0 \tag{32}$$

Solutions to Eq. (32) take on many forms depending on the values of q and the nature of $F(u)$. These solutions can be sinusoidal, localised, structured kinks and pulses, and chaotic; two solutions are illustrated in Fig. 5 (Peletier and Troy, 2001). Some special forms of Eqs. (30) and (32) as discussed later in this paper are:

(i) If $F(u)$ is linear then Eq. (32) reduces to the standard biharmonic equation discussed widely in structural geology (Ramberg, 1961, 1963; Biot, 1965; Ramsay, 1967; Smith, 1977) for the buckling of a strong layer embedded in a weaker material. In this case $F(u)$ expresses the reaction forces exerted by the embedding material on the layer as the layer buckles. The solutions to the biharmonic equation for a linear $F(u)$ are strictly sinusoidal and play a prominent role in the classical Biot theory of folding where u is the displacement of the layer normal to its initial orientation.

(ii) If $F(u)$ is a non-linear softening function then the application of Eq. (32) to the buckling of layered materials results in fold

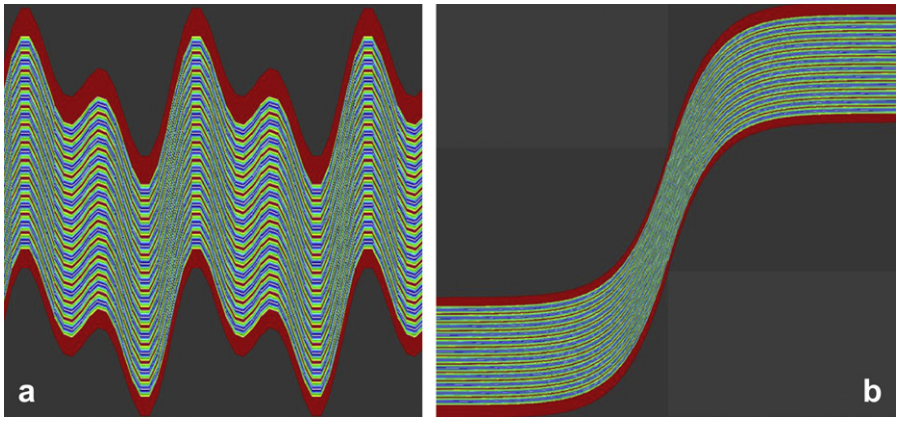

Fig. 5. Two solutions to the Swift–Hohenberg Equation (from solutions reported by Peletier and Troy, 2001). (a) A "multi-bump periodic" solution given by equations of the form $u = \alpha(\frac{\sin\beta_1 x}{\beta_1} + \frac{\sin\beta_2 x}{\beta_2})$ where α, β_1 and β_2 are constants. (b) A localised "kink" solution given by $u = 1 - \exp(-\alpha x)[\cos\beta x - \frac{\beta}{\sqrt{8-\beta^2}}\sin\beta x]$ where α and β are constants. For details of these equations and the values of the constants see Peletier and Troy (2001).

systems more complicated than those arising from the Biot theory. The buckles are now "multi-bumped" but periodic (Fig. 5a), localised (Fig. 5b) and can be chaotic (Whiting and Hunt, 1997). The structures that develop in the embedding material are also localised and represent the development of microlithons and axial plane cleavages.

(iii) If Eq. (30) is thought of as applying to N coupled chemical reactions then chemically unstable behaviour can lead to metamorphic differentiation and/or compositional zoning in growing mineral grains.

(iv) Metamorphic differentiation resulting from Eq. (30) leads to a sinusoidal reaction response of the embedding material on a buckling layer which in turn, through Eq. (32), produces localised folding with the metamorphic layering axial plane to the folds.

Eqs. (30) and (32) have profound implications for structural-metamorphic geology. Understanding the rich assemblage of deformed metamorphic fabrics observed in Nature depends on developing physically realistic and geologically relevant descriptions of q and of $F(u)$. The book by Peletier and Troy (2001) is devoted to a detailed discussion of Eq. (32) and various forms of the solutions developed by those authors are discussed in this paper.

3.5. The scale issue

Many processes that operate during deformation of rocks can be expressed as diffusion equations. Thus diffusion of heat, of chemical components and of fluid pressure is governed by equations of the form: $\frac{\partial c}{\partial t} = \kappa^{process}\frac{\partial^2 c}{\partial x^2}$ involving a diffusivity, $\kappa^{process}$, for the process. c represents temperature, chemical concentration or fluid pressure. If this process is coupled with deformation then the length scale, $l^{process}$, over which feedback is important is given by the standard diffusion relationship (Carslaw and Jaeger, 1959), $l^{process} = \sqrt{\kappa^{process}\tau}$, where τ is a time scale associated with the deformation. We take $\tau = (\dot{\varepsilon})^{-1}$ where $\dot{\varepsilon}$ is the strain-rate; then $l^{process} = \sqrt{\kappa^{process}/\dot{\varepsilon}}$. Values of $l^{process}$ are given in Table 6 which shows that the length scale likely to characterise a particular coupled process varies from kilometres to microns depending on the process and the rate of deformation. For thermal–mechanical coupling at tectonic strain-rates the length scale is the kilometre scale (Regenauer-Lieb and Yuen, 2004; Hobbs et al. 2008). Other scales have been considered in Regenauer-Lieb et al. (2009) and Hobbs et al. (2010a) where it is shown that the same fold mechanism (namely, strain-rate softening) operates at outcrop and thin-section scales as does at regional scales although different physical and chemical processes are involved at the different scales.

As an example consider a shear zone of thickness h. Then the heat dissipated by mechanical processes at a strain-rate $\dot{\varepsilon}$ will be conducted out of the shear zone on a characteristic time scale $\tau = h^2/\kappa^{thermal}$ where $\kappa^{thermal}$ has a value for most rocks of 10^{-6} m^2 s^{-1}. For a shear zone 1 km thick $\tau = 10^{12}$ s whereas for a shear zone 1 m thick $\tau = 10^6$ s (note that 1 year $\cong 3.1536 \times 10^7$ s). If the shear zones deform at a shear strain-rate of 10^{-13} s^{-1} then the time taken to reach 20% shear strain is 2×10^{12} s. Thus the thick shear zone has the potential to heat up whereas the thin shear zone remains isothermal. Note that if other endothermic processes such as endothermic mineral reactions occur within the thick shear zone then any heat generated by deformation may be used to enhance reaction rates and the thick zone may remain close to isothermal. If on the other hand the strain-rate is 10^{-2} s^{-1} (representing a slow seismic event) then both the thick and thin shear zones heat up. Further discussion on this matter is presented by Burg and Gerya (2005) who point out that for a shear strain-rate of 10^{-12} s^{-1} and a shear stress of 10 MPa the resulting dissipation compares in value with radiogenic dissipation in crustal rocks. We consider these aspects in Section 6.

3.6. Overview of Section 3

In Section 3 we have presented the foundations, derived from Biot (1955, 1958) and from Rice (1975), for the remainder of this paper by reviewing the thermodynamic basis for coupling various processes such as deformation, mineral reactions, mass, and fluid and thermal transport. It is perhaps surprising that the evolution of systems not at equilibrium can be discussed in terms of just two functions: (i) a function that defines the energy of the system (usually the Helmholtz energy, Ψ) and (ii) the dissipation function, $\Phi = T\dot{s} \geq 0$, which specifies the rate of entropy production. Having defined these two functions the coupling between processes is governed by the manner in which the total rate of entropy production is partitioned between the processes according to the second law of thermodynamics Eq. (1).

The literature on systems not at equilibrium over the past 80 years has been dominated by attempts to arrive at extremum principles for the rate of entropy production (Onsager, 1931a, b; Prigogine, 1955; Biot, 1954, 1965, 1978; Ziegler, 1963, 1983) but in the past 5 years the situation has been clarified by Ross and co-workers (Ross and Vlad, 2005 and Ross, 2008, Chapter 12) who show that for systems where the thermodynamic flux is a linear function of the thermodynamic forces, an extremum exists for the entropy production rate and this corresponds to a stationary state that is not an equilibrium state. Ziegler (1963) showed that for many plastically deforming systems this stationary state is a maximum. If the relationship between thermodynamic fluxes and forces is non-linear then only one extremum in the entropy production rate exists and that is an equilibrium state. This has the unfortunate repercussion that many of the claims made in the past

Table 6
Length scales associated with various processes when coupled to deformation.

Process	Diffusivity, m^2 s^{-1}	Strain-rate, s^{-1}	Length scale for process, m	Reference
Heat conduction; slow deformations (tectonic deformations)	10^{-6}	10^{-12}	1000	Hobbs et al., 2008
Heat conduction; fast deformations (slow to fast seismic)	10^{-6}	10^{-2} to 10^{2}	10^{-2} to 10^{-4}	Veveakis et al., 2010
Chemical diffusion; slow deformations (tectonic deformations)	Say 10^{-10} to 10^{-16}	10^{-12}	10 to 10^{-2}	Regenauer-Lieb et al., 2009
Chemical diffusion; fast deformations (slow to fast seismic)	Say 10^{-10} to 10^{-16}	10^{-2} to 10^{2}	10^{-4} to 10^{-7}	Veveakis et al., 2010
Fluid diffusion	Depends on permeability	10^{-12} to 10^{-2}	Any value from 10^3 to 10^{-4} depending on permeability	
Chemical reactions	No diffusivity. Coupling depends on chemical dissipation		All scales from 10^3 to 10^{-4}	Hobbs et al., 2009a; Regenauer-Lieb et al. 2009; Veveakis et al. 2010

for processes such as thermal conduction and chemical reactions (and even the origin of life!) are not generally true. For the assumptions made by Biot (1955, 1965, 1978) his proposition of minimum entropy production rate turns out to be identical to Ziegler's principle of maximum entropy production rate; the considerable confusion arises from the manner in which the two "principles" were phrased. For simple plastic systems Ziegler's principle of maximum entropy production rate remains true.

The outcome is that for general systems one needs to track the total entropy production rate and hence recourse has to be made to the Clausius–Duhem relation which is an expression for the total dissipation rate in a coupled system and is in fact simply an expression of the second law of thermodynamics. This is especially true for systems that are characterised by multiple stationary states and non-linear relations between the thermodynamic forces and the thermodynamic fluxes (all chemical and thermal conduction systems). Combining the Clausius–Duhem relation with the first law of thermodynamics results in the Energy Equation which expresses the rate of change of temperature in the system arising from all of the dissipative processes. For most situations the Energy Equation reduces to some form of reaction-diffusion equation or a set of coupled reaction-diffusion equations. The study of these systems is accompanied by an immense literature. Reaction-diffusion equations take on many forms but a particularly relevant form for structural geology is the stationary form of the Swift–Hohenberg Equation which describes all forms of buckling as well as the development of axial plane structures such as microlithons and crenulated metamorphic layering. For many systems of interest to structural geologists the situation is simplified because specific processes dominate the entropy production rate at particular length scales. We explore these length scales in what follows. It turns out that for some important systems the evolution of the system can be considered incrementally as a series of steps that minimise the Helmholtz energy; this approach seems to be fundamental to the development of structures at all scales in deformed rocks and turns out to be the essence of the development of criticality in deforming-reacting systems.

4. The microscale

At the scale of approximately 1 m or less heat arising from any dissipative process will diffuse out of a system of size L on a time scale, τ, given by $\tau = L^2/\kappa^{thermal}$. Taking $L = 1$ m and $\kappa^{thermal} = 10^{-6}$ m^2 s^{-1} we obtain $\tau = 10^6$ s which is small compared to 10^{11} s, the time taken to reach 10% strain at a strain-rate of 10^{-12} s^{-1}. Thus, given these assumptions, a cube of rock 1 m on edge and undergoing finite tectonic deformations can be considered to remain isothermal. This means that the Energy Equation (26) reduces to Eq. (27) and the processes at this scale can now be coupled and considered in terms of reaction-diffusion or reaction-diffusion-deformation equations of the type portrayed in Eqs. (28)–(32).

4.1. Chemical reactions with no coupled diffusion

Many mineral reactions in deformed metamorphic rocks are coupled in the sense that one mineral reaction proceeds in cooperation with others. In other words the product of one reaction acts as the reactant for another reaction. This concept was introduced by Carmichael (1969) and has been explored by many others (Vernon, 2004 and references therein). These coupled reactions are called cyclic reactions by Vernon and are well known in the chemical literature as networked reactions (Clarke, 1976, 1980; Epstein and Pojman, 1998). An example is the reaction:

$$\text{kyanite} \rightarrow \text{sillimanite} \tag{33}$$

which microstructural evidence (Carmichael, 1969) indicates is better represented in many rocks by at least one pair of coupled reactions of the form:

$$\begin{gathered} 4\text{kyanite} + 3\text{quartz} + 2K^+ + 3H_2O \rightarrow 2\text{muscovite} + 2H^+ \\ 2\text{muscovite} + 2H^+ \rightarrow 4\text{sillimanite} + 3\text{quartz} + 2K^+ + 3H_2O \end{gathered} \tag{34}$$

In this set of coupled reactions quartz acts as a catalyst in the sense that it appears in both the products and the reactants and muscovite acts as a catalyst in the sense that it participates in the reactions but does not appear in the final product of the reactions, sillimanite. Carmichael (1969) gives other more complicated forms of such coupled reactions and emphasises the importance of catalysts in metamorphic reactions. If one is solely interested in thermodynamic equilibrium and the construction of mineral phase diagrams, Eq. (33) is all that is needed; if one is interested in the processes that operate during metamorphism then Eq. (33) is irrelevant and Eq. (34) is fundamental. An example of networked reactions from Whitmeyer and Wintsch (2005) is given in Fig. 6.

The opportunity exists in cyclic reactions for competition between production and consumption of a particular chemical component so that its concentration may oscillate in time if the production and consumption occur at different rates. As the equations for cyclic reactions are written by metamorphic petrologists the systems are never autocatalytic (Fisher and Lasaga, 1981; Epstein and Pojman, 1998) with respect to mineral species and so much of the rich variety of behaviour of coupled reactions discussed in the extensive literature on non-linear chemical kinetics is not to be expected from the form of such equations. However if intermediate reactions (especially redox reactions) are written in combination with the standard equations then autocatalytic behaviour appears. Moreover we will see below that heterogeneity in the spatial distribution of reaction sites, and coupling of other processes such as diffusion (Epstein and Pojman, 1998), deformation (Ortoleva, 1989) and fluid flow (Ortoleva et al. 1987; Rusinov and Zhukov, 2000, 2008) can produce instability in otherwise stable coupled chemical systems resulting in a rich variety of spatial and temporal patterning. The definitive treatment for chemical systems both with and without coupled diffusion is by Murray (1989) but see also Epstein and Pojman (1998). The systematics behind the behaviour of such systems is important for a variety of processes (Sections 4.9, 6.3) other than chemical reactions and so a brief review is given below. One should consult the above two books for details.

Consider a set of cyclic reactions involving two chemical components of interest, A and B, and where the rate equations of the form of Eq. (28) may be written

$$F = \frac{dA}{dt} = F(A,B);\ G = \frac{dB}{dt} = G(A,B) \tag{35}$$

and for the moment we have neglected the diffusion terms. In Eq. (35) A and B are written as the concentrations of A and B. The units of concentration depend on the problem to be studied and because of the diverse mathematical treatments reported in the literature no firm rules can be laid down. The units are suitable to the problem being considered and can be dimensionless (volume% or mass%), mass per volume or moles per volume; these concentrations may be in the solid or in an inter-granular fluid. The behaviour of this system of cyclic reactions is best understood by plotting the stationary states for the reactions in (A–B) compositional concentration space (Fig. 7a and b). This means we plot the curves for $F = \frac{dA}{dt} = 0$ and $G = \frac{dB}{dt} = 0$. Such curves represent all values of the

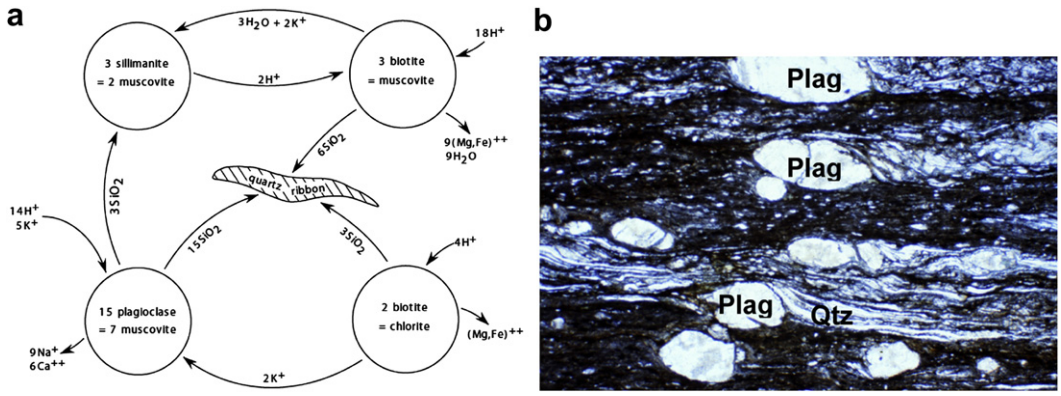

Fig. 6. Cyclic reactions (from Whitmeyer and Wintsch, 2005). (a) Quartz, biotite and muscovite act as catalysts. (b) Quartz ribbons produced by networked reactions in (a). Details of specimen are in Whitmeyer and Wintsch (2005).

stationary (non-equilibrium) states and are called null-clines. In Fig. 7(a) the F null-cline is plotted where we have assumed that F is a cubic. We see that for a specific concentration B^* there are three possible stationary values of A. The stability of a particular stationary state can be seen by plotting arrows that indicate the direction the relevant concentration will evolve if displaced from the stationary state. In Fig. 7(a) points above the null-cline represent conditions where $F = \frac{dA}{dt} < 0$ (that is, the reaction that produces A at constant B moves the concentration of A to smaller values) whereas points below represent conditions where $F = \frac{dA}{dt} > 0$ (that is, the reaction that produces A at constant B moves the concentration of A to larger values). Thus the arrows in Fig. 7(a) indicate the ways in which the concentration of A will move if displaced from the stationary state by a perturbation in concentration. If $\frac{\partial F}{\partial A} < 0$ then the stationary state is stable and if $\frac{\partial F}{\partial A} > 0$ then the stationary state is unstable. These conditions are derived by Murray (1989) and Epstein and Pojman (1998). In Fig. 7(b) the G null-cline is plotted. The behaviour of the system is governed by the ways in which the two null-clines intersect and by the magnitude of the non-stationary perturbation that is introduced. In Fig. 7(c) a small displacement from the point P will cause the system to oscillate as shown however a large displacement from P would cause the system to evolve to one of the stable states where $\frac{\partial F}{\partial A} < 0$. In Fig. 7(d) a perturbation that moves the system to the point B means that the system undergoes large oscillations in time. The oscillations are sustained in time so long as the system is maintained far from steady state. In Fig. 7(e and f) a small displacement from O to L causes the system to spiral in to a steady state whereas a large displacement from O to B causes the system to move to a new steady state or to undergo a large amplitude migration back to the initial steady state depending on the relations between the F and G null-clines.

We define

$$F_1 = \left(\frac{\partial F}{\partial A}\right)_o ; F_2 = \left(\frac{\partial F}{\partial B}\right)_o ; G_1 = \left(\frac{\partial G}{\partial A}\right)_o ; G_2 = \left(\frac{\partial G}{\partial B}\right)_o \quad (36)$$

and

$$J = \begin{bmatrix} \frac{\partial F}{\partial A} & \frac{\partial F}{\partial B} \\ \frac{\partial G}{\partial A} & \frac{\partial G}{\partial B} \end{bmatrix}_o = \begin{bmatrix} F_1 & F_2 \\ G_1 & G_2 \end{bmatrix} \quad (37)$$

The subscript o indicates that the quantity is evaluated at a stationary state when $F = 0$ and $G = 0$. That is, the derivatives are calculated at $A(x,t) = A_o \neq 0$ and $B(x,t) = B_o \neq 0$. The trace and determinant of J are written

$$Tr = F_1 + G_2 \quad \text{and} \quad \Delta = F_1 G_2 - F_2 G_1 \quad (38)$$

The stability of the set of coupled equations is now determined by the values that Tr and Δ take along with another quantity we will call $\Gamma = (Tr(J))^2 - 4\Delta$. Details of the calculations involved are given by Murray (1989) and Epstein and Pojman (1998) and the results are given in Table 7 taken from Hobbs and Ord (2010a).

As an example, let us consider one of the simplest expressions of homogeneous coupled reactions that can exhibit instability. The rate equations are linear and given by:

$$F = \frac{dA}{dt} = aA - bB \quad \text{and} \quad G = \frac{dB}{dt} = cA - dB \quad (39)$$

where a, b, c, d are rate constants. We then have $F_1 = a$; $F_2 = -b$; $G_1 = c$; $G_2 = -d$ so that $Tr = a - d$; $\Delta = bc - ad$ and $\Gamma = (a+d)^2 - 4bc$. We see from Table 7 that the following stability states arise if $bc > ad$; that is if $\Delta > 0$. The system is stable if $d > a$, but in the stable mode can exhibit a stable node if $4bc < (a+d)^2$ or a stable focus if $4bc > (a+d)^2$. If $d < a$ then the system is unstable and exhibits an unstable focus if $4bc < (a+d)^2$ or an unstable node if $4bc > (a+d)^2$. On the other hand, if $bc < ad$ then the system exhibits a saddle point. If $a = d$ and $bc > ad$ a Hopf bifurcation arises. This very simple system is capable of exhibiting all of the temporal instabilities that are possible in such coupled systems. It has an additional point of interest in that if diffusion is added to the processes involved then the system is capable of exhibiting spatial instabilities (Turing patterns) if $d > a$. An important characteristic of the system with respect to the development of spatial instabilities is that F_1 has the opposite sign to G_2 (Epstein and Pojman, 1998).

In simple systems these kinds of behaviour are relatively easy to explore (Murray, 1989; Cross and Hohenberg, 1993; Epstein and Pojman, 1998) but in highly non-linear reactions, such as are common in metamorphic rocks, the details of such instabilities may be impossible to establish. By highly non-linear here we mean that F and G in (35) are highly non-linear functions. An important theorem in this regard is the Poincare–Bendixson theorem (Andronov et al., 1966; Strogatz, 1994; Epstein and Pojman, 1998) which states that if a two component system is confined to a finite region of concentration space then it must ultimately reach either a steady state or oscillate periodically. Thus if one can demonstrate instability then periodic oscillations of the system must exist although it may prove impossible to define these explicitly. Clearly compositional zoning can form by these oscillatory processes as suggested by Ortoleva (1994) and we explore this topic in Section 4.8.

Carmichael (1969) presents highly non-linear coupled reactions where one such reaction is:

$$43\text{albite} + 7K^+ + 18(\text{Mg, Fe})^{++} + 7H_2O \rightleftharpoons 17\text{sillimanite} + 6\text{biotite} + \text{muscovite} + 91\text{quartz} + 43Na^+$$

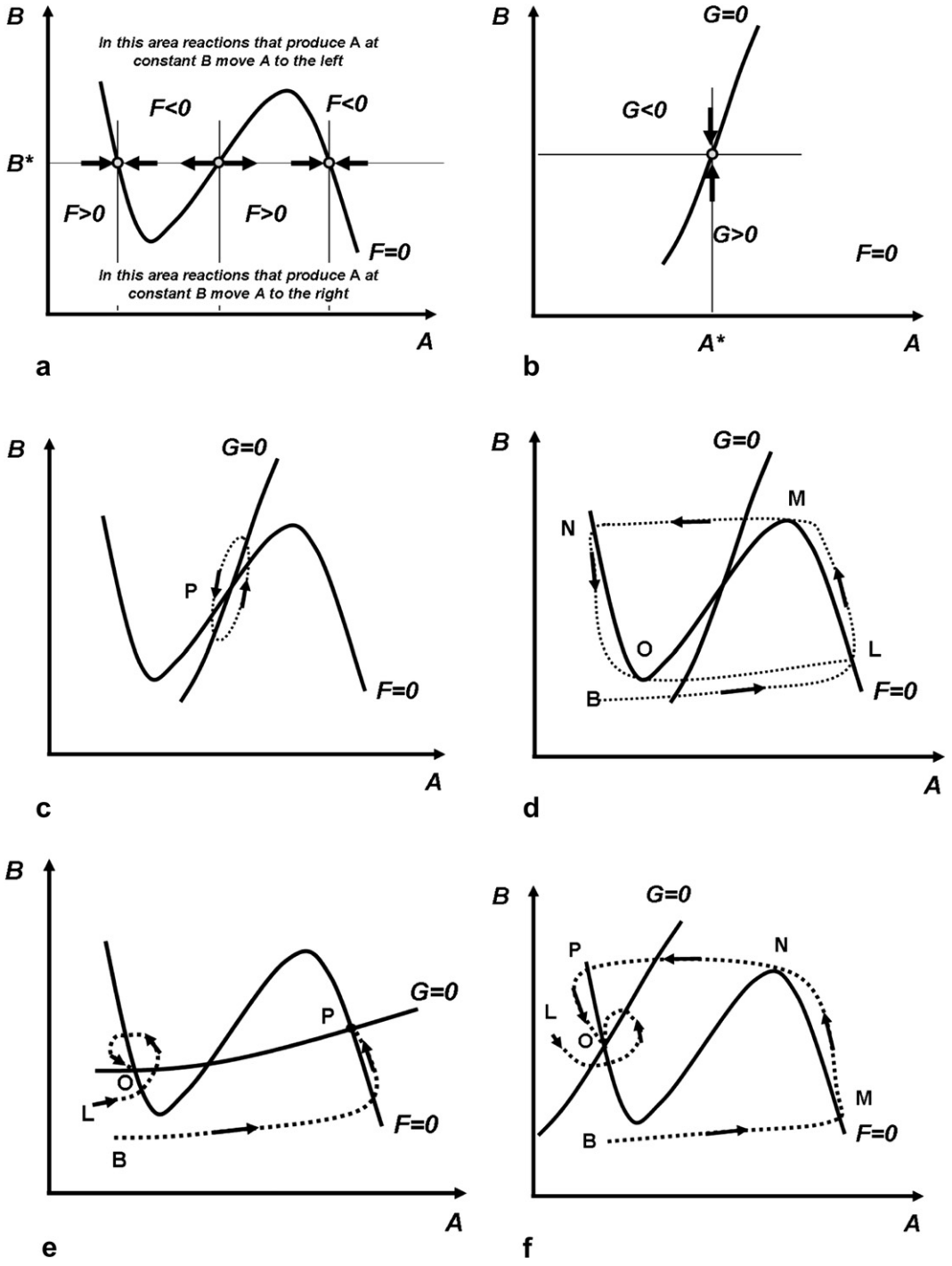

Fig. 7. Stable and unstable oscillatory behaviour of systems in (*A*, *B*) composition concentration space depending on the relation between null-clines and the size of the perturbation from steady state. (a) The *F* null-cline. Notice that above the *F* null-cline reactions that produce A at constant *B* move the concentration of A to the left whereas below the *F* null-cline reactions that produce A at constant *B* move the concentration of A to the right. (b) The *G* null-cline. (c) Intersection of *F* and *G* null-clines. A small perturbation away from the intersection P causes the system to oscillate about P. (d) A perturbation of the system to the point B causes large oscillations in composition. (e) A perturbation to L causes the system to spiral back to the stationary state O. A perturbation to B causes the system to move to a new stationary state P. (f) A perturbation to B results in the system moving to the stationary state O but through a large compositional loop.

In these reactions it will probably prove quite difficult to define the conditions for stability or instability (especially with respect to redox and pH states) due to the algebraic opacity of the relations involved and for such highly non-linear systems a number of theoretical and graphical approaches has been developed. An excellent summary of these methods is given in Epstein and Pojman (1998, Chapter 5). In particular, the network methods developed by Clarke (1976, 1980) deserve special consideration. Recent developments are discussed by Schreibner and Ross (2003).

The behaviour of two component systems such as given in Eq. (35) may thus be of the following types:

Table 7
Stability criteria for two component coupled chemical reactions (From Hobbs and Ord, 2010a).

Tr(J)	Δ	Γ	Behaviour	Phase Diagram
<0	>0	>0	Stable node	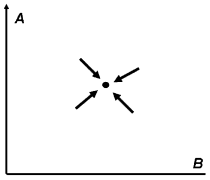
<0	>0	<0	Stable focus	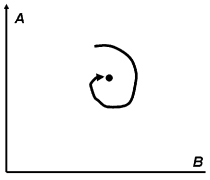
>0	>0	<0	Unstable focus	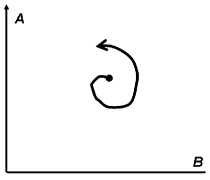
>0	>0	>0	Unstable node	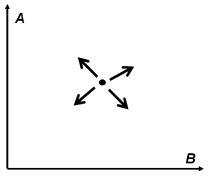
	<0		Saddle point	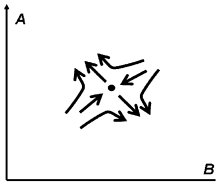
=0	>0		Hopf bifurcation	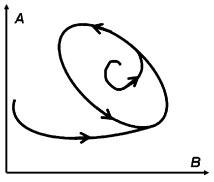

(i) *Stable behaviour* expressed as either a stable node or a stable focus (Table 7). This seems to be the behaviour of many cyclic metamorphic reactions. If these systems also involve diffusion of A and B then the system is defined in terms of reaction-diffusion equations (such as those given in Eq. 28). Then, subject to other conditions considered in Section 4.2, stationary spatial patterns known as Turing instabilities can form spontaneously in an otherwise homogeneous material.
(ii) *Unstable behaviour* expressed as an unstable focus, an unstable node, a saddle point or a Hopf bifurcation (Table 7). The closed ellipse in the phase portrait of a Hopf bifurcation in Table 7 is known as a limit cycle.

4.2. Reactions with coupled diffusion: metamorphic differentiation

Up until now we have considered equations of the form Eq. (35) where no diffusion is coupled to the mineral reactions. If diffusion is included as in Eqs. (27)–(29) then the possibility of spatial instabilities arises. Of particular interest in structural geology is the development of metamorphic differentiation which is a compositional patterning developed in an initially homogeneous lithology. This is expressed as a differentiated slaty cleavage, a schistosity or gneissosity, developed with or without close association with crenulation cleavage, or as a mineral lineation, or as a combination of both. By *mineral lineation* we mean elongate domainal structures composed of high concentrations of a single mineral and do not mean lineations defined by preferred orientations of inequant mineral grains. One way in which such structures could form would be as Turing instabilities (Turing, 1952). Such instabilities consist of the spontaneous development of spatial compositional patterns in an otherwise homogeneous material and can comprise spot-like, linear or planar patterns or combinations of all three. The five conditions for a Turing instability to form in a two-fold coupled mineral reaction system, together with the wave-number, k^{Turing}, that ultimately develops in an infinite domain are given by (Murray, 1989; Epstein and Pojman, 1998):

$$\begin{aligned}
&\text{(i)} \quad Tr = F_1 + G_2 < 0;\\
&\text{(ii)} \quad \Delta = F_1G_2 - F_2G_1 > 0;\\
&\text{(iii)} \quad F_1 \text{ is opposite in sign to } G_2;\\
&\text{(iv)} \quad \tfrac{D_A}{D_B} > 1 \ \textit{for}\ F_1 < 0;\\
&\text{(v)} \quad D_BF_1 + D_AG_2 > 2\left[D_AD_B(F_1G_2 - F_2G_1)\right]^{\frac{1}{2}} > 0
\end{aligned} \tag{40}$$

The resulting wave-number is

$$k^{Turing} = \left(\frac{2\pi}{\lambda^{Turing}}\right) = \left(\frac{F_1G_2 - F_2G_1}{D_A/D_B}\right)^{\frac{1}{4}} \tag{41}$$

Thus important criteria for a Turing instability to form are that the system be stable in the absence of diffusion, that one diffusion coefficient be much larger than the other and that F_1 be of opposite sign to G_2. We have seen that the simple set of linear networked reactions defined by Eq. (39) is capable of fulfilling these conditions. One can show that *Tr* for the cyclic reactions as written by Carmichael (1969) and by Wintsch et al. (2005) and Whitmeyer and Wintsch (2005) are negative (stable) and that F_1 for these reactions has the same sign as G_2. Thus spatial patterning is not possible in these systems as they are expressed and without additional coupling. An important additional requirement for such reactions is that one diffusion coefficient is much smaller than the other and this is the normal assumption in metamorphism (Carmichael, 1969) where the diffusion of aluminium is taken to be much slower than other elements such as Si, Na and so on.

4.3. Examples involving redox reactions

4.3.1. Autocatalytic reactions

Networked chemical reactions that involve changes in redox state are particularly susceptible to instabilities (Epstein and Pojman, 1998). One reason for this seems to lie in that many redox reactions can be expressed in an autocatalytic manner. Thus the oxidation of Fe^{2+} can be written:

$$Fe^{2+} + 2Fe^{3+} \rightarrow 3Fe^{3+} + \text{electron}^- \tag{42}$$

We take an example where a mineral, A, reacts to produce another mineral, B, A → B and in the process A dissolves in an intergranular fluid to contribute Fe^{2+} to that fluid. An example could be biotite reacting to produce garnet. A set of networked reactions that describes the redox part of the reaction is:

$$\text{Reaction of A to produce } Fe^{2+}: \quad A \xrightarrow{k_1'} Fe^{2+} \tag{43a}$$

$$\text{Non}-\text{catalytic step}: \quad Fe^{2+} \xrightarrow{k_2'} Fe^{3+} \tag{43b}$$

$$\text{Autocatalytic step}: \quad Fe^{2+} + 2Fe^{3+} \xrightarrow{k_3'} 3Fe^{3+} \tag{43c}$$

$$\text{Production of B from } Fe^{3+}: \quad Fe^{3+} \xrightarrow{k_4'} B \tag{43d}$$

where the k_i' are the reaction rates for the four reactions.

The set of equations that describes the coupling between these reactions is:

$$\begin{aligned} \tfrac{\partial A}{\partial t} &= -k_1 A \\ \frac{\partial \left[Fe^{2+}\right]}{\partial t} &= k_1 A - k_2\left[Fe^{2+}\right] - k_3\left[Fe^{2+}\right]\left[Fe^{3+}\right]^2 \\ \frac{\partial \left[Fe^{3+}\right]}{\partial t} &= k_2\left[Fe^{2+}\right] + k_3\left[Fe^{2+}\right]\left[Fe^{3+}\right]^2 - k_4\left[Fe^{3+}\right] \\ \tfrac{\partial B}{\partial t} &= k_4\left[Fe^{3+}\right] \end{aligned} \tag{44}$$

where the square brackets denote the concentration of the relevant redox species and the k_i are functions of the k_i' and of the concentrations of any other components that may be involved in the reactants. Solutions to these equations are shown in Fig. 8(a–c) where the system oscillates in time with respect to the concentration of Fe^{2+} and Fe^{3+} in solution with the resulting compositional zonal sequence within a growing grain illustrated in Fig. 8 (c,d).

4.3.2. A second example with redox changes

Fisher and Lasaga (1981) consider a classical networked reaction (the Brusselator) described in the context of redox reactions by the coupled reaction-diffusion equations:

$$\begin{aligned} \frac{d\left[Fe^{3+}\right]}{dt} &= D_A \frac{\partial^2\left[Fe^{3+}\right]}{\partial x^2} + \alpha + \left[Fe^{3+}\right]^2\left[Fe^{2+}\right] - (\beta+1)\left[Fe^{3+}\right] \\ \frac{d\left[Fe^{2+}\right]}{dt} &= D_B \frac{\partial^2\left[Fe^{2+}\right]}{\partial x^2} + \beta\left[Fe^{3+}\right] - \left[Fe^{3+}\right]^2\left[Fe^{2+}\right] \end{aligned} \tag{45}$$

Here the $[Fe^{3+}]^2[Fe^{2+}]$ term arises from autocatalytic reactions of the form Eq. (43c) and so could be relevant in many networked metamorphic reactions. In fact the reactions described by Eq. (45) are similar to Eq. (43) except that both the reactant and the product in Eq. (45) involve Fe^{3+} (Epstein and Pojman, 1998, p. 39). The networked series of reactions which result in the net reaction A → E with intermediaries B and D are:

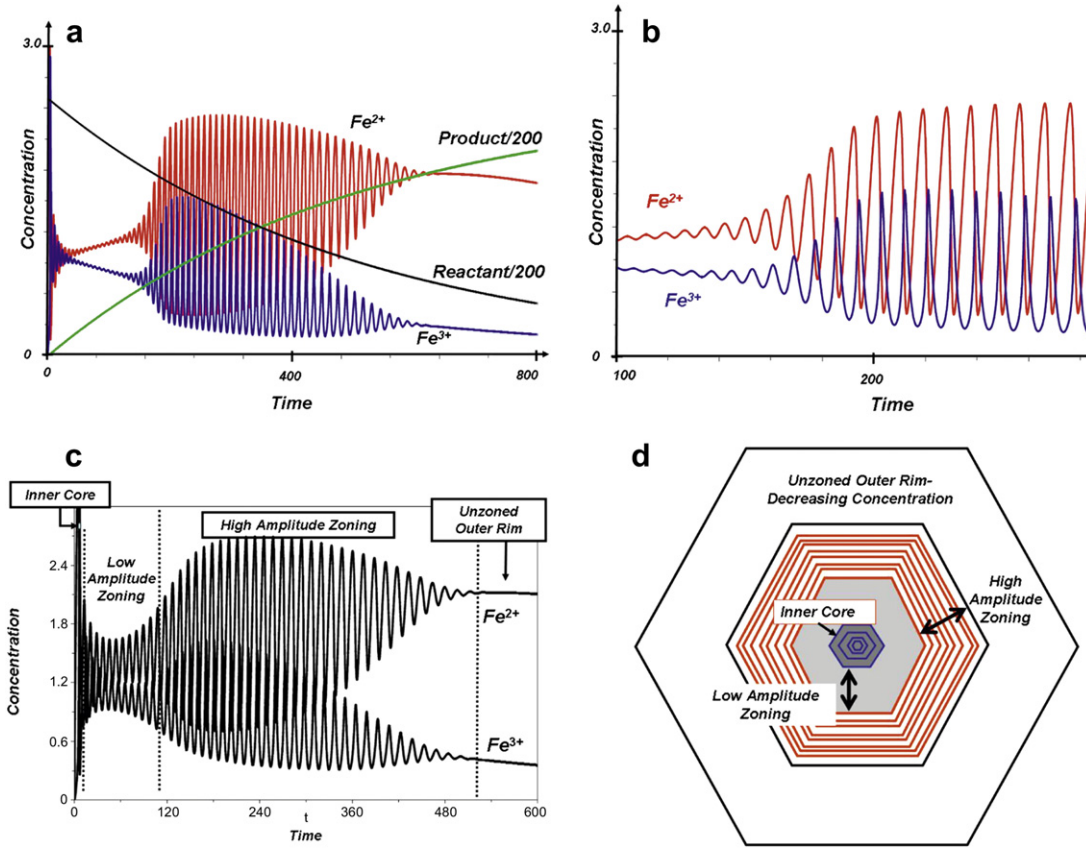

Fig. 8. Behaviour of the autocatalytic reaction (43). (a) Concentrations of Fe^{2+}, Fe^{3+}, the reactant A and the product B with dimensionless time. Notice that the concentrations of A and B have been divided by 200. Equilibrium conditions do not develop until a dimensionless time of about 3000. (b) Zoom into part of (a) showing detail. The parameters from Eq. (44) are $k_1 = 0.002$, $k_2 = 0.08$, $k_3 = 1.0$, $k_4 = 1.0$ so that the dissolution of A is much slower than the formation of B. (c) The behaviour of Eq. (43) but with A dissolving faster than in (a). $k_1 = 0.05$, $k_2 = 0.08$, $k_3 = 1.0$, $k_4 = 1.0$. Regions are marked that correspond to compositional zonal patterns that would develop in growing porphyroblasts illustrated in (d). For details of the calculations involved see Boyce and DiPrima (2005). (After Ord and Hobbs, 2011).

$$\text{Reaction of A to produce } Fe^{3+}: \quad A \xrightarrow{k_1'} Fe^{3+}$$

$$\text{Non}-\text{catalytic step involving B and D}: \quad B + Fe^{3+} \xrightarrow{k_2'} Fe^{2+} + D$$

$$\text{Autocatalytic step}: \quad Fe^{2+} + 2Fe^{3+} \xrightarrow{k_3'} 3Fe^{3+} \qquad (46)$$

$$\text{Production of E from } Fe^{3+}: \quad Fe^{3+} \xrightarrow{k_4'} E$$

The reader is referred to Fisher and Lasaga (1981) who treat this system in detail. In particular they derive the conditions under which compositional differentiation will arise and the expression for the rate of growth of such layering from an initial compositional distribution that consists of small perturbations, $g(x)$, above a background steady state composition, c_o, defined by a Fourier series:

$$g(x) = c_o + \sum_{n=1}^{N} a_n \sin\left(\frac{n\pi x}{L}\right) \qquad (47)$$

In Eq. (47) L is some length scale associated with the system and a_n is the initial compositional fluctuation, around a background composition c_o, associated with the nth wave-number. The spatial evolution of the composition, c, of the system with time is given by

$$c(x,t) = c_o + \sum_{n=1}^{N} a_n \sin\left(\frac{n\pi x}{L}\right) \exp(w_n t) \qquad (48)$$

where w_n is the amplification of the nth mode and is discussed by Fisher and Lasaga (1981). The two dimensional evolution of a system described by Eq. (48) using values of w_n derived by Fisher and Lasaga (1981) is shown in Fig. 9(a,b). Fig. 9(c) shows the result of growing the spatial pattern in Fig. 9(b) during a homogeneous shortening normal to the layering. The material has been treated as a Maxwell solid with shortening of 80%.

The system of equations in (45) is also capable of undergoing oscillations in time so that as the system passes across the condition $Tr = 0$ the system passes from one characterised by the Turing instabilities shown in Fig. 9(b) through a Hopf bifurcation to one characterised by oscillations in time as shown in Fig. 9(d). The oscillations in this case comprise a series of bursts and would produce the spiked zonal patterns observed in the concentrations of Ca and Mg in some garnets (Chernoff and Carlson, 1997).

4.4. Reaction-diffusion processes with deformation and heterogeneity

There are ways however, other than the classical Turing instability, in which metamorphic differentiation may develop. Most of the vast literature on instability in networked chemical systems involves homogeneous systems. Ortoleva and Ross (1973, 1974) consider systems where heterogeneities exist. Such systems are of fundamental importance in metamorphic systems where heterogeneities comprised of localised reaction sites, localised dissipation arising from heterogeneous deformation and gradients in chemical potential are hallmarks of the processes that operate. Eq. (28) is replaced by equations of the form

$$\begin{aligned} \frac{du_1}{dt} &= D_1 \frac{\partial^2 u_1}{\partial x^2} + F(u_1,u_2) + \varepsilon_1 E(x,u_1,u_2) \\ \frac{du_2}{dt} &= D_2 \frac{\partial^2 u_2}{\partial x^2} + G(u_1,u_2) + \varepsilon_2 H(x,u_1,u_2) \end{aligned} \qquad (49)$$

where now F and G are non-linear functions of composition representing homogeneous reactions and E and H are non-linear

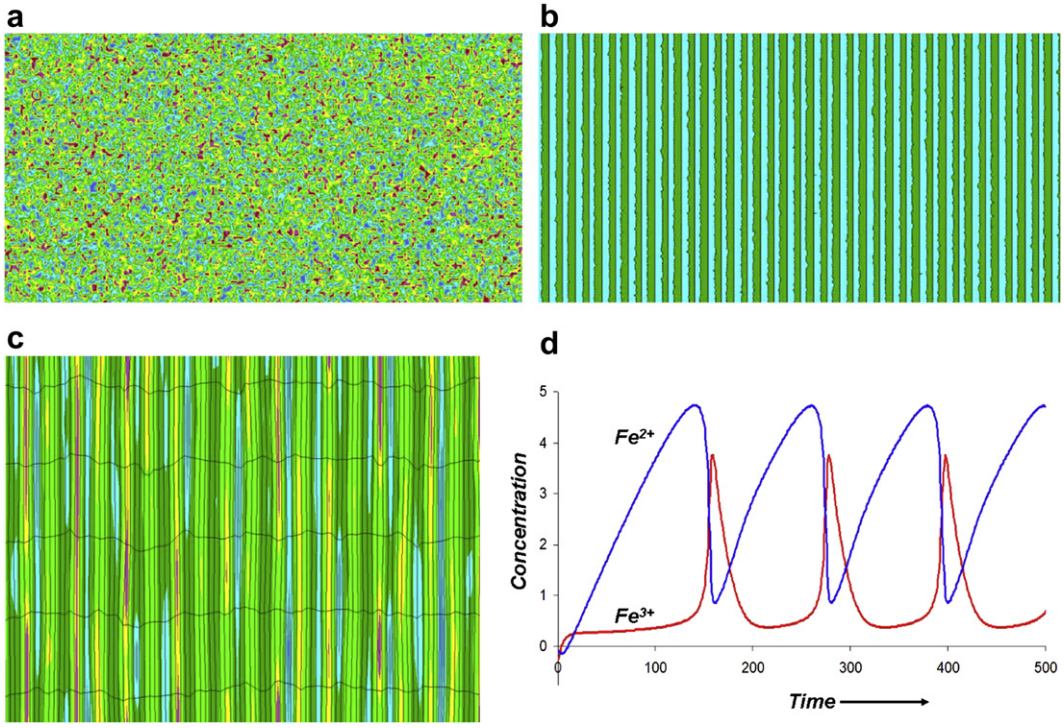

Fig. 9. The behaviour of the Fisher and Lasaga (1981) Brusselator system as expressed by Eqs. (45) and (46). (a) Initial random spatial distribution of Fe^{2+} and Fe^{3+}. The colours represent fluctuations of 10^{-2} about an initial background of Fe^{2+} concentration; red high, blue low. (b) Spatial distribution of Fe^{2+} (light green high Fe^{2+}) and Fe^{3+} after dimensionless time = 1.0 for the conditions, parameters and dimensionless units proposed by Fisher and Lasaga (1981). (c) Effect of growing the spatial instability in (b) during horizontal shortening of 80%. The horizontal lines are passive markers. Such a structure could represent many differentiated slaty cleavages. (d) The behaviour of the Fisher and Lasaga (1981) Brusselator system for $\alpha = 2$, $\beta = 4$, $D_A = D_B = 0$ in Eq. (45). In this case the material remains homogeneous spatially but oscillates in time.

functions of composition and of space arising from heterogeneities in reaction sites and/or deformation or from gradients in chemical potential; ε_1, ε_2 measure the magnitude of the effect of E and H. Ortoleva and Ross (1974) show that a wide range of unstable behaviour can arise from Eq. (49) including oscillating reactions but also travelling compositional waves including spirals. In particular spatially static compositional differentiation patterns can develop even in systems where the diffusion coefficients, D_1 and D_2, are equal. The approach of Ortoleva and Ross (1973, 1974) for heterogeneous systems means that even if one can demonstrate that a metamorphic networked reaction system is stable (that is, $Tr < 0$), then the presence of heterogeneities will almost certainly induce some form of instability so that compositionally zoned metamorphic grains and some form of compositional differentiation should be common-place in metamorphic rocks as of course they are.

This work is the basis for a series of papers by Ortoleva and co-workers (Dewars and Ortoleva, 1990, and Ortoleva et al., 1982, 1987a, b). In particular, Ortoleva et al. (1982) show that even the simple uncoupled reactions:

$$A \rightarrow X$$

$$B \rightarrow Y$$

can become unstable and produce spatial patterns when coupled with deformation effects that influence the concentration of X and Y.

As an example, the simple quartz–muscovite system has been analysed in terms of equations of the form of Eq. (35). Consider the networked set of reactions given by:

$$\begin{aligned} \text{Quartz} &\rightleftharpoons SiO_2 \textit{ in solution} \\ \text{Muscovite} &\rightleftharpoons 3\text{Quartz} + K^+ + H_2O + AlO^{3-} \end{aligned}$$

One can readily confirm (Hobbs and Ord, 2010a) that for such a network Tr is always negative so the system is always stable but F_1 always has the same sign as G_2 and hence a classical Turing instability can never form. Ortoleva and co-workers have shown that this system can develop spatial differentiation by a number of mechanisms but each mechanism ultimately depends on the approach taken in Ortoleva and Ross (1974). Dewars and Ortoleva (1989) develop a model whereby the mineral reactions are coupled to deformation via dependence of the chemical potential of each mineral phase upon the mineral composition of its surroundings; this is referred to as a texture dependent chemical potential. The dependence arises because for a given imposed far field stress, the mean stress on a grain is dependent upon the strength of the surrounding material. Thus a grain of quartz will have a larger mean stress imposed upon it if it is surrounded by quartz-rich material (strong) rather than mica-rich material (weak). The dependence of the chemical potential of a stressed solid on the mean stress (Kamb, 1959, 1961) then results in a texture dependent chemical potential. The dissolution or growth of the grain is expressed as a stress dependent function of the chemical potential. There is a positive feedback between the texture dependent chemical potential and the texture so that gradients in this chemical potential not only drive migration of material but reinforce further dissolution of stressed grains in domains rich in strong minerals or growth (precipitation) of the same mineral grains where surrounded by weaker minerals (see Fig. 10 where the feedback arrows are particularly important). An important additional component of such models is that the growth of grains is also dependent on the texture and/or the stress via relations of the form

$$\frac{\partial r_u}{\partial t} = F(u,v) - G(\boldsymbol{\Theta}, \boldsymbol{\sigma})$$

where r_u is the radius of a grain composed of the chemical phase, u, $F(u,v)$ is a function that expresses the kinetics of formation of u in competition with v, G is a function of the texture, $\boldsymbol{\Theta}$, and the stress $\boldsymbol{\sigma}$ as discussed by Ortoleva (1994). This equation says that the increase in the radius of a grain is governed by the rate at which u is produced minus the rate at which texture and stress influence growth rate. Thus the model illustrated in Fig. 10 becomes a classical diffusion-reaction-deformation model Eq. (29) where there is a continuous competition between texture/stress driven dissolution and diffusion and texture/stress driven grain growth (represented by the feedback arrows in Fig. 10). Ortoleva (1994, Fig. 11-2) illustrates that for critical parameters such a system can develop spatial patterning.

All of the processes discussed in the Ortoleva model result in metamorphic differentiation at the grain scale so that the differentiation documented by Whitmeyer and Wintsch (2005) and by Wintsch et al. (2005) are at the scale expected of the Ortoleva type of process. An additional but related process for developing metamorphic differentiation arises through the reaction-diffusion-deformation equations expressed by Eqs. (27) and (29). Examples are given in Hobbs and Ord (2010a). Although the processes discussed by Ortoleva and co-workers represent a specific form of Eqs. (27) and (29), these equations are more general and point to the development of metamorphic differentiation at the scale of heterogeneities in the deformation but still presumably limited by the scale of the transport mechanisms involved. Thus the classical metamorphic differentiation associated with crenulation cleavages (Fig. 11) would seem to be an example of this more general coupling but presumably in an open system where quartz can leave the system (see Hobbs and Ord, 2010a).

The coupling of deformation to reaction-diffusion equations leads to relationships (Hobbs and Ord, 2010a) that are of the same form as the Ortoleva–Ross equations (49) for a heterogeneous reacting system. The physical significance of this coupling can be seen from Fig. 12 that shows how a stable reacting system can become unstable due to relative displacement of null-clines by compositional dependent dissipation.

4.5. Reaction processes with coupled fluid flow

The coupling of fluid flow to networked chemical reaction systems can induce instability in the system in exactly the same manner as does coupling mass diffusion and has been explored by Ortoleva et al. (1987a,b) and by Rusinov and Zhukov (2000, 2008) who write a set of equations that couple chemical reactions to fluid flow in the form of reaction-transport equations:

$$\frac{\partial\left(\varphi c_i^{fluid} + c_i^{solid}\right)}{\partial t} = \frac{\partial J_i}{\partial x} + F_i\left(c^K\right) \tag{50}$$

where φ is the porosity, c_i^{fluid} and c_i^{solid} are the dimensionless concentrations (volume% or mass%) of the component i in the fluid and rock respectively, x is a spatial coordinate and F_i is a function of the dimensionless concentrations of all the K chemical components, c^K, and expresses the kinetics of the ith reaction. J_i is the flux of the ith component and is given by

$$J_i = j c_i^{fluid} - D_i\left(\frac{\partial c_i^{fluid}}{\partial x}\right) \tag{51}$$

and so includes components arising from both infiltration due to the fluid flux, j, and diffusion arising from the diffusivity, D_i. Eqs.

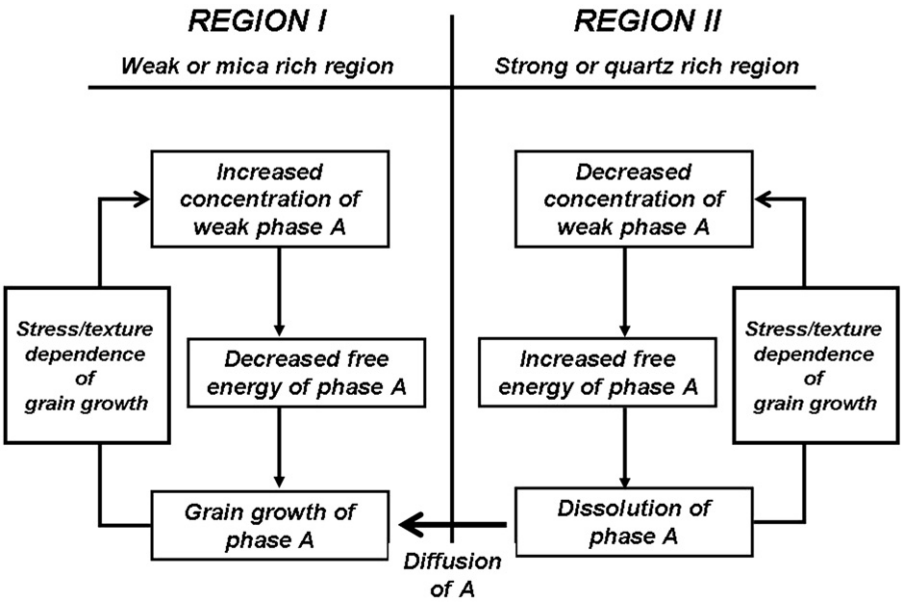

Fig. 10. The positive reinforcement of grain growth and dissolution of a weak grain A, embedded in a mixture of A and B where B is strong. The reinforcement arises from a texture dependent chemical potential in a deforming material (After Ortoleva et al. 1987a). Also portrayed is a texture or stress dependence of the dissolution/precipitation rates. Without this dependence the system moves towards homogenisation. Ortoleva et al. (1987a) and Ortoleva (1994) shows that there are regions of a phase space defined by the competition between diffusion and the texture/stress dependent growth rates that enable metamorphic differentiation to grow.

(50) and (51) combined have the same form as the reaction-diffusion equations (28).

Rusinov et al. (1994) and Rusinov and Zhukov (2000, 2008) consider reactions, involving wollastonite and hedenbergite, which they write in a form that involves the autocatalytic oxidation–reduction step

$$Fe^{2+} + 2Fe^{3+} \rightleftharpoons 3Fe^{3+} + \text{electron}^{-} \tag{52}$$

This system with coupling to fluid flow is unstable and produces a limit cycle for the concentrations of Fe^{2+} and Fe^{3+} in solution and an associated spatial patterning of wollastonite and hedenbergite as shown in Fig. 13. A similar study involving redox reactions is that of Ortoleva et al. (1986).

If the complete reaction-infiltration coupled problem is solved then the system becomes unstable in time and space and a number of compositional travelling wave structures develop. The nature of these instabilities is shown in Fig. 14 and corresponds to a travelling front in Fig. 14(a and b), oscillating but decaying travelling waves in Fig. 14(c and d) and a limit cycle representing sustained oscillations in Fig. 14(e and f). These instabilities only develop for an infiltration velocity that is below a critical value set by the reaction kinetics (Rusinov and Zhukov, 2008) and so would not develop in rocks of high permeability. The observation that such infiltration instabilities only develop for small infiltration velocities opens the possibility that such instabilities may be important in many metamorphic rocks where the permeability is presumably always small but infiltration, or at least local transport, of H_2O is commonly postulated (Wintsch et al. 2005).

The possibility of coupling to other species in solution involving multivalent elements such as manganese, titanium and so on is suggested by Rusinov et al. (1994) through relations of the form

$$Fe^{2+} + Mn^{3+} \rightleftarrows Fe^{3+} + Mn^{2+} \tag{53}$$

which implies that the concentrations of Mn^{2+} and Mn^{3+} can vary in the same manner as Fe^{2+} and Fe^{3+} shown in Figs. 8, 9, 13 and 14. This becomes an important consideration when one considers metamorphic compositional zoning. Rusinov et al. (2006) and Rusinov and Zhukov (2008) also show that fractal and multifractal

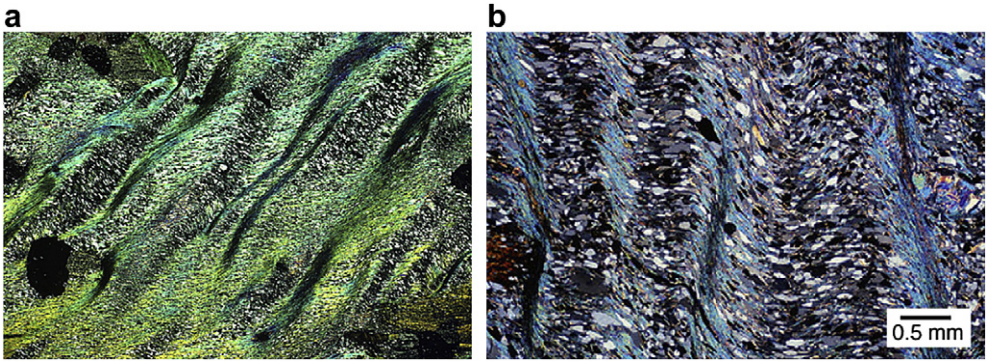

Fig. 11. Metamorphic differentiation in quartz–muscovite schists associated with the development of crenulation cleavages (photomicrographs from Ron Vernon; Picuris Range, New Mexico, USA). The scale is identical in both images. These kinds of structures presumably involve open systems where SiO_2 can be removed from the system.

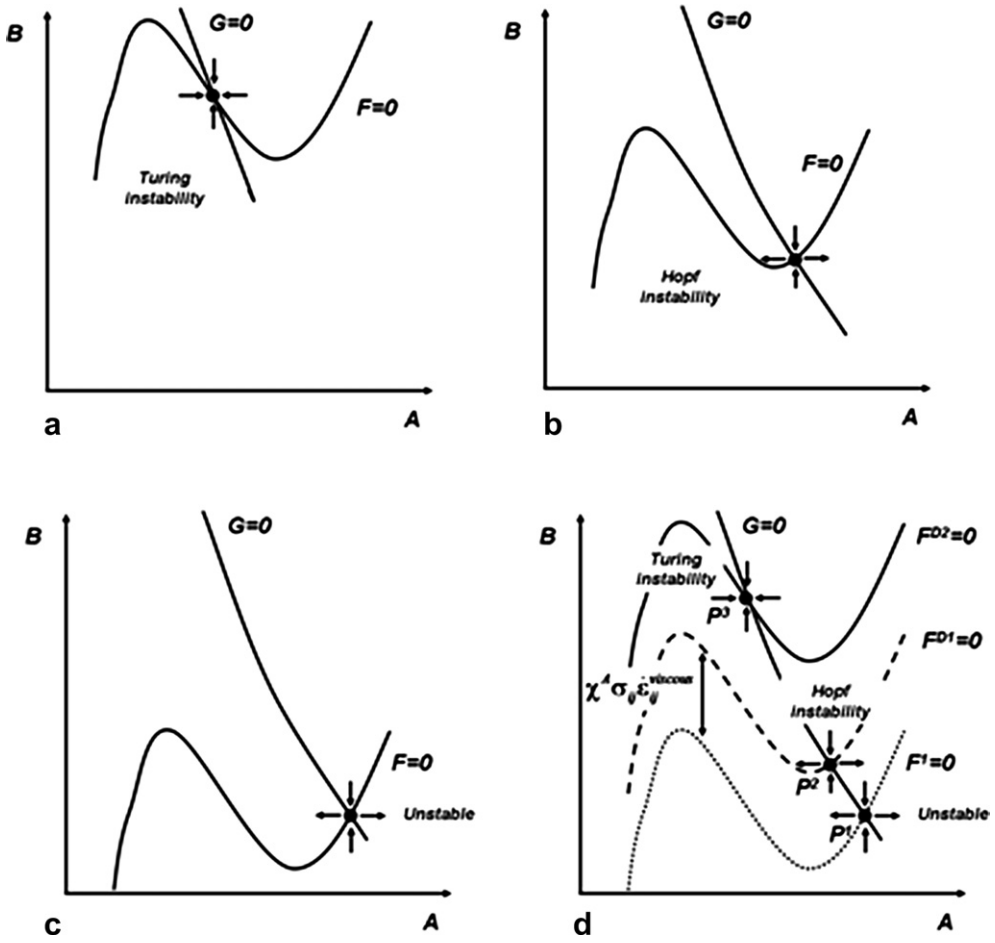

Fig. 12. (A–B) compositional phase space showing progression of system behaviour with progressive changes in a dissipative process that effects reaction rates. In this diagram the effect on the reaction rate that produces A (the F null-cline) is large compared to the effect on B (the G null-cline). (a) Intersection of the F and G null-clines results in temporal stable behaviour but such that Turing instabilities are possible. (b) The dissipative process has moved the F null-cline relative to the G null-cline such that now a Hopf bifurcation occurs. (c) Further relative movement of the two null-clines results in oscillatory temporal behaviour. (d) Summary of a system where the proportion of total mechanical dissipation partitioned to the production of A, $\chi^A \sigma_{ij} \dot{\varepsilon}_{ij}^{dissipative}$, moves the F null-cline relative to the G null-cline from an intersection at P^1 (unstable in time) to P^2 (Hopf bifurcation) to P^3 (Turing instability).

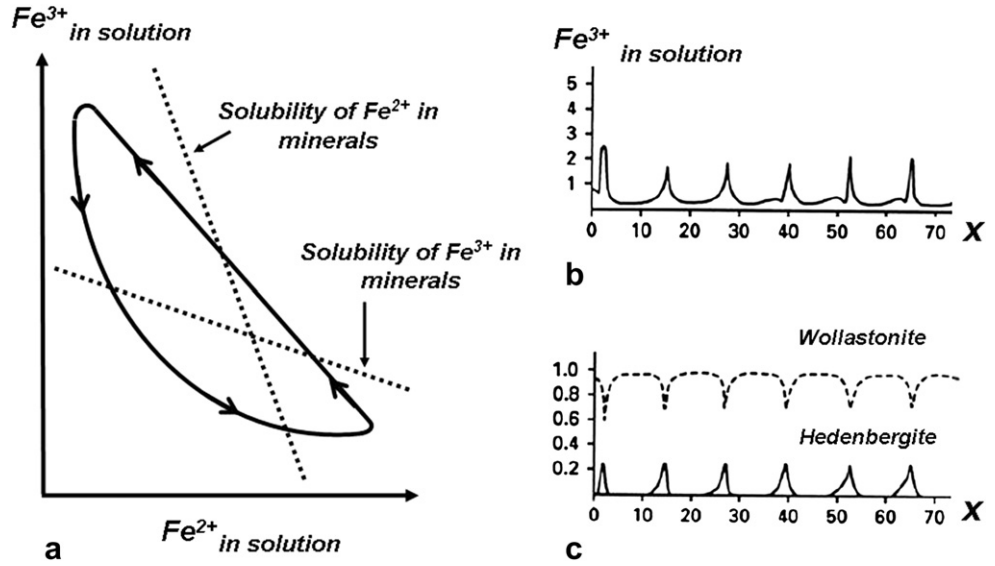

Fig. 13. Instabilities in the wollastonite-hedengergite system. (a) Limit cycle for Fe^{2+} and Fe^{3+} in solution. (b) The limit cycle of (a) as a function of dimensionless distance, x. (c) The precipitation of hedenbergite in a matrix of wollastonite as a function of dimensionless distance. After Rusinov and Zhukov (2000). The dimensionless distance x is defined by Rusinov and Zhukov (2000).

fabrics can develop through coupling reactive-diffusion-infiltration processes and propose that whether the fabric is fractal or multi-fractal may be diagnostic of whether infiltration dominates over diffusive processes.

4.6. The relationship of microfabric elements to strain and deformation-rate

A common assertion is that fold axes form normal to a principal axis of strain and that the axial planes of folds are parallel to a principal plane of strain. This assertion is not supported by analytical models of fold development. An analytical finite amplitude analysis of fold development in 3 dimensions is given by Mühlhaus et al. (1998) who show that for a general coaxial deformation history the factor that governs the orientation of the fold axis is the deformation-rate tensor. The dispersion function that relates the growth rate of a particular wave-number (Fig. 15) has a strong and sharp maximum in the plane parallel to the axis of maximum deformation-rate, D_1. The growth rate decreases rapidly away from this sharp maximum in all directions although there is a weaker, broader maximum parallel to D_2. The wave vector corresponding to the sharp maximum is parallel to the principal axis of deformation-rate, D_1.

This relationship holds also for non-coaxial deformation histories so that as a general statement one expects fold axes to initiate normal to a principal axis of deformation-rate and not of strain. Moreover the analysis of Mühlhaus et al. (1998) is also true for thick plates so that these results show that the axial planes of folds form

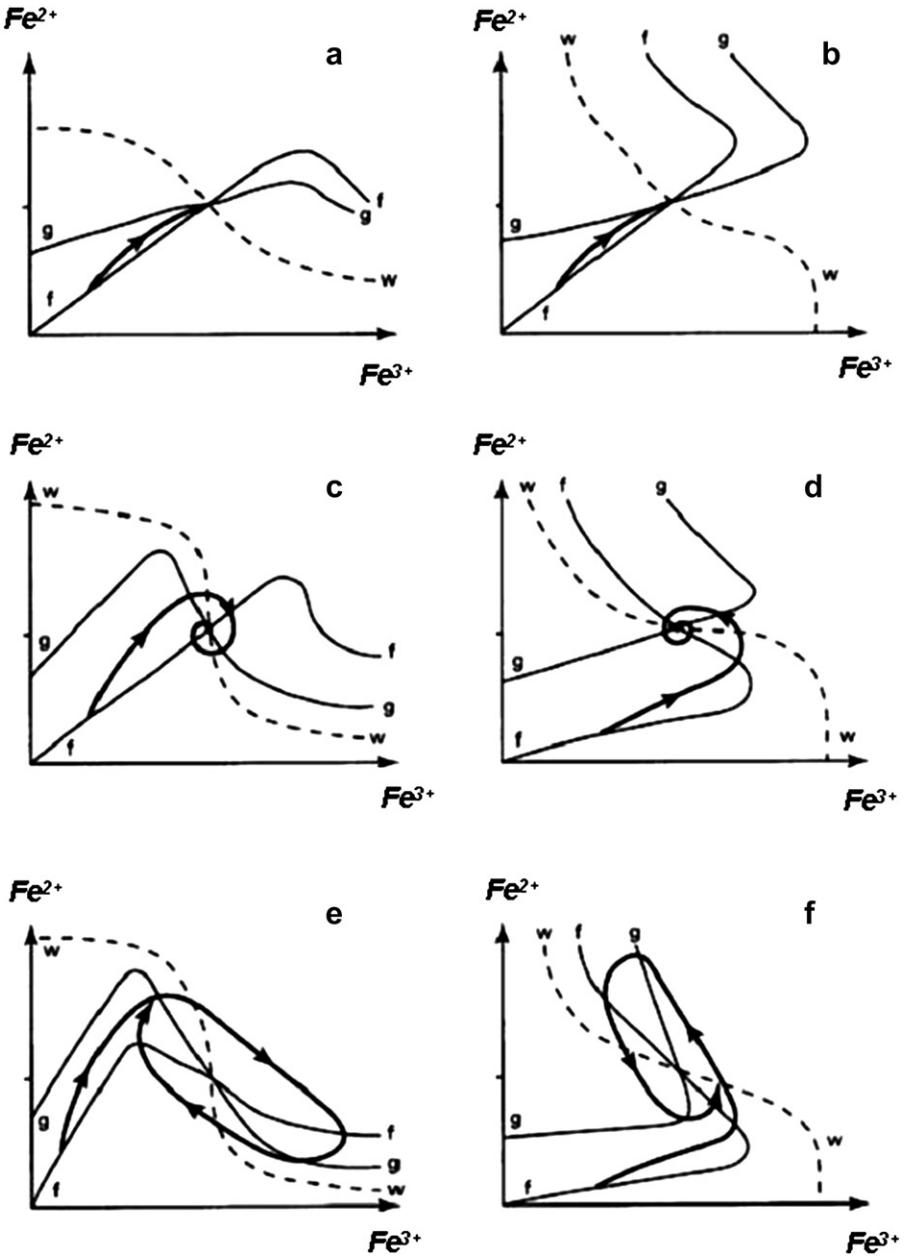

Fig. 14. Phase portraits for Fe^{2+} and Fe^{3+} in solution for various combinations of null-clines. *f*, *g* and *w* are the null-clines for a reduced component in the system, under the conditions: *redox kinetics only* for *f*, *redox kinetics combined with mass exchange kinetics between solution and solid* for *g*, and *mass exchange kinetics between solution and solid only* for *w*. (a) and (b): A stable focus corresponding to a single travelling front in solution. (c) and (d): Stable focus corresponding to a travelling wave in solution with decreasing amplitudes of oscillations. (e) and (f): An unstable focus evolving into a limit cycle corresponding to a travelling front with sustained oscillations. After Rusinov and Zhukov (2000).

parallel to a principal plane of deformation-rate. Such a conclusion also follows from the small deformation analysis of Johnson and Fletcher (1994a, b) corresponding to the initiation of folding. This of course is at odds with the widely acclaimed doctrine (Ramsay, 1967) that proposes the axial plane of folds to be a principal plane of strain. For a coaxial strain-history the principal planes of strain and of deformation-rate remain coincident so that the Ramsay proposition is true but for a non-coaxial deformation history this is no longer true. For instance, in a simple shearing deformation history the principal planes of deformation-rate remain fixed at 45° to the shearing plane whilst the principal planes of strain rotate towards the shearing plane (Fig. 16).

In a general argument, Ortoleva et al. (1982) show that the metamorphic layering produced by the model shown in Fig. 10 forms normal to a principal axis of stress. We commonly assume that the constitutive relations pertinent to deformed rocks are coaxial (that is, the stress tensor always remains parallel to the deformation-rate tensor). Thus a common form of Eq. (8) is

$$\boldsymbol{\sigma} = \mathcal{A}\,\boldsymbol{D}\left(\frac{J_2}{J_2^0}\right)^{\left(\frac{1-N}{2N}\right)}\exp\left(\frac{Q}{RT}\right) \tag{54}$$

where for rocks, N is a number between 1 and about 8, $\mathcal{A}$ is a material constant with dimensions of viscosity, Q is an activation enthalpy and R is the gas constant. J_2 is the second invariant of the stretching tensor and J_2^0 is this same quantity in a reference state. Eq. (54) says that the principal axes of stress remain parallel to the principal axes of deformation rate throughout the deformation history.

The argument of Ortoleva et al. (1982) means that metamorphic layering forms parallel to a principal plane of deformation-rate and not a principal plane of strain. Thus we interpret these results to mean that the metamorphic layering that commonly develops parallel to the axial planes of folds at the microscale is parallel to a principal plane of deformation-rate. This statement would also be true for slaty cleavage formed by differentiation at the microscale.

Eq. (27) also shows that the general influence of deformation on the metamorphic differentiation process is controlled by the $\sigma_{ij}\dot{\epsilon}_{ij}$

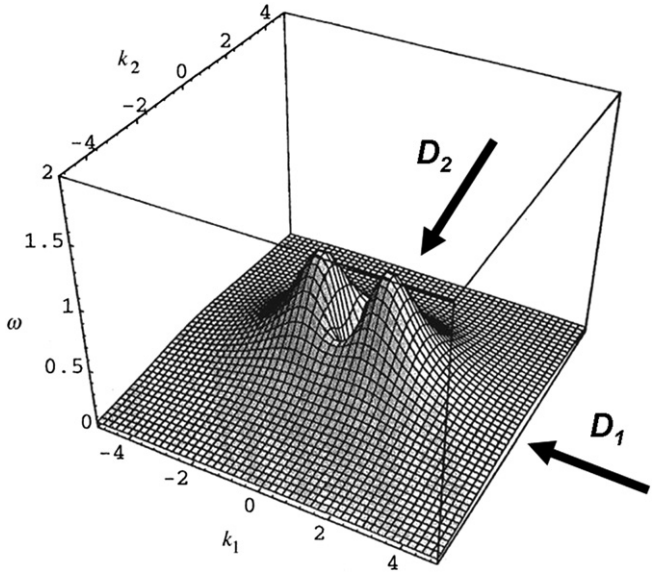

Fig. 15. Analytical dispersion relation linking growth rate, ω, to the wave-number $k_i = \frac{2\pi}{\lambda_i}$ for a plane straining history of single layer folding with the maximum principal deformation-rate D_1. Materials are Newtonian viscous (after Mühlhaus et al., 1998). The sharp maxima correspond to a wave vector parallel to D_1 and the smaller maxima correspond to a broader distribution of wavelengths with variable wavelength and with a wave vector parallel to D_2.

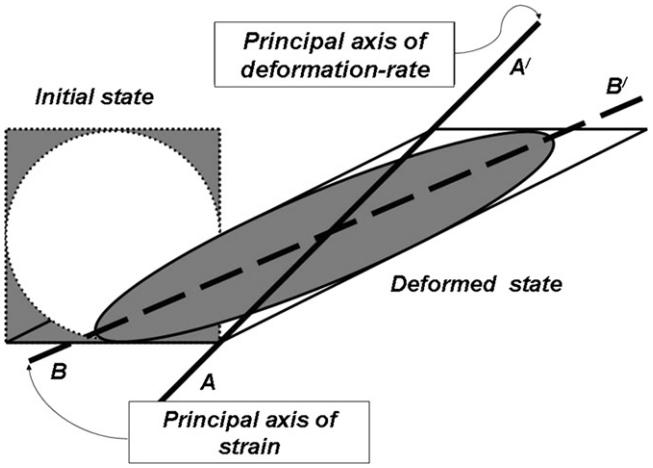

Fig. 16. Relationship of the principal axis of deformation-rate to the principal axis of strain in a simple shearing deformation history.

term. Thus the geometrical aspects of the fabric that forms reflect the symmetry of the ellipsoid representing the deformation-rate tensor. If the stretching history is a plane stretching, for instance, then planar differentiation will develop with the plane of differentiation parallel to a principal plane of deformation-rate (or equivalently, stress). If the stretching history is a simple progressive elongation then the fabric that develops is a mineral lineation parallel to a principal axis of deformation-rate. The differentiation illustrated in Fig. 17 is interpreted as forming parallel to a principal plane of deformation-rate and (for a non-coaxial deformation history) at an angle to a principal plane of strain so that shear displacements parallel to the metamorphic layering are permissible as part of the overall kinematics as illustrated by shear displacements of the bedding in the central part of Fig. 17. We emphasise that only for a coaxial deformation history do these fabric elements form parallel to a principal plane or axis of strain. However such a relationship is incidental; the control on the orientation and geometrical character of the fabric element is the deformation-rate tensor no matter if the deformation history is coaxial or non-coaxial. This is of course exactly what Sander (1911) said: *The symmetry of the fabric reflects the symmetry of the movement picture (kinematics)*. This issue is revisited in Sections 5.3 and 5.4.

The above discussion does not preclude some foliations (or lineations) forming parallel to a principal plane (or axis) of strain by distortion of initial more or less equant objects such as clasts, mineral grains or compositional heterogeneities. This form of fabric element tracks the symmetry of the strain ellipsoid precisely but it is fundamental that a distinction be made between fabric elements that form in response to thermodynamic coupling through the deformation-rate tensor and those that are simply a distortion of other fabric elements in the strain field. Of course one expects both types of fabric elements to form synchronously in suitable rocks although traditional interpretations of such occurrences might commonly be mistaken as overprinting relations.

4.7. Minimal surfaces

In the following the term *interface* applies to the boundary between domains of different mineral composition in a deformed rock whereas the term *surface* means a mathematical entity that is parallel to an interface or is defined solely by some mathematical expression.

Mecke (1996, 1997), De Wit et al. (1992, 1997), Leppanen et al. (2004), Alber et al. (2005) and Glimm and Hentschel (2008) have

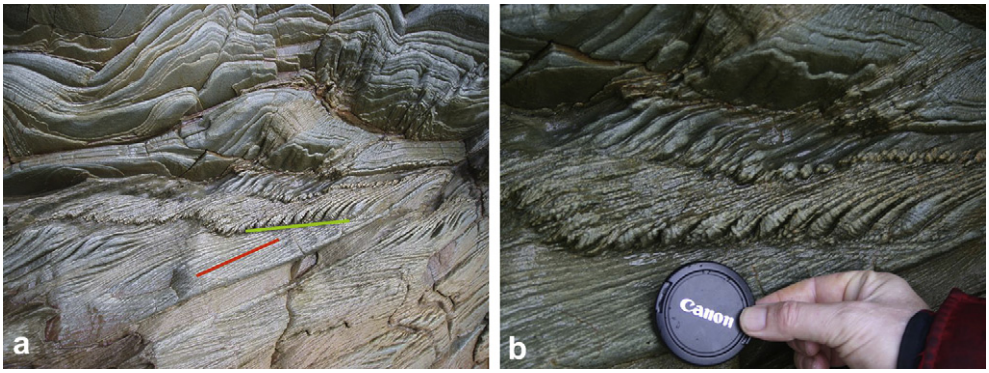

Fig. 17. Differentiated layering (red line) at Rhoscolyn. Anglesey, Wales, UK. Note (b) the shear displacements on the differentiated foliation clearly marked by displacements of bedding (green in a) in the central part of the figure. In outcrop it is observed that this differentiated layering is slightly oblique to the fold axis.

pointed out that the spatial segregation of phases resulting from Turing instabilities forms interfaces separating the segregations that approximate minimal surfaces, a minimal surface being one where the mean curvature is zero. The mean curvature, H with dimensions [per unit length], at any point is defined as $H = 0.5(\frac{1}{r_1} + \frac{1}{r_2})$ where $\frac{1}{r_1}$ and $\frac{1}{r_2}$ are the principal curvatures of the surface at that point (Lopez-Barron and Macosko, 2009). In addition, the types of interfaces that develop for reaction-diffusion equations are saddle shaped or hyperbolic and are characterised by values of the Gaussian curvature K, with dimensions [per unit length^2], that are less than zero (hyperbolic) or zero (planar). K is given by $K = \frac{1}{r_1 r_2}$. H and K are useful in discriminating between various types of surfaces (Table 8). Aksimentiev et al. (2002) and Lopez-Barron and Macosko (2009) show that during the annealing of immiscible polymer blends the microstructures can evolve in both self-similar and non self-similar manners and that the evolution along various paths is represented in the shapes and standard deviations of plots of the mean and Gaussian curvatures. Paths towards minimum energy configurations are characterised by decreases in the standard deviations of both H and K, and a transition in the mean value of K ranging from zero to a distribution with skewness towards negative values indicating a transition to a dominance of hyperbolic or saddle shaped topologies.

In metamorphic rocks quartz-rich and mica-rich domains commonly interweave in the system whilst individual grains of other phases such as garnet and feldspar are embedded in this topology. An interweaved set of interfaces separates these domains; in S-tectonites these are flattened lozenges whilst in L-tectonites these domains are strongly elongate and perhaps approximate flat elongate ellipsoids. A typical example of such domainal structure is the “millipede” structure of Bell (1981) in three dimensions. Reaction-diffusion theory proposes that the topology of this interweaved network is or evolves towards that of a minimal surface.

The outcome of the analysis in Sections 4.1–4.5 is that spatial patterning is to be expected in most if not all deforming-reacting mineral systems leading to a variety of forms of metamorphic differentiation such as layering in gneisses, mineral lineations and differentiated crenulation cleavages (Hobbs and Ord, 2010a).

As part of this argument a number of authors including in particular De Wit et al. (1997), Leppanen et al. (2004), Alber et al. (2005) and Glimm and Hentschel (2008) have pointed out that the iso-concentration interfaces produced by reaction-diffusion equations are minimal surfaces or close to minimal surfaces. In particular, Alber et al. (2005) and Glimm and Hentschel (2008) have shown that the types of minimal surfaces (or surfaces close to minimal) that develop from reaction-diffusion equations are represented parametrically by

$$u = s_1 \cos x + s_2 \cos y + s_3 \cos z \tag{55}$$

where u is a parameter; different values of u result in different surfaces. These surfaces are not strictly minimal surfaces but

Table 8
Mean and Gaussian curvatures for various regular surfaces.

Surface	Mean Curvature, m^{-1}	Gaussian Curvature, m^{-2}
 Sphere, radius 1m	+1	+1
 Circular cylinder, radius 1m	+0.5	0
 Plane	0	0
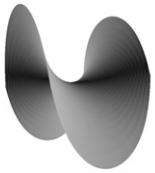 Scherk surface, principal curvatures $\pm 1 m^{-1}$	0	−1

approximate minimal surfaces. Alber et al. (2005) show that there are three possible cases:

(i) $s_1 \neq 0$, $s_2 = s_3 = 0$ representing sheet or lamellae structures which would be represented in rocks as foliation planes,
(ii) $|s_1| = |s_2| \neq 0$, $s_3 = 0$ representing cylindrical-like structures which would be represented in rocks as mineral lineations and,
(iii) $|s_1| = |s_2| = |s_3| \neq 0$ representing undulating surfaces that can encompass a sphere or "nodule" which would be represented in rocks as foliation surfaces encompassing porphyroblasts or lozenge shaped regions such as lithons. The surface $s_1\cos x + s_2\cos y + s_3\cos z = 1$ is shown in Fig. 18(a) together with histograms of the mean, (b), and Gaussian, (c), curvatures across the surface. The case $s_1\cos x + s_2\cos y + s_3\cos z = u$ is very close to a Schwarz P-surface which is a triply periodic minimal surface (Aksimentiev et al. 2002) although only part of the surface is shown in Fig. 18(a); for the complete P-surface see Aksimentiev et al. (2002). These types of structures are common in polymers (Aksimentiev et al. 2002; Lopez-Barron and Macosko, 2009).

Glimm and Hentschel (2008) show that curved interfaces such as that shown in Fig. 18(a) represent conditions for maximum diffusive flux normal to the surface if there are gradients in the chemical field (that is, gradients in the rates of production defined by the functions F and G in Eq. 32) and are surfaces of maximum diffusive flux if the chemical field is constant. Gabrielli (2009) shows that minimal surfaces represent conditions for minimising stress concentrations in a loaded aggregate. Thus if the metamorphically differentiated foliations and/or lineations that evolve as interfaces between quartz and biotite concentrations in a quartz–biotite schist develop as instabilities arising from reaction-diffusion-deformation reactions then one expects these interfaces to define or approximate minimal surfaces. To date there has been relatively little study of such interfaces in metamorphic rocks but examples perhaps are the 3D images generated in anatexite by Brown et al. (1999) and in a garnet–staurolite schist by Ketcham and Carlson (2001). The opportunity exists to analyse the microstructures in metamorphic rocks using the concepts developed by the above workers and by Aksimentiev et al. (2002). Fig. 18(d) shows one of the sets of interfaces described by Bell and Bruce (2006, 2007) for the shapes of foliation surfaces in porphyroblastic schists while Fig. 18(e,f) show histograms of the mean and Gaussian curvatures for that surface (Hobbs and Ord, 2010a). The Bell and Bruce interface is similar to the surface shown in Fig. 18(a) that results from reaction-diffusion equations and is also similar to the computer-simulated interfaces that arise in the lamellar phase of surfactant systems (Holyst, 2005). The observations that, for the Bell and Bruce interface, the mean value of H is zero, the standard deviation of H is less than that for the theoretical surfaces of Glimm and Hentschel (2008) and K is negative supports the suggestion that the Bell and Bruce interface is part of an evolution towards a minimal surface. Demonstration of the widespread existence of interfaces defining foliations and lineations that approach minimal surfaces would be a good test of the proposition that the microstructures developed in deformed metamorphic rocks form by reaction-diffusion processes.

4.8. Compositional zoning

Ortoleva and Ross (1973, 1974) discuss the development of wave-like instabilities in chemically reacting systems when heterogeneities exist in the distribution of reaction sites. Depending on the nature of the equivalent reactions in a homogeneous situation, a number of types of chemical waves can originate at the individual reaction sites. These include planar waves of concentration, oscillations (increasing, decreasing or constant in amplitude) of concentration and spiral compositional waves. These waves are not material waves and travel with a phase velocity that is invariably different to the transfer of material by diffusion or advection alone and that is a function of the non-linear kinetics of the chemical reactions. This means that in some situations the influence of a wave may be restricted at any instant to a small part of the system whereas in other situations the influence of the wave may extend throughout the system. In particular spiral compositional waves are restricted to the reaction site. A growing grain interface that incorporates chemical components from these waves will preserve a record of the nature of these waves: a dominantly monotonic change in concentration arising from planar waves, oscillatory changes in concentration arising from oscillatory waves and spiral shaped distributions arising from locally developed spiral waves.

A number of different types of compositional zoning within porphyroblasts have been reported in the literature (Fig. 19). A review of observations up until 2004 is presented by Vernon (2004). Three types are: (i) more or less monotonic increases or decreases in the concentration of an element from the inferred site of nucleation of a porphyroblast towards the rim of the grain with some discontinuities in the case of Ca and Mg in particular (Chernoff and Carlson, 1997); (ii) oscillatory zoning superimposed on variable trends in concentration of an element towards the rim (Schumacher et al., 1999; Yang and Rivers, 2002; Meth and Carlson, 2005) and (iii) spiral zoning of the concentration of an element (Yang and Rivers, 2001). Note that in this latter case we are specifically referring to *spiral compositional zoning* and not to the spiral shaped distribution of inclusions common in garnets. In most cases the zoning is interpreted in terms of variations in the flux of nutrients towards the growing porphyroblast either by diffusion or advection in a fluid. The classical interpretation in terms of variations in the supply of nutrients remains if one adopts the Ortoleva and Ross approach but the origin of these variations is now proposed as specifically arising from competition in the production and consumption of nutrients in nearby unstable networked chemical reactions. The spatial scale at which these compositional waves occur is controlled by the phase velocity of the chemical waves and it may therefore be dangerous to base arguments of the scale of equilibration in such situations on chemical diffusivities alone. An example of compositional zoning in a growing porphyroblast is proposed in Fig. 8.

4.9. Dislocation interactions and subgrain-size

4.9.1. Dislocation patterns arising from reaction-diffusion equations

Walgraef and Aifantis (1985a, b, c) and Aifantis (1986) have applied the concepts of pattern formation arising from reaction-diffusion equations to the development of localised deformation patterns. The results of these latter analyses indicate that such localisation should develop both as temporal oscillations in deformation intensity (a Hopf instability) and spatial fluctuations in deformation intensity (a Turing instability). Both of these kinds of instabilities are observed in deforming metals (Aifantis, 1987). The approach is motivated by work on dislocation dynamics (Walgraef and Aifantis, 1985a, b, c; Aifantis, 1986; Pontes et al., 2006; Zbib et al., 1996; Shizawa and Zbib, 1999; Shizawa et al., 2001). Such an approach suggests that dislocation pattern formation results from interactions during deformation between different dislocation populations, a process that tends to localise dislocation densities, and diffusion which tends to homogenise dislocation densities. Patterns develop when a critical stress is reached corresponding to

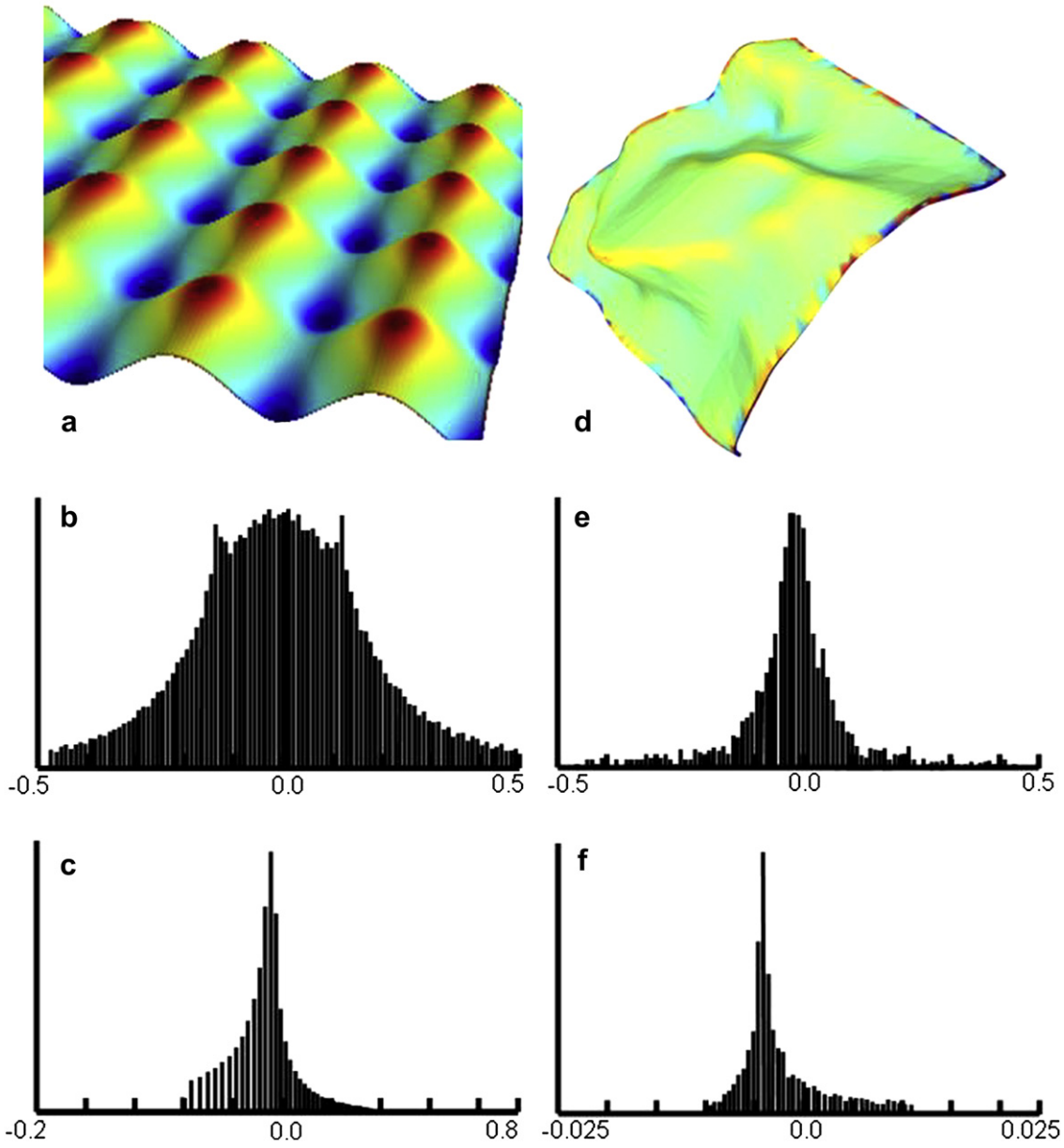

Fig. 18. Surfaces resulting from reaction-diffusion systems and natural interfaces. (a) The surface $u = \cos(x) + \cos(y) + \cos(z)$ predicted as arising from reaction-diffusion equations by Glimm and Hentschel (2008) shaded according to the mean curvature. Red is high positive mean curvature and blue is negative. (b) Histogram of the values of mean curvature for the surface in (a). (c) Histogram of the values of Gaussian curvature for the surface in (a). (d) A Bell and Bruce interface shaded according to mean curvature. Red is high positive mean curvature and blue is negative. (e) Histogram of the values of mean curvature for the surface in (d). (f) Histogram of the values of Gaussian curvature for the surface in (d). Note that many of the values in the tails of the histograms arise from artefacts that we have not removed, at the edges of the surfaces. The vertical scale in the histograms is the number of nodes, normalised to 1, on the triangulated surface that have a given curvature. Images produced using *Meshlab* (MeshLab, Visual Computing Lab – ISTI – CNR, http://meshlab.sourceforge.net/).

a balance between these two competing processes. In the original version of this model (Walgraef and Aifantis, 1985a) two populations of dislocations were considered: mobile and less mobile populations with instantaneous densities ρ_m and ρ_{lm} with units $m^{+1}\ m^{-3}$ The four processes that contribute to the total dislocation density in a one dimensional model are proposed as (Schiller and Walgraef, 1988):

(i) *Dislocation diffusion*: which contributes terms such as $D_k \frac{\partial^2 \rho_k}{\partial x^2}$ to the total rate of change of the density of the kth population where D_k is the diffusion coefficient for the kth population density and x is a spatial coordinate. Note that it is the diffusion of the *density* of the *dislocation population* that is referred to here and not the diffusion of the population itself. As in the models for the development of classical Turing instabilities it is important that the diffusion coefficient of densities of mobile dislocations is much larger than that of less mobile dislocations in order for dislocation patterns to form.

(ii) *Dislocation interaction and pinning:* leading to a non-linear source term in the rate of change of less mobile dislocations and a corresponding sink term in that for mobile dislocations. In the original model the source term is a quadratic, $+\varpi\rho_m\rho_{lm}^2$, where ϖ is the rate for this process with units $m^4\ s^{-1}$. However the important point is that this term is non-linear so more

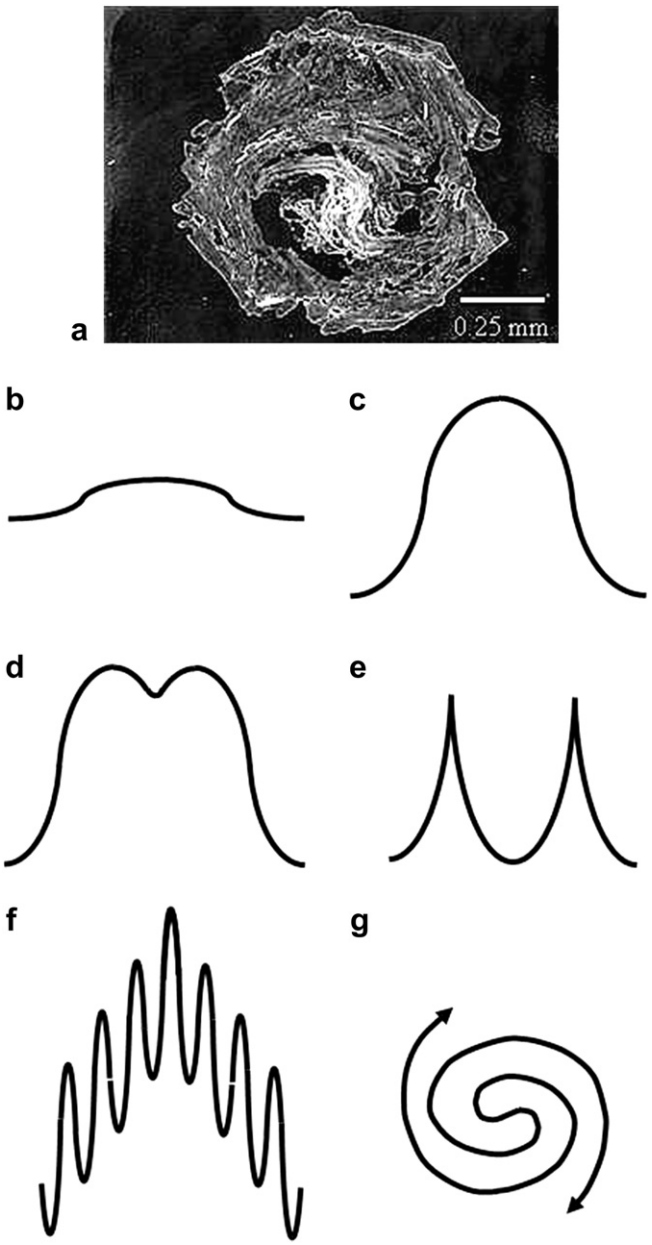

Fig. 19. (a) Back-scattered electron image of a garnet in a metapelite showing spiral compositionally zoned fabric, a white core due to high Y concentration, and small white rectangular inclusions of ilmenite (from Yang and Rivers, 2001). Summary of compositional zoning relationships from Yang and Rivers (2001, 2002). (b) and (c) Monotonic decreases in composition as would arise from the propagation of planar compositional waves. (d) and (e) Patterns that would develop from behaviour in Fig. 9 (d). (f) Oscillatory pattern that would arise from behaviour in Fig. 8. (g) Spiral pattern that would arise from spiral compositional wave of Ortoleva and Ross (1974).

complicated interaction/pinning processes leading to higher order terms lead to the same kinds of results (Schiller and Walgraef, 1988; Pontes et al., 2006).

(iii) *Dislocation generation:* by some mechanism such as Frank-Read sources or the like that adds a rate term $g(\rho_{lm})$ into the balance equation for less mobile dislocations, the assumption being that all newly generated dislocations are immediately pinned.

(iv) *Dislocation liberation:* which adds a source term $b\rho_{lm}$ to the balance equation for mobile dislocations and a corresponding sink term for less mobile dislocations.

The above discussion indicates that the overall evolution of dislocation arrays is described by two coupled reaction-diffusion equations which express the relationships and coupling between diffusion, generation, annihilation and pinning of dislocations:

$$\frac{\partial \rho_{lm}}{\partial t} = D_{lm}\frac{\partial^2 \rho_{lm}}{\partial x^2} + g(\rho_{lm}) - b\rho_{lm} + \varpi\rho_m\rho_{lm}^2 \tag{56}$$

$$\frac{\partial \rho_{m}}{\partial t} = D_{m}\frac{\partial^2 \rho_{m}}{\partial x^2} + b\rho_{lm} - \varpi\rho_m\rho_{lm}^2 \tag{57}$$

This is the set of reaction-diffusion equations introduced by Walgraef and Aifantis (1985a) and has been intensively studied over the past 25 years. One notes that Eqs. (56) and (57) are precisely those of the Fisher and Lasaga (1981) Brusselator reaction discussed in Section 4.3. In particular one can confirm that this coupled set of equations has the following properties (see Eq. (40) which are the conditions for a Turing instability to develop):

- The homogeneous, steady state of the system is defined by

$$g(\rho_{lm}^o) = 0 \text{ and } \rho_m^o = \frac{b}{\varpi\rho_{lm}^o} \tag{58}$$

- Instability represented by temporal oscillations (a Hopf instability) of the dislocation densities occurs when

$$b = b_{Hopf} = a + \varpi(\rho_{lm}^o)^2 \tag{59}$$

where a is the rate of change of the initial density of less mobile dislocations, ρ_{im}^o.

- An instability represented by spatial patterning (a Turing instability) occurs when the stress becomes high enough that

$$b = b_{Turing} = \left(a^{1/2} + \sqrt{\varpi\rho_{lm}^o D_{lm}/D_m}\right)^2 \tag{60}$$

- The wave vector for such spatial patterning is from Eq. (41)

$$q_{Turing} = \frac{2\pi}{\lambda_{Turing}} = \left(\frac{a\varpi\left(\rho_{lm}^o\right)^2}{D_{lm}D_m}\right)^{1/4} \tag{61}$$

where λ_{Turing} is the wavelength of the patterning.

- The Turing instability is reached before the Hopf instability if

$$\frac{D_{lm}}{D_m} < \frac{a}{\varpi\left(\rho_{lm}^o\right)^2}\left(\sqrt{1 + \frac{\varpi\left(\rho_{lm}^o\right)^2}{a}} - 1\right)^2 \tag{62}$$

Thus the analysis indicates that an initial homogeneous distribution of dislocations will spontaneously develop into a spatial pattern whose wavelength depends on the diffusion coefficients of the densities of the two families of dislocations, the rates of generation (a) and of interaction (ϖ) of dislocations, and the initial density of less mobile dislocations (ρ_{lm}^{0}).

This discussion has been for a one dimensional model but the discussion is readily extended to three dimensions (Walgraef and Aifantis, 1985c) and to more complicated dislocation processes (Pontes et al., 2006 and references therein). A result that immediately appears from models of this type is that if one takes the Orowan relation $\dot{\varepsilon} = \rho_m v_m b$, where v_m is the velocity of the mobile dislocations and b is the Burgers vector, then using Eq. (61) one can arrive at the relation (Schiller and Walgraef, 1988):

$$\lambda_{Turing} = \left(\frac{l_{lm}\dot{\varepsilon}}{b^2}\right)^{\frac{1}{2}} \rho^{-\frac{1}{2}} \tag{63}$$

where l_{lm} is the mean free path of less mobile dislocations and ρ is taken to be the total dislocation density. If one considers the Turing wavelength to be equivalent to subgrain-size then Eq. (63) gives a relation between subgrain-size and dislocation density which is a function of strain-rate and hence stress depending on the constitutive relation.

The arguments presented above for the development of dislocation patterning apply to any set of defects in a deforming rock mass where the densities of one population of defects diffuses at a different rate to another. Ord and Hobbs (2010) have applied this model to the development of joint patterns in deformed rocks.

4.10. Energy minimisation and the development of microstructure

A different approach to the development of dislocation patterns and other types of microstructure arises from the extensive theoretical work on the development of microstructure associated with martensitic transformations (Ball, 1977; Ericksen, 1980; Ball and James, 1987). The subject is highly mathematical and relies heavily on the mathematics of convex analysis. The following is an attempt at a brief summary of recent work that extends the work on martensitic transformations to crystal plasticity in metals and to the development of other microstructures including folding and fracturing.

Although five independent slip systems are necessary in any crystal to achieve a general homogeneous isochoric strain (Paterson, 1969), this same strain can also be achieved with fewer slip systems if the development of microstructure (that is, inhomogeneous deformation) is allowed. Moreover this alternative mechanism requires less energy and leads to smaller yield and flow stresses than a homogeneous deformation. As an example (Fig. 20), Ortiz and Repetto (1999) show that in BCC metals deformed in plane strain, the deformation can be accommodated by single slip or double slip depending on the type of deformation (extension, pure shortening, simple shearing or combinations of these as measured by the values of ($\varepsilon_{11}-\varepsilon_{22}$) and of ε_{12} where ε_{ij} are the strains). The energy is less for single slip deformations than for double slip orientations as shown in Fig. 20(d). In fact as the orientation of the crystal is changed with respect to the imposed deformation a series of low energy wells is generated corresponding to the orientations where single slip dominates (Fig. 20d).

In addition to this observation, the operation of single slip is commonly associated with mechanical softening, the two common mechanisms being geometrical softening as the slip plane rotates relative to the imposed stress, or latent hardening (Ortiz and Repetto, 1999; Ord and Hobbs, 2011). The development of softening in rate dependent materials is further explored by Carstensen et al. (2002) and for rate independent materials by Miehe and Lambrecht (2003) and Miehe et al. (2004). This softening leads to non-convexity in the Helmholtz energy as shown in Figs. 20 and 21.

However there is another constraint on the development of microstructure as a process of minimising the energy in that the developed microstructure must be capable of producing an array of deformed domains that are themselves compatible and that together are compatible with the imposed deformation in order to ensure no long range stresses. This leads to a hierarchy of microstructure represented by a progressive refinement in the length scale of the microstructure as shown in Fig. 22. The opportunity exists here to develop fractal geometries due to self-similar refinement of the microstructure as it approaches a boundary where strain compatibility is achieved.

In Fig. 21(d) two sets of shears are developed with deformation gradients $\boldsymbol{F}^{-}$ and $\boldsymbol{F}^{+}$. These approximate the imposed deformation represented by the deformation gradient $\boldsymbol{F}$ and the approximation becomes better the finer the spacing of the two sets of shear bands. However strain compatibility can never be achieved by this process alone and other deformation histories are necessary at the ends of the shear bands to produce compatibility. This leads to a spatial hierarchy of deformation histories that is shown as an example in Fig. 22 and is represented by a "tree" structure in Fig. 23(a). The tree is divided into a number of "*levels*" each with a number of "*nodes*" as shown. The top node in Level 0 is the deformation history that represents the large scale homogeneous deformation, $\boldsymbol{F}$. The two deformation histories in level 1 combine together to approximate $\boldsymbol{F}$ and this relationship holds for each level below that so that for instance $\boldsymbol{F}_4$ and $\boldsymbol{F}_5$ combine to approximate $\boldsymbol{F}_2$. Ortiz and Repetto (1999) show that the number of independent degrees of freedom, d, for the complete array of nodes is given by $d = 4n_i - 3n_l$ where n_i is the number of nodes such as $\boldsymbol{F}_2$ in Fig. 23(a) that have "*daughters*" $\boldsymbol{F}_4$ and $\boldsymbol{F}_5$ whereas n_l is the number of "*leaves*" such as $\boldsymbol{F}_6$ that have no daughters. This means that to match the nine independent components of an arbitrary three dimensional deformation tensor $\boldsymbol{F}$ we need $d \geq 9$. This cannot be accomplished by only two levels of the tree and complete matching needs at least three levels. Fig. 23(b) shows one such arrangement.

At large strains the microstructure can become refined so that eventually inhomogeneous deformation is no longer required for compatibility and any inhomogeneity becomes simpler even to the extent of vanishing (Fig. 24). Fig. 24 shows this evolution of microstructure for simple shearing by single slip of an initial square with the slip direction, $\boldsymbol{S}$, lying in the plane whose normal is $\boldsymbol{T}$, at various initial angles to the shearing direction as measured by the angle α. The kink bands that form in order to minimise the Helmholtz energy and at the same time accommodate the imposed deformation gradient have different orientations relative to the shearing direction depending on α and rotate towards the shearing direction as the strain increases; at high strains inhomogeneous deformation may not be necessary to accommodate the imposed deformation gradient and a steady state homogeneous microstructure remains.

Fundamentally different types of microstructure form depending on the nature of the stored Helmholtz energy function. The literature on finite non-linear elasticity (see Antman, 1983 and Ball, 1998 for reviews) distinguishes four different types of energy functions: convex, poly-convex, quasi-convex and rank-1 convex functions. Since, from Eq. (21), $V_o\sigma_{ij} = \frac{\partial \Psi}{\partial \varepsilon_{ij}}$, the stress strain curve corresponding to a particular Helmholtz energy function can be obtained by differentiation of the energy function. Three of these types of functions are illustrated in Fig. 25 together with the stress–strain curve associated with that particular energy function and an example of the resulting microstructure.

Fig. 25(a) shows a convex (quadratic) energy function with the derived linear stress strain curve. In general, convex energy

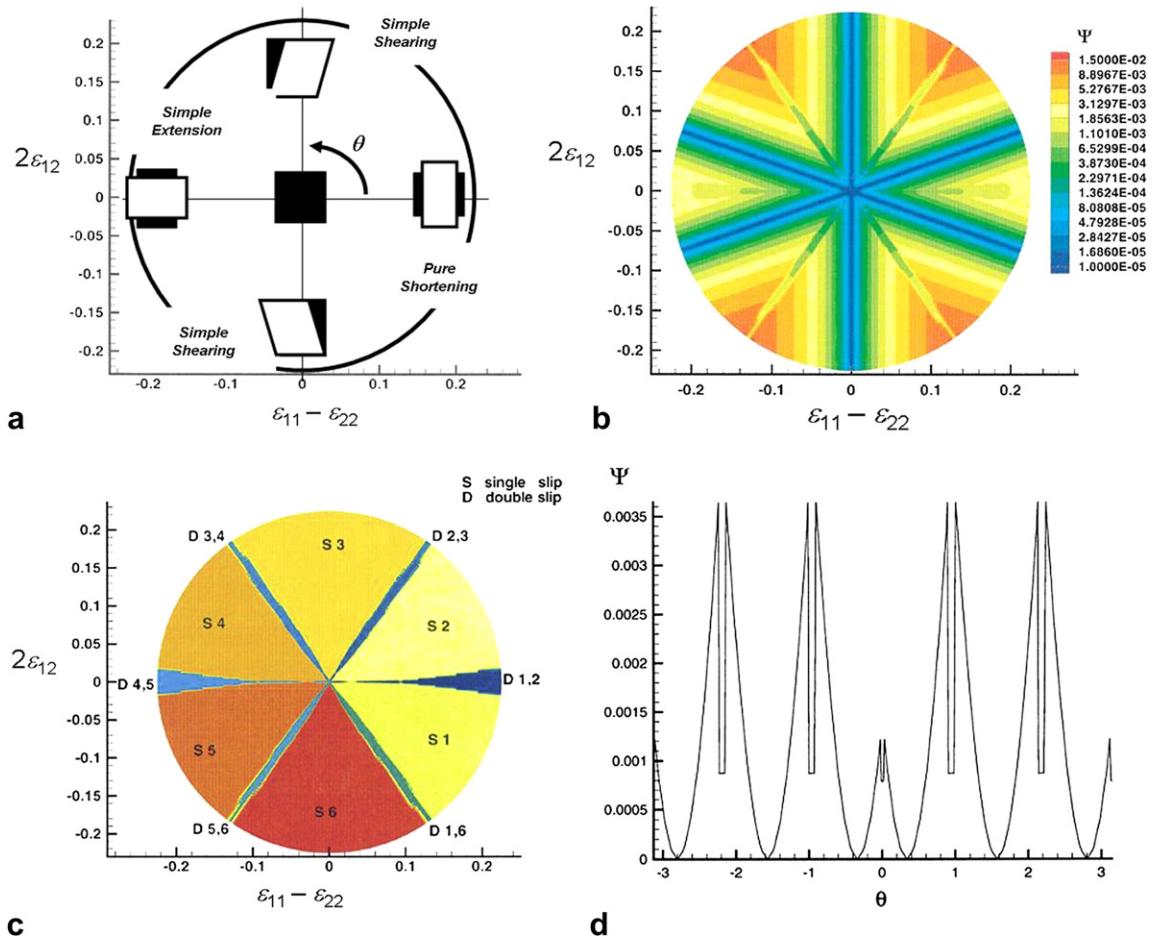

Fig. 20. Low energy wells generated for single slip in BCC metals for various orientations of the crystal with respect to the imposed deformation. (a) Plane strain deformations defined by various values of $2\varepsilon_{12}$ with respect to $(\varepsilon_{11}-\varepsilon_{22})$ where ε_{ij} are the incremental strains. (b) Plot of the energy, Ψ, for various deformations (c) Operating slip systems to accommodate the imposed strain. See Ortiz and Repetto (1999, Fig. 5) for slip system nomenclature. (d) Plot of Ψ for a circular traverse around Fig. 20b showing the development of low energy wells. θ is defined in Fig. (a). (After Ortiz and Repetto, 1999, Fig. 5).

functions inhibit the formation of instabilities such as buckles, kinks and other forms of microstructure so that the resultant deformation is homogeneous. An example of a poly-convex function is not shown but involves matrices and so is ideal for use in finite elasticity to represent the stored elastic energy of anisotropic materials such as single crystals. Poly-convexity results in the development of microstructure and is a major tool in understanding the microstructures that develop in martensite transformations. Fig. 25(b) shows an example of a quasi-convex energy function (possessing a discontinuity at the origin) with the derived stress strain curve showing softening behaviour. The resultant microstructure comprises buckling of any layers that are present (Ball, 1977). Fig. 25(c) shows a rank-1 convex energy function which is non-convex with two energy wells. An example has already been discussed in Fig. 21. The derived stress strain curve shows both softening and hardening. The microstructure that develops consists of chevron style folds.

If materials characterised by different energy functions are inter-layered with each other then the opportunity exists for layering of microstructure as shown in Fig. 26. In this way axial plane crenulation cleavages and axial plane kink structures can form.

Several important aspects of the microstructures developed in polycrystalline rocks deforming by single slip follow from this approach:

(i) *Fractal grain boundaries.* The microstructure shown in Fig. 22 becomes finer towards the original grain boundary in order to produce compatibility of strain across the boundary and to minimise the Helmholtz energy. If one considers each domain to be a subgrain then a traverse through the array of domains approximately parallel to $X-Y$ resembles a fractal Koch curve (remembering that the traverse is a two dimensional one across a three dimensional structure) with a fractal dimension somewhere between 1.1 and 1.5 (Mandlebrot, 1977 pp. 44–50). This corresponds to the observations made on serrated grain boundaries in deformed quartz aggregates (Kruhl and Nega, 1996). Moreover the details of the distribution and magnitudes of the deformation gradients depend on both the yield stress for the material and the magnitude of the strain hardening (Carstensen et al. 2002) and hence depend on temperature and strain-rate. This is suggested as the mechanism behind the observed fractal dependence of subgrain shapes reported by Takahashi et al. (1998).

(ii) *Rotation recrystallisation.* It is well known since the experimental demonstration of Hobbs (1968) that some forms of dynamic recrystallisation develop through successive rotation of subgrains. The microstructural mechanisms described above that minimise the Helmholtz energy seem to produce this phenomenon in that the domains shown in Fig. 22 eventually undergo a large rotation although the misorientation between

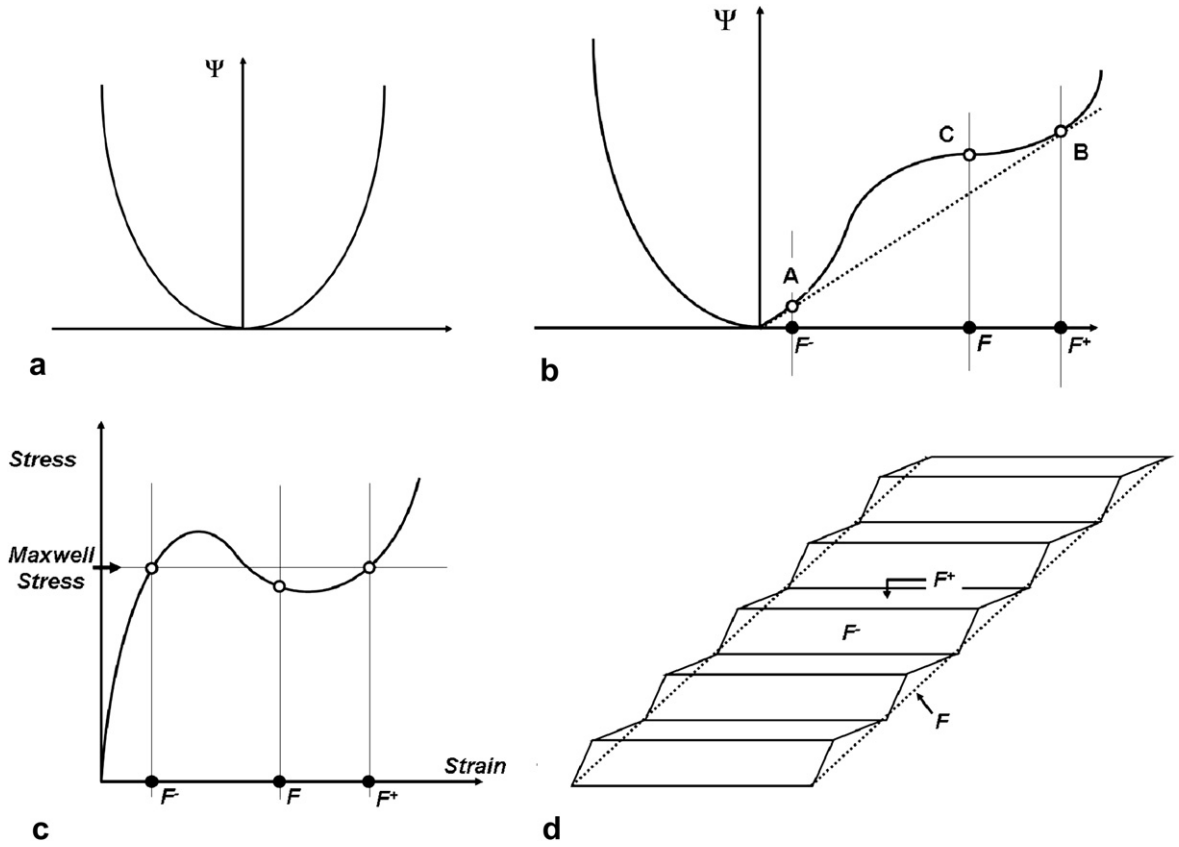

Fig. 21. Development of microstructure from a non-convex energy function. (a) The normal convex form of the Helmholtz energy plotted against some measure of the deformation gradient. (b) A non-convex form of the Helmholtz energy plotted against the deformation gradient for systems with a single slip system. The energy at C corresponds to a homogeneous deformation gradient, *F*, and can be minimised by decreasing the energy to the tangent line AB. The homogeneous deformation gradient is unstable and evolves to a stable form of microstructure consisting of two spatially alternating deformation gradients F^- and F^+ which together approximate the homogeneous deformation, *F*. (c) The stress–strain curve that results from the non-convex form of the Helmholtz energy in (b); the strains corresponding to F^-, *F* and F^+ are shown. The horizontal line which divides the stress strain curve into equal areas above and below the curve corresponds to the Maxwell stress. This has a direct analogue in the Equilibrium Chemical Thermodynamics of two phase systems. (d) The microstructure that minimises the Helmholtz energy.

adjacent domains may be quite small. This mechanism is discussed in detail in Section 4.11.

(iii) *Core and mantle structure.* The type of structure illustrated in Fig. 22 is suggested as a possible mechanism for the development of core and mantle structures in partially recrystallised materials. The progressive development of the mantle structure with the associated changes in grain orientation from core to grain boundary is a mechanism for producing compatibility of strain

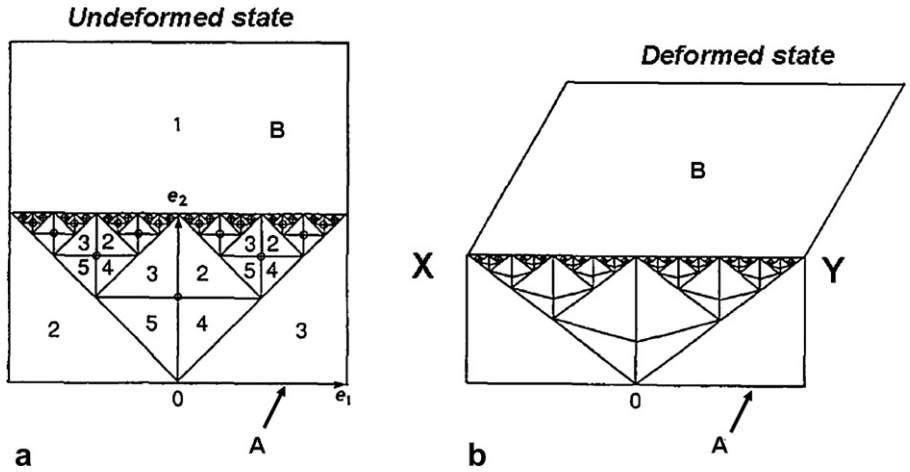

Fig. 22. Progressive refinement of microstructure towards a boundary in order to produce compatibility of strain across the boundary X–Y between two crystals A and B and at the same time minimise the energy in the crystal. (a) The distribution of five different deformation gradients in the undeformed state. The sizes of the domains become finer towards the boundary between two crystals A and B. Each domain is associated with a rotation of the lattice with respect to adjacent domains. (b) The deformed state where grain B is sheared by 45° with respect to grain A and A is shortened normal to the boundary. The distribution of the five deformation gradients produces compatibility of strain between the two grains. (After Ball and James, 1987).

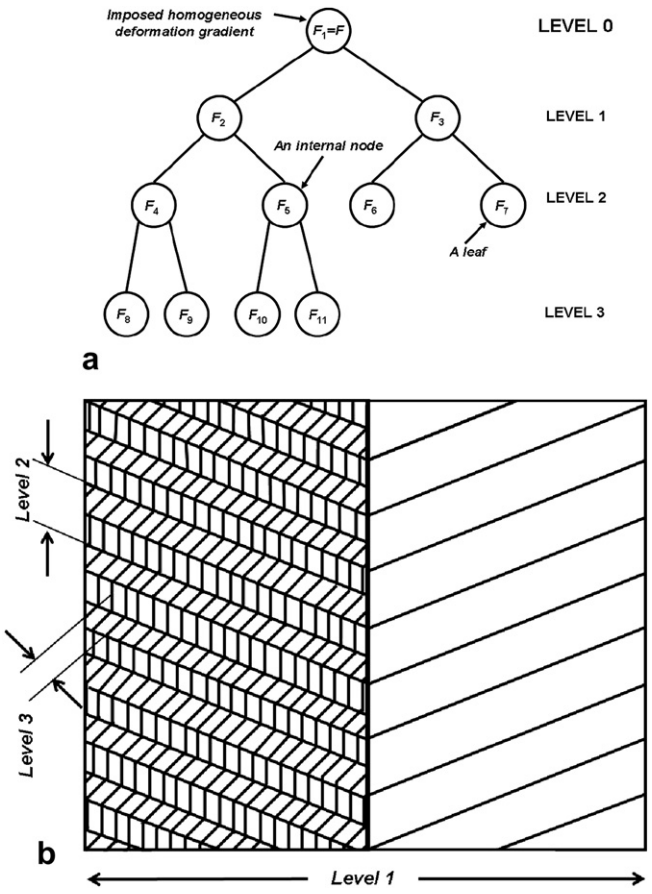

Fig. 23. A hierarchy of deformation histories (a) represented by a "tree" structure in which the tree is divided into a number of "*levels*" each with a number of "*nodes*". The top node in Level 0 is the deformation history that represents the large scale homogeneous deformation, *F*. The two deformation histories in level 1 combine together to approximate *F* and this relationship holds for each level below that so that for instance F_4 and F_5 combine to approximate F_2. Ortiz and Repetto (1999) show that the number of independent degrees of freedom, *d*, for the complete array of nodes is given by $d = 4n_i - 3n_l$ where n_i is the number of nodes such as F_2 in (a) that have "*daughters*" F_4 and F_5 whereas n_l is the number of "*leaves*" such as F_6 that have no daughters. This means that to match the nine independent components of an arbitrary three dimensional deformation tensor *F* we need $d \geq 9$. This cannot be accomplished by only two levels of the tree and complete matching needs at least three levels. (b) shows strain compatibility achieved by one such arrangement (after Ortiz and Repetto, 1999).

between two initially undeformed and adjacent grains with the operation of a single slip system.

(iv) *Fractal subgrain-size distribution.* In three dimensions the structure illustrated in Fig. 22 can be approximated as a fractal packing of spheres. Lind et al. (2008) have shown that a two dimensional cut across such a packing will result in a distribution of circles with a fractal dimension of 1.7–1.8. This is suggested as the origin of such relations observed in deformed metals (Hahner et al. 1998).

4.11. Crystallographic preferred orientations; rotation recrystallisation

The introduction of X-ray and electron diffraction techniques to examine the crystallographic preferred orientations (CPO) in both naturally and experimentally deformed rocks has led to the conclusion that slip on a single slip system is a common process in the development of CPO (Schmid and Casey, 1986; Schmid, 1994; Reddy and Buchan, 2005; Heilbronner and Tullis, 2006). This is at odds with the postulate made in the Taylor–Bishop–Hill theory of CPO development that five independent slip systems operate within each grain (Lister et al. 1978; Lister and Hobbs, 1980) in order to accommodate a homogeneous strain that is imposed on the aggregate and on each grain. The observation that single slip operates implies that the deformation within each grain is inhomogeneous. We have seen in Section 4.10 that single slip is a mechanism for minimising the Helmholtz energy in a crystal and results in non-convex energy functions. This in turn leads to the development of heterogeneous deformation within a grain in an attempt to match the imposed deformation gradient. Since a general imposed deformation gradient has nine independent components, nine independent deformation gradients must develop in each grain to match a general imposed deformation. Ord and Hobbs (2011) develop a model for rotation recrystallisation based on the formation of subgrains as a mechanism for minimising the Helmholtz energy and using the arguments developed in Section 4.10, particularly those derived from Ortiz and Repetto (1999). The model proposes that a self-similar hierarchy of subgrains develops in each grain represented by a tree structure as in Fig. 23(a). A specific tree structure is shown in Fig. 27(a) for an imposed simple shearing deformation history and for a quartz grain that has the most number of adjustments to make before its deformation matches the imposed deformation gradient at each instant. Part of the resulting array of subgrains is shown in Fig. 27 (b,c) and the complete list of orientations developed is portrayed for the A side of the tree in Fig. 27(d). The CPO in this case develops through the operation of single slip in each subgrain and the process of refinement continues until the aggregate is dominated by orientations that do not continue to evolve with increased deformation (in this case with *prism*$\langle \boldsymbol{a} \rangle$ aligned parallel to the imposed shear plane and shear direction). The CPO then is a steady state CPO and no further evolution of the microstructure occurs in a manner analogous to the microstructural evolution described in Fig. 24 from Miehe et al. (2004). At each stage in the development of the CPO, compatibility of deformation is guaranteed between adjacent grains by the compatibility requirement (Ord and Hobbs, 2011, Appendix) expressed by

$$\left(\boldsymbol{F}^{+} - \boldsymbol{F}^{-}\right) = \boldsymbol{a} \otimes \boldsymbol{N} \tag{64}$$

where $\boldsymbol{F}^{+}$ and $\boldsymbol{F}^{-}$ are the deformation gradients in adjacent subgrains labelled (+) and (−), $\boldsymbol{N}$ is the normal to the subgrain boundary and may be a rational or non-rational crystallographic direction, $\boldsymbol{a}$ is an arbitrary vector and $\otimes$ is the dyadic product operator (Section 2.1; Ord and Hobbs, 2011). For single slip the deformation gradients, $\boldsymbol{F}^{\pm}$, in the two adjacent subgrains are given by:

$$\boldsymbol{F}^{\pm} = \boldsymbol{R}^{\pm}\left(\boldsymbol{I} + \gamma^{\pm}\boldsymbol{s}^{\pm} \otimes \boldsymbol{m}^{\pm}\right) \tag{65}$$

where $\boldsymbol{R}^{\pm}$, are the rotations in each subgrain, $\boldsymbol{I}$ is the identity matrix and $\gamma^{\pm}$, $\boldsymbol{s}^{\pm}$, $\boldsymbol{m}^{\pm}$are the shear strains, the slip directions and the slip plane normals in each grain respectively (Ortiz and Repetto, 1999; Ord and Hobbs, 2011).

The compatibility condition Eq. (64) means that although the deformation of the aggregate is heterogeneous and during its evolution, the aggregate passes through many levels of microstructural refinement, the deformation field throughout the aggregate remains compatible from one subgrain to the next and on average, approximates the imposed deformation gradient. This means that all sub- and grain boundaries obey Eq. (64) whether they are rational or non-rational in orientation. Some additional self-similar refinement as discussed in Section 4.10 is necessary to

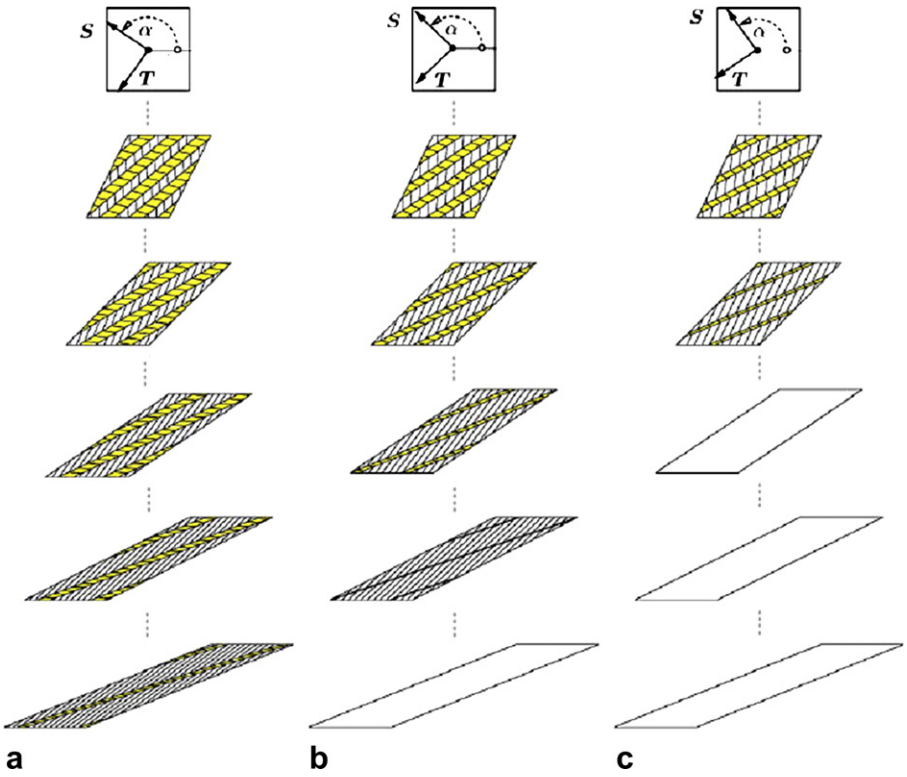

Fig. 24. From Miehe et al. (2004, their Fig. 10). Simple shear test. Comparison of evolution of microstructures for simple shear test with three differently oriented slip systems. ***S*** is a unit vector parallel to the initial slip direction and ***T*** is an initial unit vector normal to the slip plane. α is the angle between the initial slip direction and the shear direction (a) $\alpha = 145°$, (b) $\alpha = 135°$, (c) $\alpha = 125°$. After loss of material stability microstructures develop which are modelled as a first order approximation to the deformation gradient with no refinements.

produce precise compatibility with the imposed deformation gradient and the total process produces a fractal geometry for the CPO illustrated in Fig. 27(f). The potential exists to link the fractal dimensions of CPO's with the environment of deformation including parameters such as amount of strain, temperature and strain-rate.

The outcome of this analysis is that CPO development by single slip minimises the Helmholtz energy but the process demands compatibility of deformation, as expressed by Eq. (64) across every grain and subgrain boundary as does the Taylor–Bihop–Hill theory. Such compatibility has yet to be tested in natural or experimentally dynamically recrystallised specimens.

4.12. Folding at the microscale due to feedback from chemical reactions

Regenauer-Lieb et al. (2009) present a model in which the reaction

$$\text{muscovite} + \text{quartz} \rightarrow \text{Kfeldspar} + \text{sillimanite} + H_2O$$

is coupled to the deformation of a stronger single layer shown in Fig. 28(a). As indicated in the Introduction to Section 4 the spatial scale involved here (tens of millimetres) is such that the system can be considered isothermal at strain-rates of 10^{-13} to 10^{-10} s^{-1} and so the Energy Equation reduces to an equation of the form:

$$\textit{Mechanical dissipation} = \textit{Diffusive dissipation} + \textit{Chemical dissipation}.$$

This means that heat generated by the deformation is used to preferentially increase the rates of diffusive processes and chemical reactions rather than be conducted out of the system. Since the mechanical dissipation in the stronger layer is larger than in the weaker embedding material and the diffusion length for H_2O is small on the time scale of the deformation, the muscovite breakdown reaction is driven faster in the stronger layer and the concentration of H_2O becomes higher in the stronger layer than in the embedding material (Fig. 28c). At this stage dissipation due to diffusion is no longer important and the system is controlled by the relation:

$$\sigma_{ij}\dot{\varepsilon}_{ij}^{dissipative} = A\dot{\xi} \tag{66}$$

Adopting a Newtonian viscous constitutive relation for the stronger layer and an Arrhenius relation for the reaction rate, $A = \mathscr{B}\dot{\xi}\exp(\frac{Q^{chemical}}{RT})$ gives:

$$\eta_{ijkl}\dot{\varepsilon}_{ij}^{dissipative}\dot{\varepsilon}_{kl}^{dissipative} = \mathscr{B}\dot{\xi}^2\exp\left(\frac{Q^{chemical}}{RT}\right) \tag{67}$$

which means that the effective viscosity, η_{ijkl}, is inversely proportional to the square of the strain-rate. This relation is of the same form as that proposed for thermal–mechanical coupling by Fleitout and Froidevaux (1980) for a two dimensional shear zone:

$$\eta_{\text{minimum}} = \frac{8K^{thermal}RT^2_{\text{maximum}}}{\dot{\varepsilon}^2h^2Q^{chemical}} \tag{68}$$

where $K^{thermal}$ is the thermal conductivity and h is the steady state thickness of the shear zone. Similar expressions may be obtained for power-law constitutive relations (Fleitout and Froidevaux (1980). The result is localisation of the deformation due to strain-rate softening and the deformation of the layer and embedding

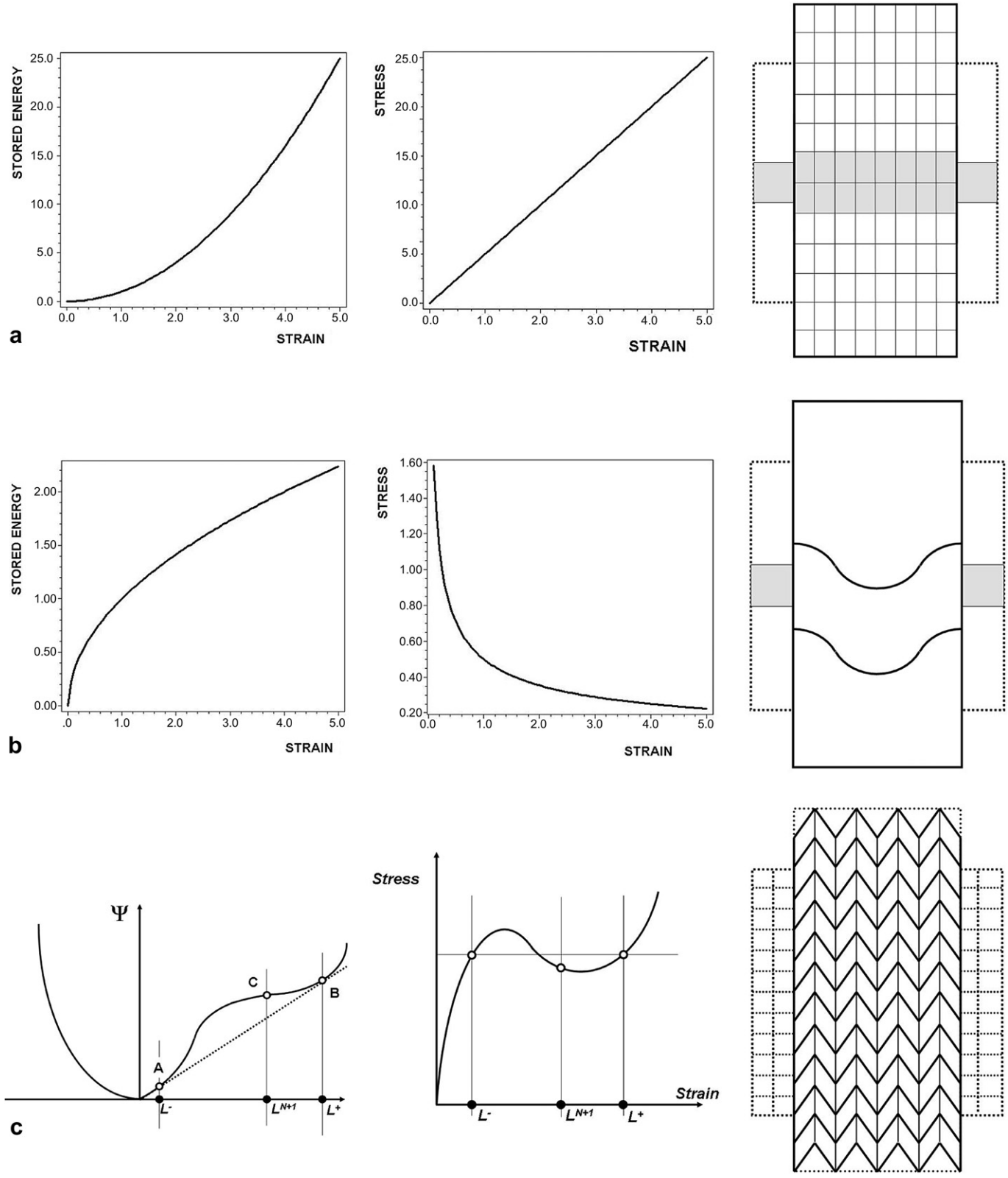

Fig. 25. Different types of stored Helmholtz energy functions and the derived stress strain curves and microstructures. (a) Convex (quadratic) stored Helmholtz energy function with derived linear stress strain curve. No microstructure develops; the deformation remains homogeneous. (b) Quasi-convex Helmholtz energy function with derived softening stress strain curve. The microstructure consists of buckles in layers that may be present. (c) Rank-1 non-convex Helmholtz energy function with derived stress strain curve that consists of both softening and hardening segments. The resultant microstructure consists of chevron folding.

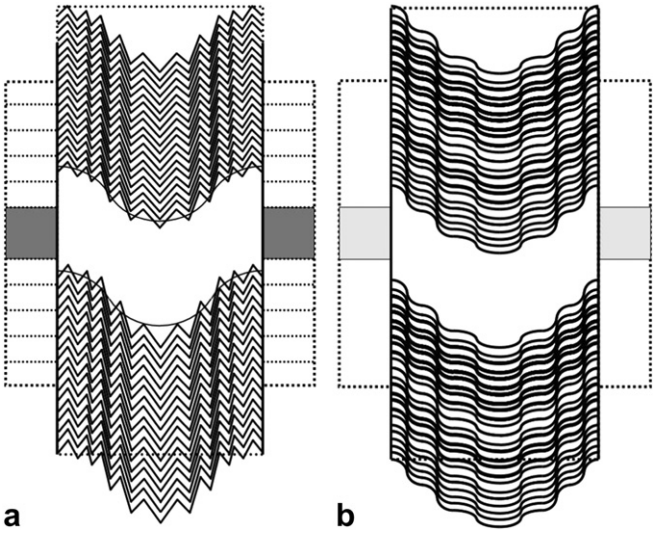

Fig. 26. Results of layering different materials with different energy functions. (a) Quasi-convex layer embedded in material with rank-1 convexity. (b) Quasi-convex layer embedded in quasi-convex material with finer scale layering. These hypothetical relationships follow from models proposed by Ball (1977) and by Carstensen et al. (2002).

material is shown in Fig. 28d. As indicated by Eq. (67) the effective viscosity is decreased in the shear zones which in turn are nucleated on initial deflections of the layer. These localised deflections ultimately grow to produce micro-folds. We leave a detailed analysis of this process to Section 5.

4.13. Chemical reactions and mechanical behaviour

One may have expected that by now there would exist a general thermodynamic treatment of deforming-reactive systems that links common mechanisms such as dislocation motion and mineral reactions. However the subject is still quite open. The general problem of deriving constitutive equations for deforming-reacting systems has not been solved but some progress has been made in restricted areas by Coussy and Ulm (1996). That work serves as a template for future developments. We consider a deforming system within which a chemical reaction occurs and some of the strain is achieved by diffusion mechanisms and/or diffusion assisted mechanisms associated with the chemical reaction. This means that deformation occurs through chemical species diffusing from regions of high chemical potential to regions of low chemical potential. Typical examples are Herring–Nabarro, Coble and "pressure solution" constitutive behaviour (Lehner, 1995). One example of coupling of diffusive mass transport to deformation is that of Fletcher (1982) who considers diffusive flux driven by gradients in chemical potential as defined by Kamb (1959, 1961). Coupling to dissipative effects is not considered. This flux is coupled to the folding of a linear viscous layered material with a constant but small porosity. For this model, diffusive transport is therefore down gradients in the rock pressure. Fletcher shows that this coupling can lead to a significant decrease in the dominant wavelength below that which would develop with no diffusive coupling. The following discussion is modified from Coussy (2004). It is to be emphasised that this approach is different to that commonly developed in the geological and metallurgical literature (eg., McLellan, 1980; Larche and Cahn, 1985) where the emphasis is on the influence of non-hydrostatic stress on chemical potential in elastic systems and dissipative processes are not considered.

We consider a chemical reaction or diffusive process where the kinetics of the reaction are given by

$$A = \eta \frac{d\xi}{dt} \exp\left(\frac{Q}{RT}\right) \tag{69}$$

where η is a constant with the dimensions of viscosity, t is time, Q is the activation enthalpy for the diffusion process or the chemical reaction and R is the universal gas constant. A is the affinity of the chemical reaction and is a linear function (with units of stress) of the difference between the sum of the chemical potentials of the reactants and that of the products (Kondepudi and Prigogine, 1998). ξ is the extent of a diffusive process or of a chemical reaction.

Following Rice (1975) we define the Gibbs Free Energy, $\mathcal{G}$ (Table 4):

$$\mathcal{G} = \sigma_{ij}\varepsilon_{ij}^{elastic} - \Psi \tag{70}$$

The state equations are then:

$$\mathcal{G} = \mathcal{G}(\sigma_{ij}, T, \xi)\ ;\ \varepsilon_{ij}^{elastic} = \frac{\partial \mathcal{G}}{\partial \sigma_{ij}};\ s = \frac{\partial \mathcal{G}}{\partial T};\ A = \frac{\partial \mathcal{G}}{\partial \xi} \tag{71}$$

Differentiating Eq. (71) we obtain:

$$d\varepsilon_{ij}^{elastic} = S_{ijkl}d\sigma_{kl} + \alpha_{ij}dT + \beta_{ij}d\xi \tag{72a}$$

$$ds = \alpha_{ij}d\sigma_{ij} + C\frac{dT}{T} - L\frac{d\xi}{T} \tag{72b}$$

$$dA = \beta_{ij}d\sigma_{ij} - L\frac{dT}{T} - ad\xi \tag{72c}$$

where S_{ijkl} is the elastic compliance tensor, α_{ij} is the thermal expansion tensor, C is the volumetric heat capacity of the solid material. L is the latent heat associated with the reaction, so that as the reaction progresses the heat produced is $Ld\xi$; the reaction is exothermic if $L > 0$ or endothermic if $L < 0$. a is the decrease in chemical affinity per unit of reaction extent under isostress and isothermal conditions. The symmetrical tensor β_{ij} is given by:

$$\beta_{ij} = \frac{\partial^2 \mathcal{G}}{\partial \sigma_{ij} \partial \xi} \tag{73}$$

$\beta_{ij}(\sigma_{ij},T,\xi)$ is the tensor of chemical strain coefficients and is dimensionless; as the chemical extent increases by an amount $d\xi$, the chemical reaction produces a strain with components $\beta_{ij}d\xi$. The associated chemical dilation is $\beta_{ii}d\xi$. The forms of the various coefficients in Eq. (72), such as β_{ij}, need to be established by experiments and at present we are sadly lacking in such data.

For a diffusion process, A represents the difference between the chemical potential of the solid subjected to the diffusion process and the chemical potential of the same chemical component elsewhere within the solid where the temperature and/or stress are different. For closed systems, the term $\beta_{ij}d\sigma_{ij}$ in Eq. (72c) describes the stress concentration effect in the solid at heterogeneities. In an isothermal system, the process is controlled by the diffusion of the species towards the regions where the solid is poorly stressed.

If we now assume that the elastic properties are not influenced by the chemical/diffusion processes and that the system remains isothermal then Eqs. (72) and (73) give (Coussy and Ulm, 1996; Coussy, 2004):

$$\sigma_{ij} = C_{ijkl}\left(\varepsilon_{kl}^{total} - \varepsilon_{kl}^{viscous}\right) \tag{74a}$$

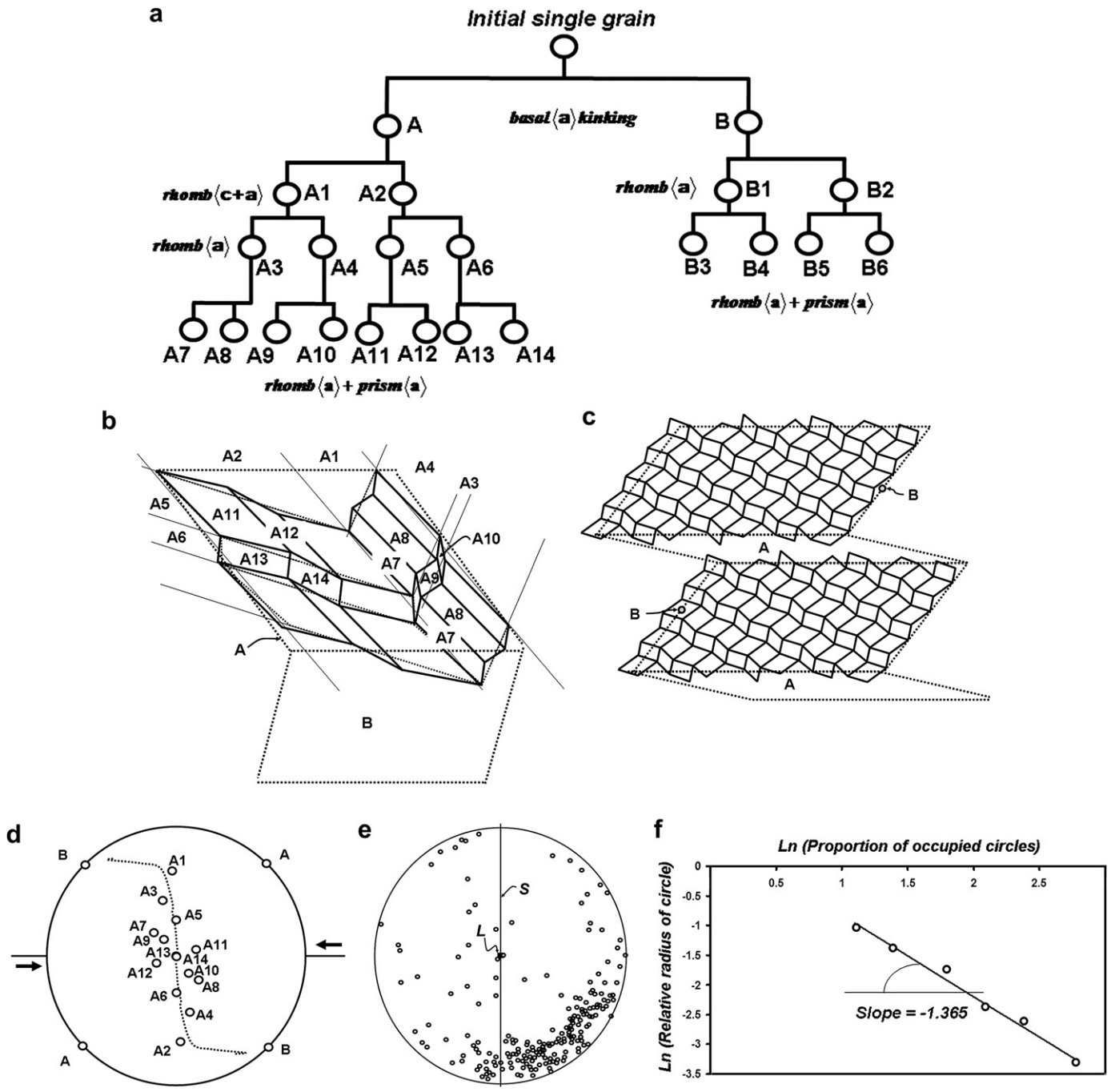

Fig. 27. (a) The tree structure for a self-similar hierarchy of subgrains for an imposed simple shearing deformation history and for a quartz grain that has the most number of adjustments to make before its deformation matches the imposed deformation gradient at each instant. (b) Part of the resulting array of subgrains arising from orientation A in Fig. (a). (c) Subgrain arrays for orientation B. (d) The complete list of orientations developed for the A side of the tree. (e) Natural CPO for 200 quartz grains from Hobbs (1966). (f) Demonstration of fractal geometry for the CPO.

$$\sigma_{ij} = C_{ijkl}\varepsilon_{kl}^{viscous} + \eta_{ijkl}\frac{\mathrm{d}\varepsilon_{kl}^{viscous}}{\mathrm{d}t} \tag{74b}$$

where

$$\varepsilon_{ij}^{viscous} = \beta_{ij}\xi \tag{75a}$$

$$C_{ijkl} = S_{ijkl}^{-1} \tag{75b}$$

$$C_{ijkl}^{-1} = a\beta_{ij}\beta_{kl} \tag{75c}$$

$$\eta_{ijkl} = \eta\beta_{ij}\beta_{kl} \tag{75d}$$

and it is assumed that the reference state is stress free with zero affinity.

Coussy and Ulm (1996) proceed to establish rheological models based on this approach. The need is to develop these models for geological materials and to extend them to deal with isotropic and kinematic hardening (or softening) as discussed by Houlsby and Puzrin (2006a, Chapters 5, 6 and 7) and for the development of anisotropy.

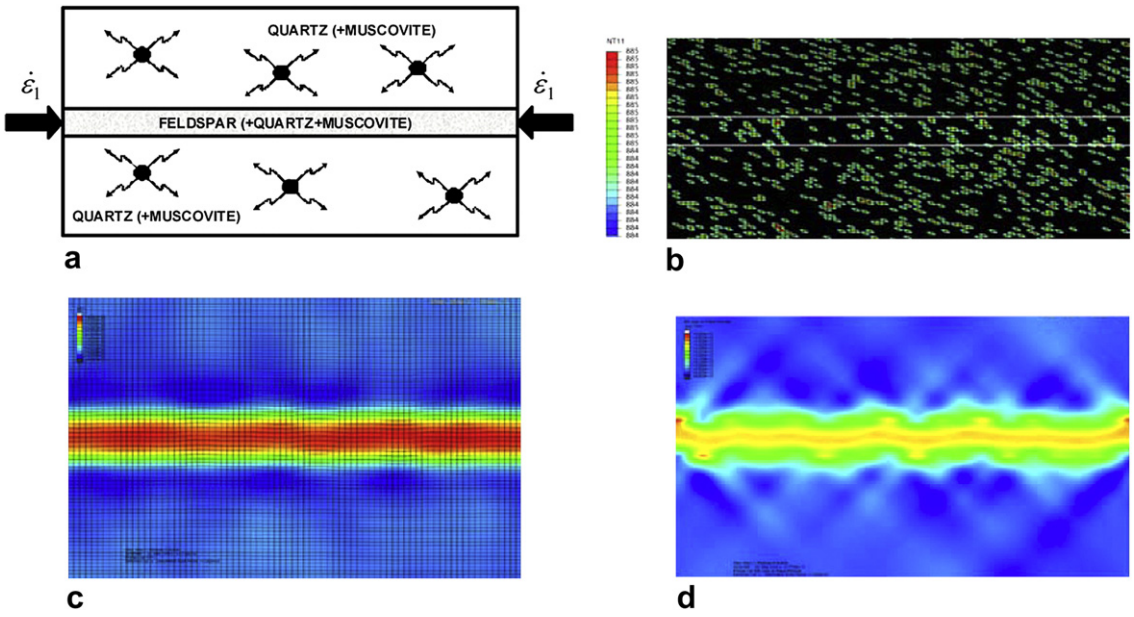

Fig. 28. Chemical-deformation coupling at the microscale. Initial growth of the model shown in (a). (b) A random set of muscovite breakdown sites is assumed as the starting condition. Contours show the concentration of water (which has an equivalent effect on rheology as a temperature perturbation of 1 K) after 1% shortening. In keeping with the thermo-chemical analogy, chemical changes are reported in terms of the effect of an equivalent temperature change on rheology. (c) The water concentration after 5.8×10^7 s shortening. The maximum hydrolytic weakening is equivalent to 6 K heating. (d) Plot of strain-rate at the same time step as (c). The interface between the stronger and the weaker material is clearly visible and decorated periodically by alternating regions of high and low strain-rates. The central strong layer buckles through weakening in the hinges defined by the maximum strain-rate/dissipation sites on the interface. This result is equivalent to the thermal–mechanical fold instabilities reported in Hobbs et al. (2007, 2008), however, localisation and buckling occur here at the centimetre scale rather than at kilometre scale.

Eq. (74b) can be interpreted as linear elastic–viscous behaviour, with $\varepsilon_{kl}^{viscous}$ representing the viscous strain and η_{ijkl} representing a "chemical viscosity". Notice that η_{ijkl} is a quadratic function of β_{ij}. In particular Eq. (75d) says that if β_{ij} decreases by an order of magnitude, then the "chemical viscosity", η_{ijkl}, decreases by two orders of magnitude. A similar situation arises from thermal–mechanical feedback (Eq. 68) where, in a zone of localised shearing, an order of magnitude increase in strain-rate leads to two orders of magnitude decrease in viscosity (Fleitout and Froidevaux, 1980). If for instance the chemical reaction involves a decrease in volume with continued straining then strong weakening occurs during the chemical reaction, with the opportunity for localisation to develop provided that such localisation is compatible with the boundary conditions (Fressengeas and Molinari, 1987).

This discussion indicates that diffusion and chemical reactions, if they are an integral part of the deformation mechanisms, can result in modification of the viscosity, with the resultant development of a "chemical viscosity" that is strongly dependent on the extent of the chemical reaction and that can lead to weakening. This is a strong mechanism for generating localisation in deforming-reactive rocks.

4.14. A synthesis of coupled processes

A paper by Veveakis et al. (2010) provides the principles by which much of the previous discussion may be integrated. Consider a shear zone of thickness h as shown in Fig. 29a in which a number of processes are operating concurrently with deformation including mineral reactions and grain-size evolution. The zone is deformed by the boundary velocity, $\boldsymbol{v}$, and the temperature is fixed on the boundaries at $T^{boundary}$. The strain-rate for stable shearing induced by $\boldsymbol{v}$ is $\dot{\gamma} = v/(h/2)$ and the shear stress is τ.

The temperature within the shear zone evolves according to the Energy Equation (26):

$$c_p\dot{T} = \chi V_o \tau\dot{\gamma} + V_o\mu^K\dot{m}^K - \sum_K \Phi_K^{chemical} - \Phi^{thermal} - \Phi^Q \qquad (76)$$

In Eq. (76) we have added the extra process, Q, with a dissipation function, Φ^Q as indicated in the Helmholtz energy Eqs. (20) and (21e). In this example Q is taken to be grain-size evolution but it could be any other dissipative process such as recrystallisation, preferred orientation development or fracturing.

If the processes involved are only deformation and heat conduction then Eq. (76) reduces to

$$c_p\dot{T} = \chi V_o \tau\dot{\gamma} + c_p\kappa^{thermal}\frac{\partial^2 T}{\partial z^2} \qquad (77)$$

We assume that the constitutive law for deformation is a power-law of the form $\tau = \mathcal{A}^{-\frac{1}{N}}\dot{\gamma}^{\frac{1}{N}}\exp(\frac{Q}{NRT})$ and we define the dimensionless quantities

$$z^* = \frac{z}{(h/2)};\ t^* = \frac{\kappa^{thermal}}{(h/2)^2}t;\ T^* = \frac{T}{T^{boundary}};\ \gamma^* = \frac{\dot{\gamma}}{\dot{\gamma}^{reference}}$$

Then, $\dot{T}^* = \frac{\partial^2 T^*}{\partial z^{*2}} + \frac{\chi V_o \tau\dot{\gamma}^{reference}}{T^{boundary}\kappa^{thermal}c_p}(\frac{h}{2})^2\dot{\gamma}^*$ which we rewrite as

$$\dot{T}^* = \frac{\partial^2 T^*}{\partial z^{*2}} + Gr\exp(-Ar) \qquad (78)$$

where $Gr = \frac{\chi V_o\dot{\gamma}^{reference}\tau}{c_p\kappa^{thermal}T^{boundary}}(\frac{h}{2})^2$ is the dimensionless Gruntfest Number and $Ar = \frac{Q}{R(T-T^{boundary})}$ is the dimensionless Arrhenius Number. The Gruntfest Number is the ratio of the time scale for heat production by deformation to the time scale for conduction of heat away from the dissipation site. If $Gr \to \infty$ then the system is adiabatic; if $Gr \to 0$ all of the heat has time to diffuse away from the dissipation site without increasing the temperature at that site. For $Gr > 1$ mechanical dissipation is faster than heat can be conducted away and the temperature of the body increases. The Arrhenius

Number is the ratio of the thermal and rate sensitivities of the material. *Ar* may be thought of as the energy threshold where the deformation becomes thermally and rate sensitive. If we take $\chi = 1$, $V_o = 3.7 \times 10^{-4}$ m^3 kg^{-1}, $\dot{\gamma}^{reference} = 10^{-13}$ s^{-1}, $\tau = 300$ MPa; $T^{boundary} = 673$ K, $\kappa^{thermal} = 10^{-6}$ m^2 s^{-1} and $c_p = 10^3$ J kg^{-1} K^{-1} then $Gr > 1$ for $h > 1.54$ km. For $h = 1$ m the reference strain-rate needs to be greater than 2.4×10^{-5} s^{-1} for $Gr > 1$. These numbers are consistent with those given in Table 6 and indicate that shear zones need to be of the order of 1 km thick for temperatures to increase within the shear zone solely by mechanical dissipation at strain-rates of 10^{-13} s^{-1}. For faster strain-rates the shear zone can be thinner and temperatures will still increase.

If we explore steady state situations where $\dot{T}^* = 0$ then equation (78) becomes the Bratu Equation (Fowler, 1997, pp 179–199) which has been widely studied especially with respect to combustion physics (Law, 2006). The steady state solutions to Eq. (78) are shown in Fig. 29(b,c) and take two forms depending on the value of *Ar*. If *Ar* is small then the plot of the temperature at the centre of the shear zone, T^{centre} against the Gruntfest Number is known as a folded S-curve (Fig. 29b); if *Ar* is large then this plot is a stretched S-curve (Fig. 29c). The lower branch, PQ, of the solid curve in Fig. 29(b) is stable against perturbations in dissipation as is the upper branch, RS. The middle branch, QR, is unstable. The stretched S-curve of Fig. 29(c) is stable throughout. Since the stretched curve develops for large values of *Ar* high temperature deformations tend to be stable. For an Arrhenius dependence of strain-rate on temperature Veveakis et al. (2010) show that "thermal runaway" is not possible since the curves shown in Fig. 29 (b,c) always have positive slopes at high temperatures.

The dissipation within the shear zone is shown in Fig. 29(d). For the lower stable branch in Fig. 29(b) and for the stretched S-curve in Fig. 29(c) the dissipation remains small and although it is higher in the centre of the shear zone the effect is small and not noticeable at the scale Fig. 29(d) is drawn. For the unstable branch however the dissipation is high and exponentially increases towards the centre of the shear zone. If the shear zone is thick and only deformation and heat conduction operate then this corresponds to an increase in temperature as described by Fleitout and Froidevaux (1980). However, independently of the thickness of the shear zone, the heat generated and corresponding to this dissipation is available to drive other processes such as chemical reactions (including melting) and grain-size reduction according to Eq. (76). The localisation of dissipation resulting from the exponential increase in dissipation towards the centre of the shear zone means that other processes such as mineral reactions and grain-size reduction (corresponding to pseudotachylites, ultracataclasites and ultramylonites) are extremely localised as discussed by Ben-Zion (2008) and Veveakis et al. (2010).

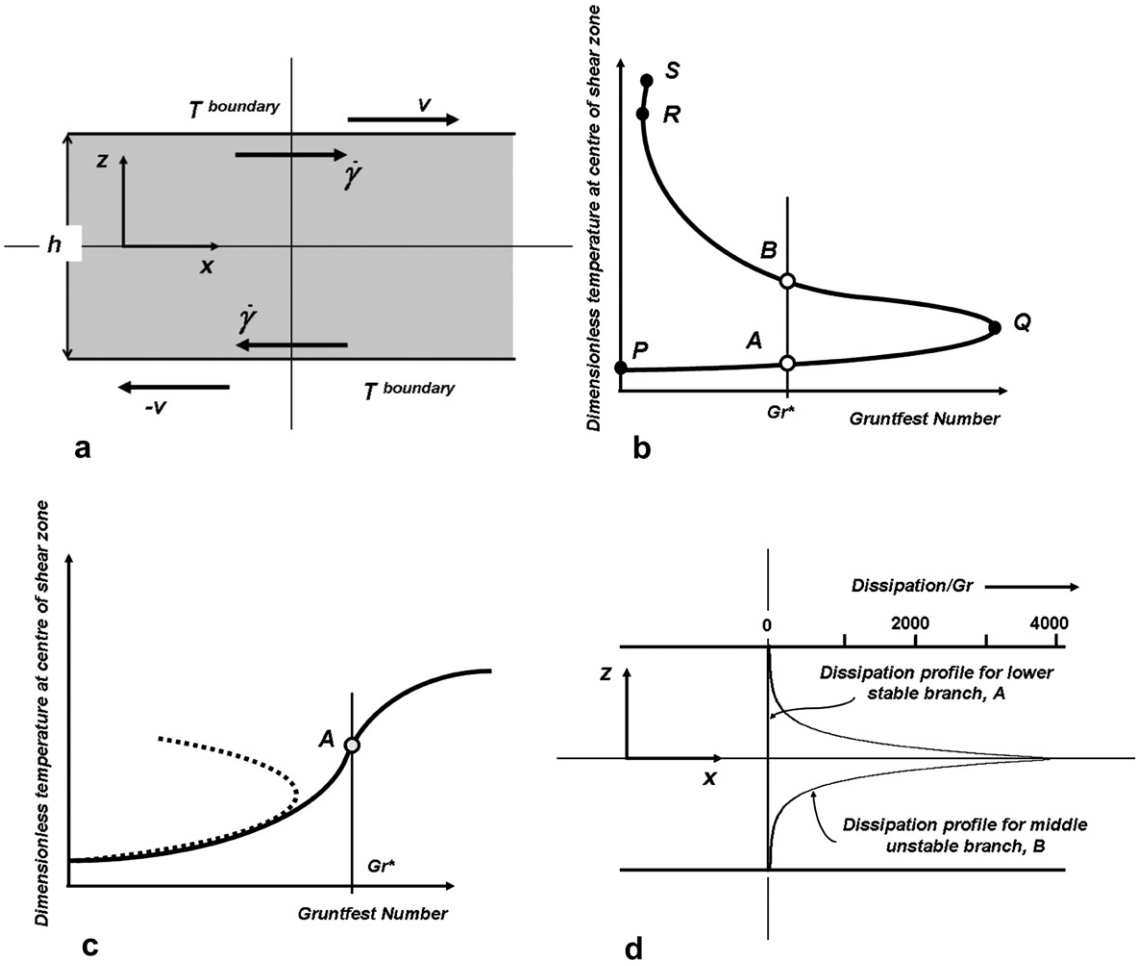

Fig. 29. (a) Shear zone of thickness *h* undergoing simple shearing forced by boundary velocity ***v*** with temperature fixed on the boundaries. (b) Steady state solution to Eq. (78) for small *Ar* demonstrating a folded S-curve on a plot of dimensionless temperature at centre of shear zone versus Gruntfest number. (c) Steady state solution to Eq. (78) for large *Ar* demonstrating a stretched S-curve on a plot of dimensionless temperature at centre of shear zone versus Gruntfest number. (d) Dissipation within the shear zone. After Veveakis et al. (2010).

If the processes involved are deformation, heat conduction and chemical reactions then the Energy Equation (76) reduces to the following two equations as quoted by Veveakis et al. (2010):

$$\dot{T} = \frac{\chi V_o \tau \dot{\gamma}}{c_p}\exp\left(\frac{-\mathcal{Q}}{NRT}\right) - k_o c \exp\left(\frac{-\mathcal{Q}^{chemical}}{RT}\right)\frac{\Delta\mathcal{H}}{c_p} + \kappa^{thermal}\frac{\partial^2 T}{\partial z^2} \tag{79}$$

and

$$\frac{Dc}{Dt} = D\frac{\partial^2 c}{\partial z^2} - k_o c \exp\left(\frac{-\mathcal{Q}^{chemical}}{RT}\right) \tag{80}$$

The solution to Eq. (79) is shown in Fig. 30a. If the $\Delta\mathcal{H}$ of the reaction is positive (an endothermic reaction) then the unstable part of the S-curve tends to be stabilised. If the reaction is exothermic, further destabilisation results. Endothermic mineral reactions correspond to the formation of the common silicates, devolatilisation reactions and melting. Exothermic reactions correspond to the formation of hydrous-silicates (Haack and Zimmermann, 1996) and the crystallisation of melts. Thus the formation of quartz in shear zones and melting are stabilisation processes whereas the formation of hydrous retrogressive mineral assemblages and the crystallisation of melts tend to be destabilising. Presumably grain-size reduction requires the input of energy to generate new surface area and is endothermic and hence is a stabilising process. The dissipation in the upper stable part of the S-curve is shown in Fig. 30b and is much broader (but larger) than in the unstable branch so that these stabilising processes tend to inhibit intense localisation. The initiation of processes such as mineral reactions and grain-size reduction is governed by the value of *Ar* (Law, 2006). Thus the points *A* and *B* in Fig. 30(a) correspond to different values of the activation energies for the reaction (or process in the case of grain-size reduction).

4.15. Overview of Section 4

The important point that simplifies the application of thermodynamics to the microscale is that at tectonic strain-rates a body of rock up to about a metre in size remains approximately isothermal so that the energy equation reduces to a set of coupled reaction-diffusion equations or a set of reaction-diffusion-deformation equations. Equations of this type are well known to exhibit instabilities either temporally, spatially or combinations of both. Some mineral reactions (especially those associated with redox reactions) reported in the literature are autocatalytic and so one expects instabilities at the grain scale with no other forms of coupling. Even though many networked mineral reactions may have the characteristics of classical stable systems one needs to remember that the theoretical background for many of these systems in the literature is for homogeneous systems. Two aspects relevant to metamorphic systems are relevant here. One is the demonstration by Ortoleva and Ross (1974) that heterogeneities arising from localised reaction sites, dissipation of energy from localised deformation sites and gradients in chemical potential can induce instability in the form of compositional oscillations in time and/or travelling diffusion waves in the simplest of stable chemical systems and could be recorded in growing mineral grains as compositional zoning. The second (related) aspect is that coupling deformation or weak infiltration of fluids to a stable reaction-diffusion system can induce instability (Ortoleva, 1989; Rusinov and Zhukov, 2008). Thus one expects a large number of phenomena to arise from networked mineral reactions in deforming metamorphic rocks including compositional zoning, metamorphic differentiation both on the scale of individual grains and on coarser scales associated with the scale of the deformation, and even more complicated patterns such as spiral compositional patterns in porphyroblasts. An additional prediction is that the detailed distribution of mineral phases in a deformed metamorphic rock should be defined by interfaces that have the topology of minimal surfaces. This opens a new field of study that has come to be known as "dissipative crystallography" (De Wit et al. 1997) that is worthy of investigation now that determination of the three dimensional geometry of microstructures by X-ray and other means is available.

A fundamental outcome from these considerations is that microfabrics that form due to coupled reaction-diffusion-deformation processes are controlled in their orientation by the deformation-rate tensor and not the strain tensor. Thus these fabrics reflect the symmetry of the kinematics (cf., Sander, 1911) and not geometrical aspects defined by the strain. In a general non-coaxial deformation history the geometry produced by the evolution of the deformation-rate tensor is quite different to that of the strain tensor. Thus foliations developed by reaction-diffusion-deformation coupling form parallel to a principal plane of the deformation-rate tensor whilst mineral lineations defined by elongate aggregates of like minerals developed by these processes form parallel to a principal axis of the deformation-rate tensor and not the strain tensor. This does not prohibit foliations and lineations formed by distortion of initially equant fabric elements developing parallel to principal planes and axes of strain. The thermodynamic arguments are quite clear that these two classes of foliations and lineations should exist in deformed metamorphic rocks.

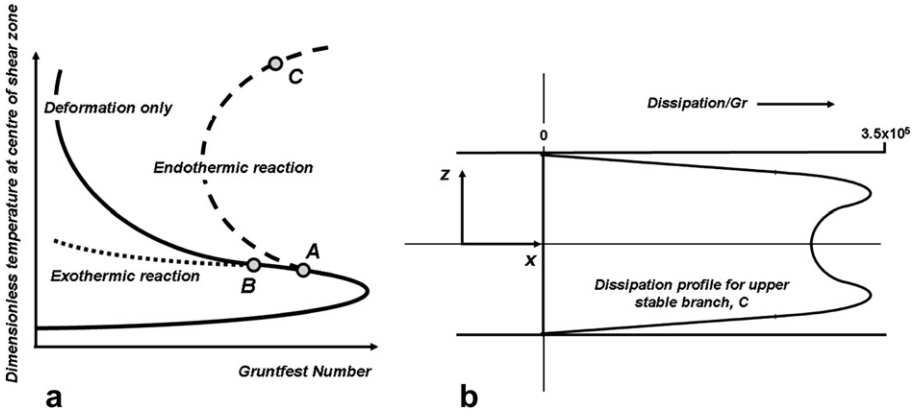

Fig. 30. (a) Solution to Eq. (79) on a plot of dimensionless temperature at centre of shear zone versus Gruntfest Number. (b) Dissipation in the upper stable part of the S-curve.

Another approach to the origin of microstructure comes from the demonstration that the Helmholtz energy of a polycrystalline aggregate is minimised if the deformation can be accomplished by shear strains parallel to a single plane as in the situation for single slip in a crystal. This however means that the Helmholtz energy as a function of the deformation, which is convex in classical theories of plasticity, becomes non-convex. The theory that develops from this lack of convexity is the same as for classical critical systems. It is identical in principle to that for the development of two phases in Equilibrium Chemical Thermodynamics, or for the development of microstructure in (non-linear elastic) martensitic transformations and for the behaviour of systems undergoing phase transitions (critical systems). A homogeneous deformation is no longer stable and the system splits into two domains in order to minimise the non-convex Helmholtz energy. Each domain is characterised by a different deformation gradient if an instant of time is considered or by a different kinematic history if integrated over the complete deformation history of the polycrystal. However there is another constraint in that two levels of microstructural development are not sufficient to match an arbitrary three dimensional deformation gradient for the polycrystal as a whole and complete matching needs at least three levels of microstructure and commonly more than three. This leads to an explanation for rotation recrystallisation, fractal measures of grain boundaries and grain-size and an explanation of core-mantle fabrics in partially recrystallised polycrystals. The process also leads to a relaxation of long range stresses at the same time as completely fulfilling strain compatibility issues so that the development of crystallographic preferred orientation solely by single slip is not only explained but emerges as the preferred mechanism in that it minimises the Helmholtz energy. Again, the symmetry of the fabric reflects the symmetry of the kinematics not of the strain. The coupling of deformation to mineral reactions also leads to strain-rate softening and hence the development of shear bands, micro-folds and micro-boudinage but the details of this form of coupling are left to Section 5.

5. The intermediate scale

At the scale of about 1–100 m and tectonic strain-rates of say 10^{-12} s^{-1} heat that is generated in a system by any dissipative process, including deformation, diffuses out of the system in 10^6–10^{10} s; these time scales are to be compared with the time scale of 10^{11} s needed to reach 10% strain. Thus a volume of rock smaller than 100 m cube will remain isothermal on time scales of say 10^{12} s (3.171×10^4 yrs). Also, dissipation due to mass diffusion takes place on a smaller spatial scale. This means that the Energy Equation (26) becomes

$$\sigma_{ij}\dot{\varepsilon}_{ij}^{dissipative} = \sum_K \left(\Phi^{chemical}\right)^K = \mathbb{C} \tag{81}$$

where $\mathbb{C}$, the total chemical dissipation arising from all of the chemical reactions. $\Phi^{chemical}$, is given by Eq. (23c). The implication of Eq. (81) is that the dissipation arising from deformation can be used to increase the rates of chemical reactions at this scale. The assumption that the $V_o\mu_K\dot{m}_K$ term in Eq. (26) is not important means that we do not expect metamorphic differentiation at this scale that arises from reaction-diffusion processes although differentiation is possible at these scales if the "diffusion" process is by mass transport in a fluid. This process is beyond the scope of this review but aspects have been treated by Ortoleva (1994) and Rusinov and Zhukov (2008). In Section 4.14 we discussed the analysis of Veveakis et al. (2010) which involves a situation similar to the one proposed here except that Veveakis et al. are concerned with faster strain-rates (associated with land-slides and seismic events). As posed, the discussion of Veveakis et al. (2010) applies to a much smaller spatial scale and is applicable at fast strain-rates; we will follow their approach at the regional scale at tectonic strain-rates. As indicated in Table 6 the scale of importance of these effects depends on the strain-rate. Below we develop the argument for the 1–100 m scale at tectonic strain-rates.

5.1. Chemical-deformation feedback

Consider a material undergoing simple shearing as shown in Fig. 29(a) in which chemical reactions may also be progressing. Then Eq. (81) reduces to $\tau\dot{\gamma} = \mathbb{C}$ which for a power-law viscous material becomes

$$\eta^{effective}\dot{\gamma}^{\frac{2}{N}} = \mathbb{C} \tag{82}$$

where the effective viscosity given by $\eta^{effective} = \eta(\gamma, \dot{\gamma}, T) = \frac{\tau(\gamma,T)}{\dot{\gamma}}$ is taken to be a function of shear strain, $f(\gamma)$, strain-rate, and temperature. Thus

$$\eta^{effective} = \mathbb{C}\dot{\gamma}^{-\frac{2}{N}} \tag{83}$$

which says that, for chemical dissipation that is independent of the strain-rate, the viscosity varies inversely with the strain-rate for $N > 0$. Note that the effective viscosity is also observed to be a function, $f(\gamma)$, of the strain. Perhaps mineral reactions are also a function of strain-rate and such dependence would alter Eq. (83) but since there appears to be no experimental work to support a dependence of mineral reaction rates on strain-rate we neglect such effects here. We also neglect the influence of strain softening or hardening as expressed by $f(\gamma)$. This means that the material softens as the strain-rate increases. This is known as *strain-rate softening* and is illustrated in Fig. 31(b) for power-law rate dependent materials. If $N > 0$ and there is no coupling to other processes then a sudden increase in strain-rate causes a jump in the stress (Fig. 31a) and if no other processes operate the stress settles down to a value larger than the stress corresponding to the initial strain-rate. This is known as *strain-rate hardening* behaviour and is an intrinsic property of rate sensitive materials with $N > 0$. The effect is greatest for $N = 1$ and becomes less important the larger N becomes, that is, as the material becomes less rate sensitive. However if some other process operates to change the effective viscosity then it is possible for the stress to settle down to a value less than that for the initial strain-rate (Fig. 31b). Typical examples include diffusion coupled with deformation in some alloys (Estrin and Kubin, 1991) and thermal–mechanical feedback (Regenauer-Lieb and Yuen, 2003; Hobbs et al., 2008). Strain-rate softening leads to localisation of deformation (Needleman, 1988; Estrin and Kubin, 1991; Wang et al. 1997) and is the important process necessary in rate sensitive materials in order to promote significant localisation.

Eq. (83) is an example of chemical strain-rate softening and is similar in form to Eq. (75). The chemical–mechanical feedback interactions here mean that mineral reactions tend to proceed to completion in some terrains whilst immediately adjacent undeformed or less deformed areas remain un-reacted (Hobbs et al. 2010a). Strain-rate hardening and softening behaviour is formally identical to velocity strengthening and weakening behaviour during frictional sliding (Ruina, 1983) and the analogue between the two classes of behaviour has been explored by Mesarovic (1995) and Kameyama (2003).

The introduction of strain-rate softening into the constitutive behaviour of rate dependent materials means that the thermodynamic flux (the strain-rate) is no longer a linear function of the thermodynamic force (the stress) and so, as shown by Ross and Vlad (2005), there is no extremum in the entropy production rate.

Hence, in particular, the principle of maximum entropy production rate of Biot and Ziegler no longer holds and in order to solve problems recourse to the Clausius–Duhem relation is necessary.

5.2. Localisation of deformation

In rate-independent materials such as are commonly represented for rocks by Mohr–Coulomb, Drucker–Prager or Cam–Clay constitutive relations, localisation of deformation derives from strain softening and/or from the presence of corners on the yield surface (Hobbs et al., 1990). This observation has lead to the widespread presumption in the geosciences that strain softening is a necessary condition for the development of localisation in all materials whether they be rate-dependent or rate-independent. One should note that localisation can occur in strain-hardening materials (Rudnicki and Rice, 1975; Ord et al. 1991). Moreover, in strain softening rate-dependent materials with $N > 0$ and no other feedback mechanisms there is always a jump in stress associated with a jump in strain-rate (Fig. 31) so that any increase in strain-rate resulting from localisation means that the associated increase in stress tends to offset any intrinsic strain-weakening. Thus it is difficult to induce intense localisation of deformation in rate dependent materials through strain softening alone as shown by Mancktelow (2002); the difficulty decreases as N increases, that is, as the material becomes more rate insensitive. Thus Mancktelow (2002) shows that localisation in strain softening power-law (with $N = 5$) is better developed than in strain softening Newtonian ($N = 1$) materials. However the localisation in such materials is not as intense as in natural examples such as those described by Ramsay (1967). Hobbs et al. (2009) show that if strain-rate softening is introduced then localisation is facilitated and is able to develop in both strain-softening and strain-hardening materials (Fig. 32). The effect has been analysed for strain-softening and strain-hardening materials by Needleman (1988) and Wang et al. (1997) and is well known in strain-rate softening alloys that show both strain softening and hardening (Estrin and Kubin, 1991). In particular Needleman (1988) shows that strain softening in rate sensitive materials is not a necessary condition for localisation.

5.3. Folding

One important discipline that has grown substantially over the past 30 years but which is poorly represented within structural geology is non-linear bifurcation theory (Guckenheimer and Holmes, 1986; Wiggins, 2003). A basic concept is that a deforming system, given the necessary boundary conditions and/or constitutive relations can behave in a number of ways with resultant patterns of deformation (Fig. 33) that are: (i) homogeneous, (ii) periodic, (iii) localised, and (iv) chaotic. As Champneys et al. (1997) point out: "*A response of a physical system that is localised to some portion of a distinguished coordinate (either space or time) is surely the next most fundamental state after homogeneous equilibrium and periodicity*". In principle a particular system can exhibit all four modes of deformation during a progressive deformation depending on the way in which the constitutive behaviour evolves during deformation.

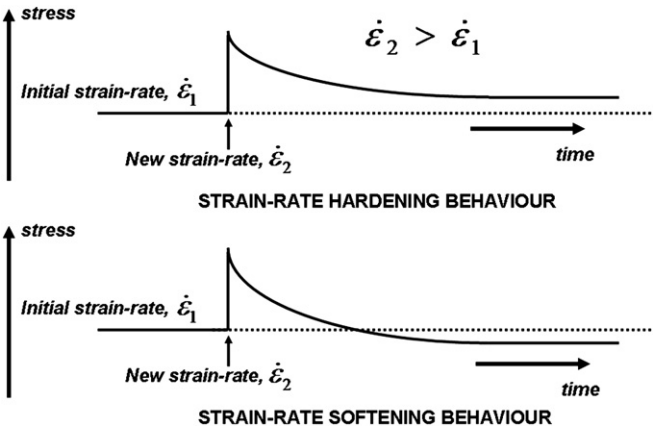

Fig. 31. Strain-rate hardening and softening behaviour in power-law rate dependent materials with $N > 0$. (a) Strain-rate hardening. A sudden increase in strain-rate leads to a rapid increase in stress followed by a slow evolution to a stress which is higher than the initial stress. (b) Strain-rate softening. After the initial response, the stress evolves to a stress lower than the initial stress.

In addition to these four fundamental modes of deformation, in both the localised mode and the chaotic mode, order can appear due to mode locking that arises when the growth of particular wavelengths reinforces the growth of others to produce periodic patterns (so called Arnol'd tongue effects, Hunt and Everall, 1999). Most of the literature within structural geology in the past 30 years has been devoted to elaborations upon Biot's theory which predicts (see discussion below) a strictly periodic response to deformation of both single- and multi-layered materials. The concept of localised folding involves the development of localised packets of folds (Tvergaard and Needleman, 1980) rather than a single periodic train of folds as shown in Fig. 33. The subject of localised and chaotic folding is yet to be fully explored and developed within structural geology but is clearly a rich and fertile field of endeavour. Natural examples of localised folding are given in Fig. 34. It is notable that the experiments by Ramsay (1967) using layered clay models produced localised folds (see Ramsay, 1967, Figs. 3–51, 7–29 and 7–35).

5.3.1. Biot's theory of folding

The emphasis over the past 30 years as far as folding theory is concerned has been on the periodic mode of deformation (Biot, 1965; Fletcher, 1974; Smith, 1975, 1977, 1998; Johnson and Fletcher, 1994a, b; Hudleston and Treagus, 2010) and has been extremely influential in guiding thoughts on natural fold systems. We briefly outline the Biot theory of folding in order to highlight its strengths and limitations. The single layer situation is shown in Fig. 35 to emphasise that two different end member boundary conditions have been considered in the literature, namely constant force (Fig. 35a) and constant velocity (Fig. 35b) conditions. In Fig. 35(a) a dead weight of X kg loads a single layer of viscosity η^L embedded in material with viscosity η^E with $\eta^L > \eta^E$ whilst in Fig. 35(b) the same model is shortened with constant velocity $\boldsymbol{v}$ at each end. It is important to appreciate the dynamic and kinematic differences between these two boundary conditions. The dead weight is rigid so that the interface with the model remains planar during subsequent deformation. This is the experimental configuration adopted by Biot et al. (1961) in the experimental confirmation of his theory except that in that study only the layer was loaded. Since the embedding material is weaker than the layer the dead weight in Fig. 35(a) is mainly supported by the layer and exerts a constant force within the layer independently of the constitutive behaviour of the material; a constant force boundary condition applied to the ends of the model without the added constraint that the ends remain planar would distort the ends of the specimen. The constant velocity boundary conditions in Fig. 35 (b) mean, by definition, that there is no acceleration at the ends and hence no force is exerted at the ends; the constant velocity conditions are purely kinematic in character and as the model shortens stresses are developed within the model depending on the deformation-rate and the constitutive behaviour of the material.

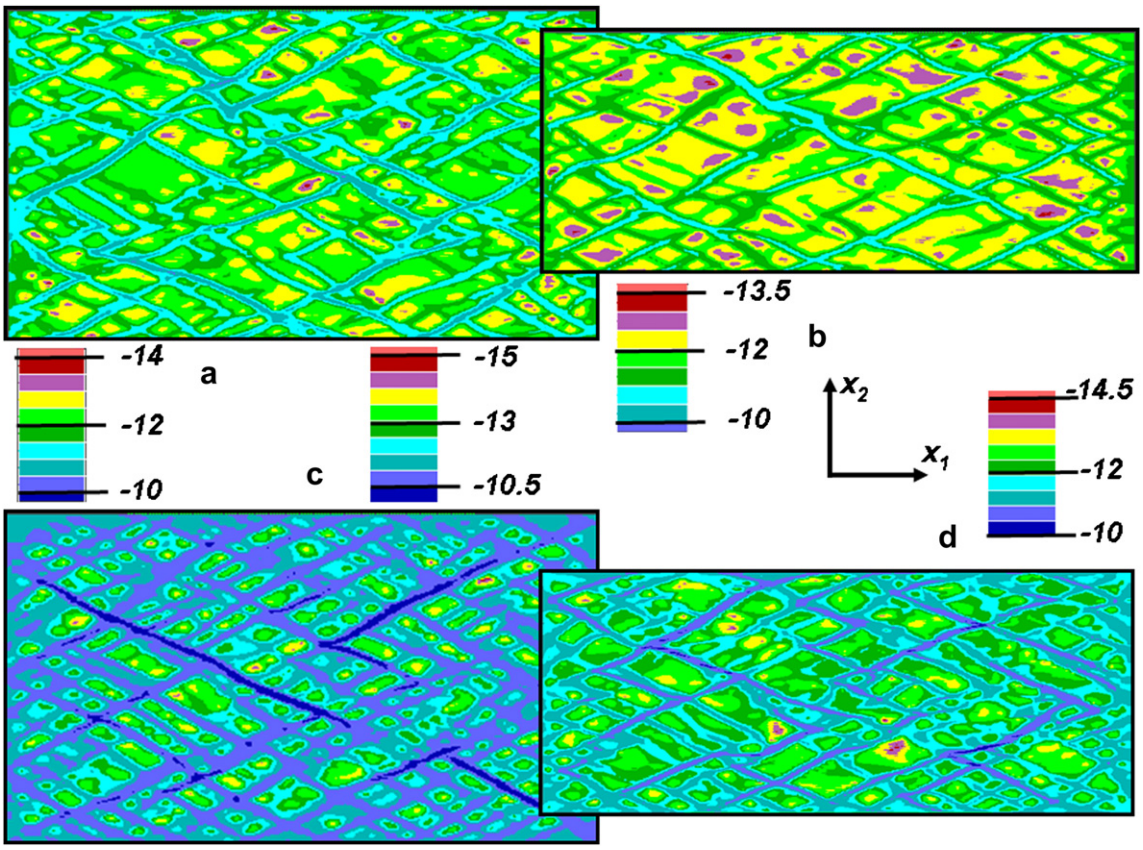

Fig. 32. Localisation of deformation in strain-rate softening materials (after Hobbs et al. 2009). Plots of the logarithm of the square root of the second invariant of the viscous strain-rate. (a) Strain softening; shortening 40%. (b) Strain softening; shortening 50%. (c) Strain hardening; shortening 40%. (d) Strain hardening; shortening 50%.

Biot (1965) developed a theory for folding in which the force in the layer remains constant (corresponding to Fig. 35a) and showed that any small perturbations from strict planarity in the embedded layer are unstable and grow with continued deformation driven by the force in the layer. The growth rates for individual perturbations are independent of all others so that the growing wavelengths can be represented as a Fourier series and the emphasis is on identifying the fastest growing wavelength; this then becomes the dominant wavelength. This wavelength is proportional to the layer thickness and depends weakly (the cubic root) on the ratio of the mechanical properties (viscosities in the case of Fig. 35) of the layers making up the model. The Biot theory is a linear theory (Hunt et al., 1997b) and holds strictly for small deflections; it has been well developed for single layers embedded in a weaker matrix (Biot, 1965; Sherwin and Chapple, 1968; Smith, 1975, 1977, 1979; Fletcher, 1974) and for multilayers (Biot, 1965; Johnson and Fletcher, 1994a, b). In particular the influence of variations in thicknesses and mechanical properties in multilayer folding has been extensively studied (Johnson and Fletcher, 1994a, b; Frehner and Schmalholz, 2006; Schmid and Podladchikov, 2006; Treagus and Fletcher, 2009). A review of some aspects of the theory is given by Hudleston and Treagus (2010). For single layer elastic–viscous systems the Biot theory predicts the development of two wavelengths for some combinations of elastic moduli and viscosity (Mühlhaus et al., 1998; Jeng et al., 2002; Jeng and Huang, 2008) although one should appreciate that the physical conditions for two wavelengths to develop by such a mechanism in natural folds is unlikely.

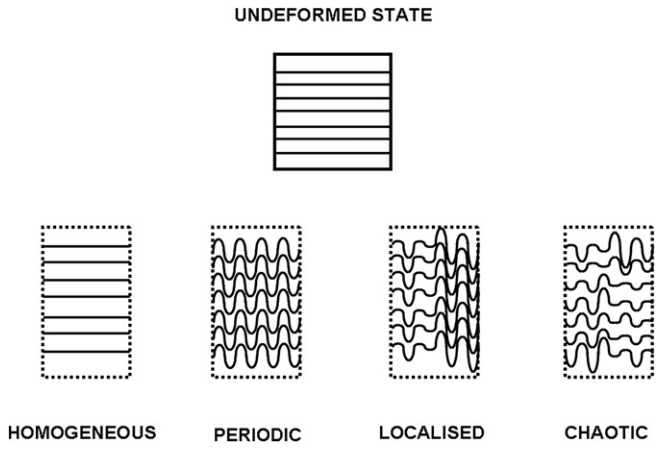

Fig. 33. The four fundamental deformation modes of a multilayer material.

For finite deformations the two types of boundary conditions in Fig. 35 result in quite different behaviours although at small strains (where the Biot theory has been mainly developed) the two behaviours are essentially the same. At large strains the constant force boundary condition produces exponential growth rates for fold development as the boundaries accelerate whereas the constant velocity boundary condition produces rapid amplification at first but a decreasing amplification rate as the force in the layer decreases (Fig. 36a) and shortening progresses (Fig. 36b). In

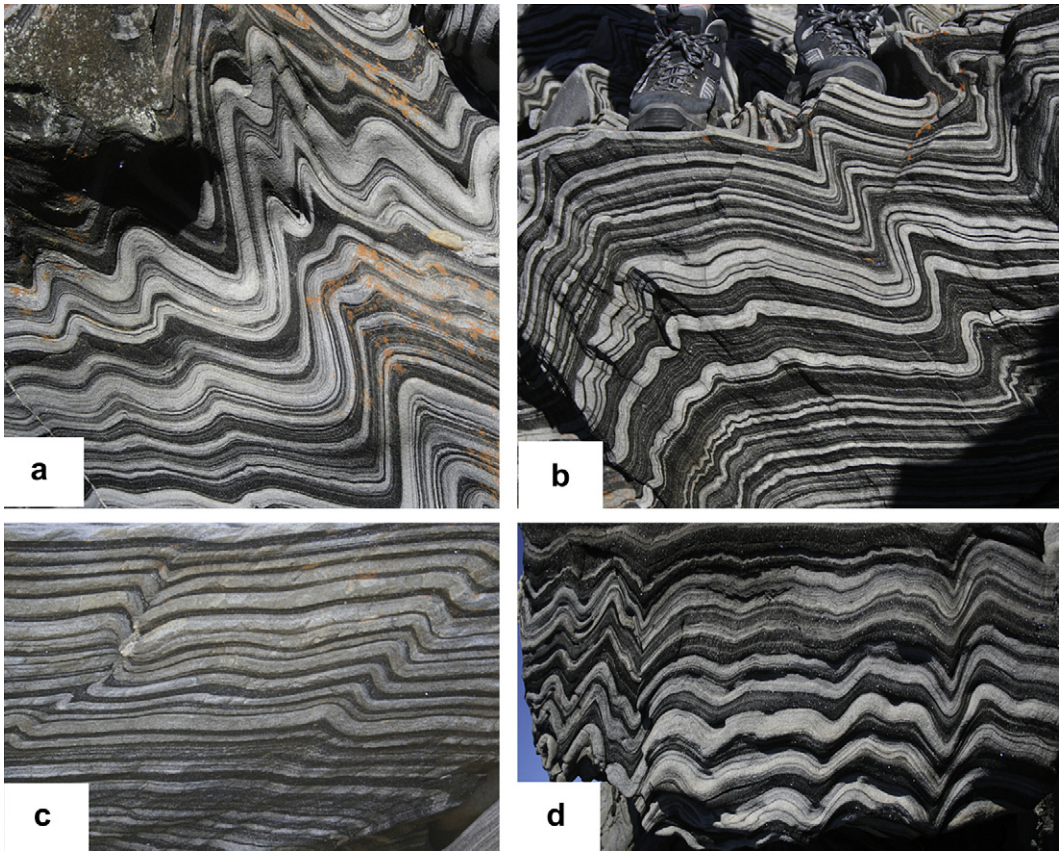

Fig. 34. Examples of localised folding. Kangaroo Island, South Australia. Scale is approximately the same in all frames and is given by the boots in (b).

the latter case initial deflections that develop early in the folding history are amplified by an essentially homogeneous deformation later in the history whereas in the former case the fold continues to grow exponentially as the boundaries of the system accelerate under the influence of the imposed force. Analytical solutions for constant velocity boundary conditions and for large deformations are given by Muhlhaus et al. (1994) and summarised by Hobbs et al. (2008). The same effect of boundary conditions exists for both single and multi-layer folding. The pragmatic outcome of the influence of boundary conditions is that one cannot say anything about the viscosity ratios (for purely viscous layers) unless one knows the nature of the boundary conditions. As an example linear viscous materials predict dominant wavelengths that are comparable to natural situations for realistic growth rates for constant force boundary conditions and for viscosity ratios as low as 20 if initial layer parallel shortening is taken into account (Sherwin and Chapple, 1968). However for constant velocity conditions amplification rates are relatively small and for the same values of amplification considered by Sherwin and Chapple (1968) realistic folds do not develop unless viscosity ratios are of the order of 1000 to 3000 (see Fig. 2 in Hobbs et al., 2008; Muhlhaus et al., 1994).

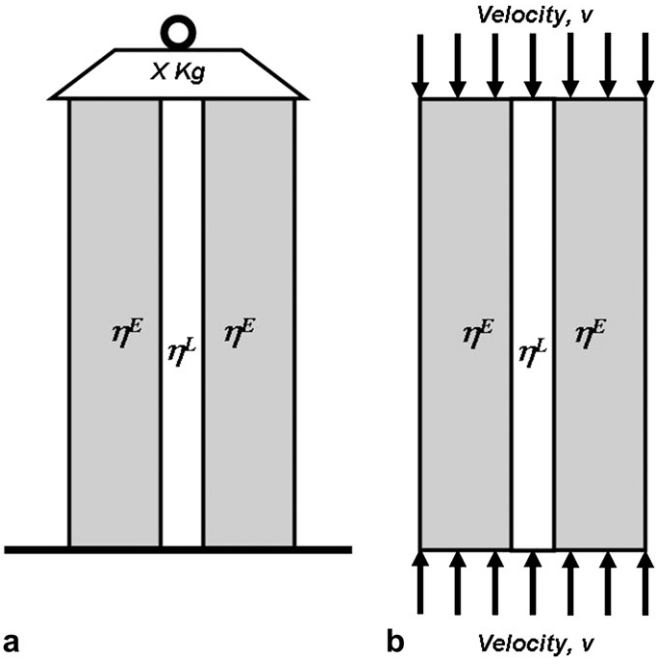

Fig. 35. Boundary conditions for folding. (a) Constant force conditions applied as a dead weight. (b) Constant velocity conditions.

The extension of the theory to large deflections for viscous single layers is made by Muhlhaus et al. (1994, 1998) where it is shown analytically that in two dimensions the fold system that develops at large deformations remains strictly periodic as predicted by the Biot theory at small deflections. In three dimensions (Mühlhaus et al., 1998; Schmid et al., 2010) another wavelength is always present, even for plane strains, along the fold axis within the axial plane and is expressed as culminations and depressions. This effect arises from the dispersion function shown in Fig. 15 where a weak maximum exists for a wave vector parallel to D_2.

There is a relatively large literature (Sherwin and Chapple, 1968; Hudleston, 1973a, b; Shimamoto and Hara, 1976; Fletcher and Sherwin, 1978) that documents a range of wavelength to thickness

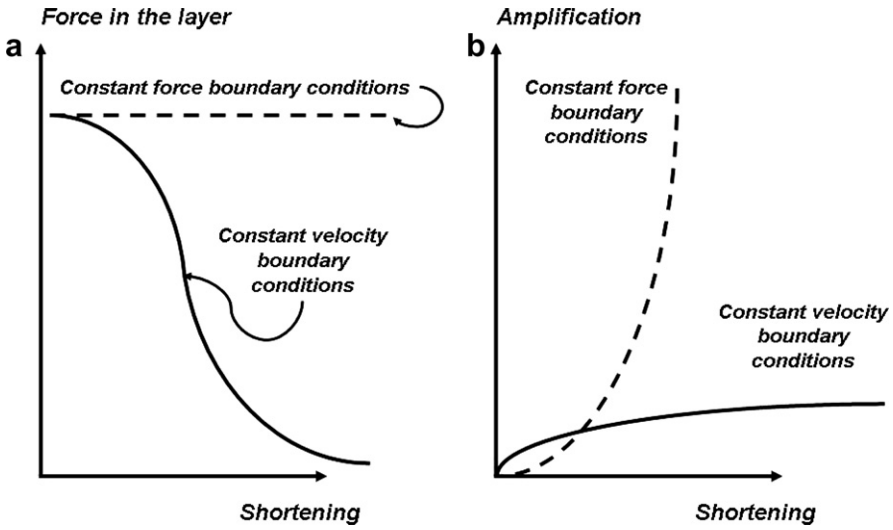

Fig. 36. Behaviour of a single layer elastic–viscous system for constant force and constant velocity boundary conditions. (a) History of force in the layer with deformation to large shortenings. As prescribed, the force in the layer remains constant for constant force boundary conditions, but for constant velocity boundary conditions there is no force at the boundary and any initial force decays to small values depending on the ratio of the viscosities in the layer and in the embedding medium. (b) Amplification of initial perturbations in the layer with increased shortening. For constant force boundary conditions the growth rate is exponential and is driven by the acceleration of the boundary. For constant velocity boundary conditions there is no force on the boundary and the amplification decreases with the amount of shortening so that eventually the only deformation consists of homogeneous amplification of early formed fold structures.

ratios within a single natural fold system. This has been taken to mean that the dispersion function as predicted by the Biot theory is relatively flat so that there is a large probability that a range of wavelengths near to the dominant wavelength will have similar amplification rates. This is not supported by analytical solutions for finite amplitude growth of initial perturbations (Mühlhaus et al., 1998) where the dispersion function is quite sharply peaked. The spread in observed wavelength to thickness ratios is not what one would expect from the Biot theory for finite deformations and one is forced to the conclusion, given the data presented in the above papers that processes other than those incorporated in the Biot theory are operating in natural fold systems.

It is possible in computer simulations of folding in materials that do not exhibit strain-rate softening to produce non-periodic fold systems or fold systems with a range of wavelength to thickness ratios (Fig. 37). Such computer simulations could be taken as confirmation of the above assertion that the Biot theory implies the aperiodic behaviour observed in natural examples. However one should be careful to observe that the irregular wave forms that appear in Fig. 37 are an artefact of the computational model and result from the finite size of the "box" in which the simulations are performed. The figure shows a progressive change of thickness of the layer from 25 units to 9 units with the same boundary conditions and viscosity ratio between layer and embedding material in all cases. In doing so the system tries to fit 9 wavelengths into the box for a thickness of 25 units and 10 wavelengths for a thickness of 9 units. For thicknesses in between the 25 and 9 units of thickness irregular fold profiles develop because of the inability of the pattern to fit into the space available. This is a purely a geometrical constraint issue and has nothing to do with predictions made by the Biot theory. The same effect will influence the shapes of folds in finite sized physical models.

5.3.2. Localised folding

What causes the development of localised folding? The answer lies in the development of softening behaviour of some form or other (Tvergaard and Needleman, 1980). In rate independent materials this involves strain softening but in rate dependent materials strain-rate softening is fundamental. In thinly layered materials geometrical softening seems to be sufficient to induce localised structures (Ortiz and Repetto, 1999); most work to date has involved elastic thinly layered materials and layers embedded in a softening matrix. The development of localised structures during martensitic transformations is well known (Ericksen, 1998). Hunt et al. (2000) have developed the theory of folding for thinly layered rate insensitive materials and have shown that geometrical softening (in the manner discussed in Section 4.10 for slip in single crystals) leads to a non-convex Helmholtz energy and the development of kink and chevron

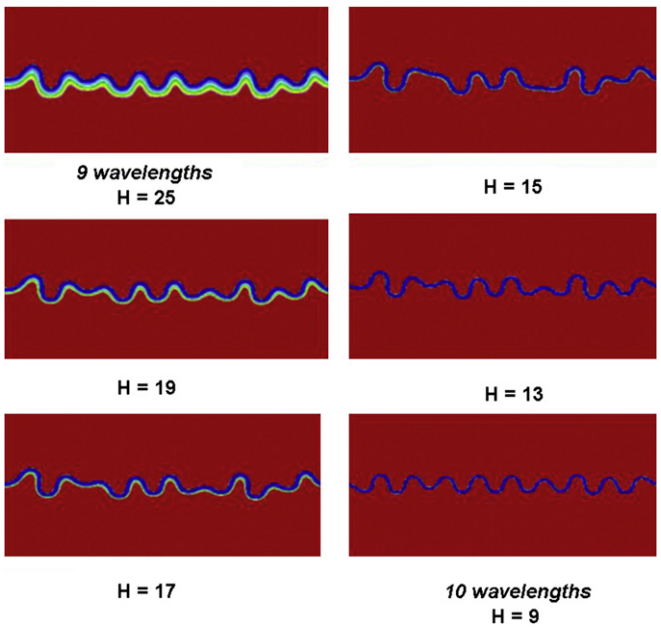

Fig. 37. Fold systems with a range of wavelength to thickness ratios. All models shortened 40%. H = initial thickness of layer. The fold train almost fits into the "box" with 9 wavelengths for $H = 25$ and fits the "box" for $H = 9$ with 10 wavelengths quite well. In between irregular fold trains develop in order better to fit the "box".

folds. The Maxwell construction is used to indicate the critical stress for the initiation of folding when the Helmholtz energy (in the form of either elastic or plastic stored energy) in the system is sufficient to promote or drive slip on the layers. The development of individual regions of homogeneous deformation in order to minimise the (non-convex) Helmholtz energy produces the structures illustrated in Fig. 21. As in Section 4.10, there is an additional requirement that the array of homogeneously deformed areas (that is, the limbs of the folds) match the imposed deformation gradient. The argument is identical to that developed in Section 4.10 except in this case there are multiple low energy wells in the Helmholtz function and the folds develop sequentially (Budd et al., 2001). Fig. 38 is presented as an example of fold systems that form in order to minimise the Helmholtz energy.

Another aspect to the development of folds in rate sensitive materials occurs if the layers are thick and some form of strain softening (such as damage-induced softening, Lyakhovsky et al., 1997) other than geometrical softening occurs. We have seen from Section 4.10 that softening implies that the Helmholtz energy becomes non-convex. Hunt et al. (1989) and Hunt and Wadee (1991) show that for a layer embedded in a softening material, localised folding is the preferred mode of deformation to minimise the non-convex energy function (Fig. 39). Hunt et al. (1997a,b) also show that the localised packets of folds that do occur are very sensitive to initial conditions and that chaotic responses can develop (Fig. 40).

In rate sensitive materials strain-rate softening can be important and examples for fold development in layered materials are shown in Figs. 41 and 42. Fig. 41(a) shows a multilayer model that exhibits strain-rate softening and strain-hardening shortened parallel to the layers by 12%. The effective viscosity, which began as uniform at 10^{20} Pa s in the layers and at 10^{19} Pa s in the matrix is now patterned in the form of localised shear zones in the matrix and as changes associated with weak buckling in the layers. At 30% shortening (Fig. 41b) the pattern of high effective viscosity on the outer arcs of buckles and low viscosity in the inner arc is well developed and shown in profile in Fig. 41(d). This kind of deformation is commonly associated with relatively high strain-rates in the inner arc as shown in Fig. 41(c) and results in reverse "dimples" on the inner arc characteristic of some natural folds. By analogy with Fig. 39 it is probable that the Biot mechanism operates to produce initial periodic deflections in the layers but strain-rate softening soon dominates and initiates localised folding. The analysis of Tvergaard and Needleman (1980) is particularly instructive here. They show that at the peak of the stress–strain curve (point A in Fig. 39) the fold system is periodic and presumably this fold system has the characteristics predicted by the Biot theory. Hunt and Wadee (1991) show that the Helmholtz energy at this point is convex. At some stage during softening after yield (Point B in Fig. 39) the Helmholtz energy becomes non-convex (due to softening) and the initial periodic wave form localises. This point is a critical point in the system evolution and localisation characterises the system with increased deformation. The system is particularly sensitive to the degree of softening and the chaotic behaviour of Fig. 40 can result. As Tvergaard and Needleman (1980) point out: the final localised pattern of folding bears little resemblance to the periodic fold pattern developed at the peak of stress.

Fig. 42 contrasts the development of folds in a single layer for materials without (Fig. 42a,b) and with (Fig. 42c,d) strain-rate softening and with constant velocity boundary conditions. The initial viscosity ratio in both cases is 200. By 44% shortening the model without strain-rate softening (a) has developed a more or less periodic train of folds whereas the model with strain-rate softening (c) has developed localised folds with no dominant wavelength. An extra 6% of shortening makes very little difference to the model with no strain-rate softening (b) because by now the deformation in that model is essentially homogeneous shortening with very little fold amplification. The model with strain-rate softening (d) shows rapid tightening and growth of the fold profiles.

Fig. 38. Chevron folds developed in thinly bedded shales and sandstones at Millook Haven, Cornwall, UK. Photograph by Giles Hunt.

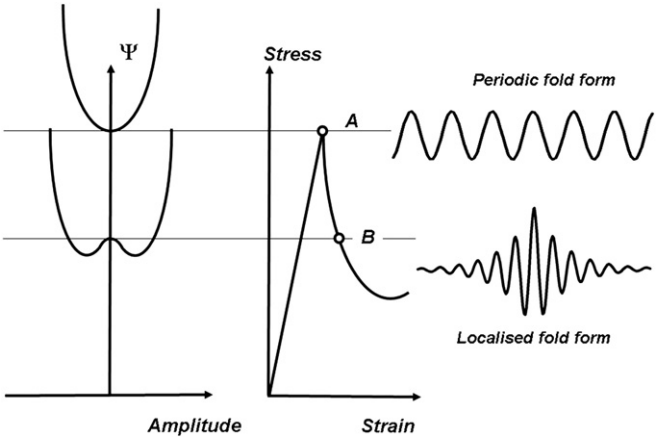

Fig. 39. Development of periodic and localised fold forms for a softening stress–strain curve. The periodic wave form develops at the peak (A) of the stress–strain curve and corresponds to a convex Helmholtz energy function (Ψ). At a smaller stress (B), a localised wave form has developed corresponding to a non-convex Helmholtz energy function. The non-convexity in Ψ arises from the softening in the stress–strain relation.

5.4. Implications of the mathematical structure of folding theory

The form of the mathematical equations that govern the development of folds in layered metamorphic rocks presents a framework that holds promise for integrating the development of folds, mineral reactions and the development of axial plane structures. A complete theory has not yet been developed and the following discussion is meant to indicate the potential for future developments. The geometry of the situation is shown in Fig. 43(a) where a layer whose thickness to wavelength ratio is small is embedded in a material that here is represented as an array of elastic springs and viscous dashpots. Such an embedding material is known as a Winkler material; other types of embedding materials are discussed by Kerr (1964) and in particular Biot (1965) considered a material where the response in Fig. 43(a) is linear. It turns out that the rheological nature of the embedding material is fundamental for the subsequent buckling behaviour of the layer and of course this rheological behaviour is controlled by the metamorphic reactions taking place in the material together with the spatial distribution of the metamorphic products.

The general expression that describes the development of a folded layer to high deflections is (Thompson and Hunt, 1973):

$$Q\left[w''''\left(1-w'^2\right)^{-1}+4w'''w''w'\left(1-w'^2\right)^{-2}+w''^3\left(1+3w'^2\right)\times\left(1-w'^2\right)^{-3}\right]+Pw''\left(1-w'^2\right)^{-3/2}+F(w)=0 \tag{84}$$

where $w(x, t)$ is the deflection of the beam, x in this case is measured along the length of the deflected beam, $w'=\frac{\partial w}{\partial x}$ with a similar definition for higher order primes, Q is a term that describes the mechanical properties of the layer, P is the force parallel to the layer and $F(w)$ is the restoring force per unit length that the embedding medium exerts on the layer.

Following Biot (1965) most authors in the geological literature assume w' is small enough that terms such as w'^2 can be neglected so that Eq. (84) reduces to

$$Q\frac{\partial^4 w}{\partial x^4}+P\frac{\partial^2 w}{\partial x^2}+F=0 \tag{85}$$

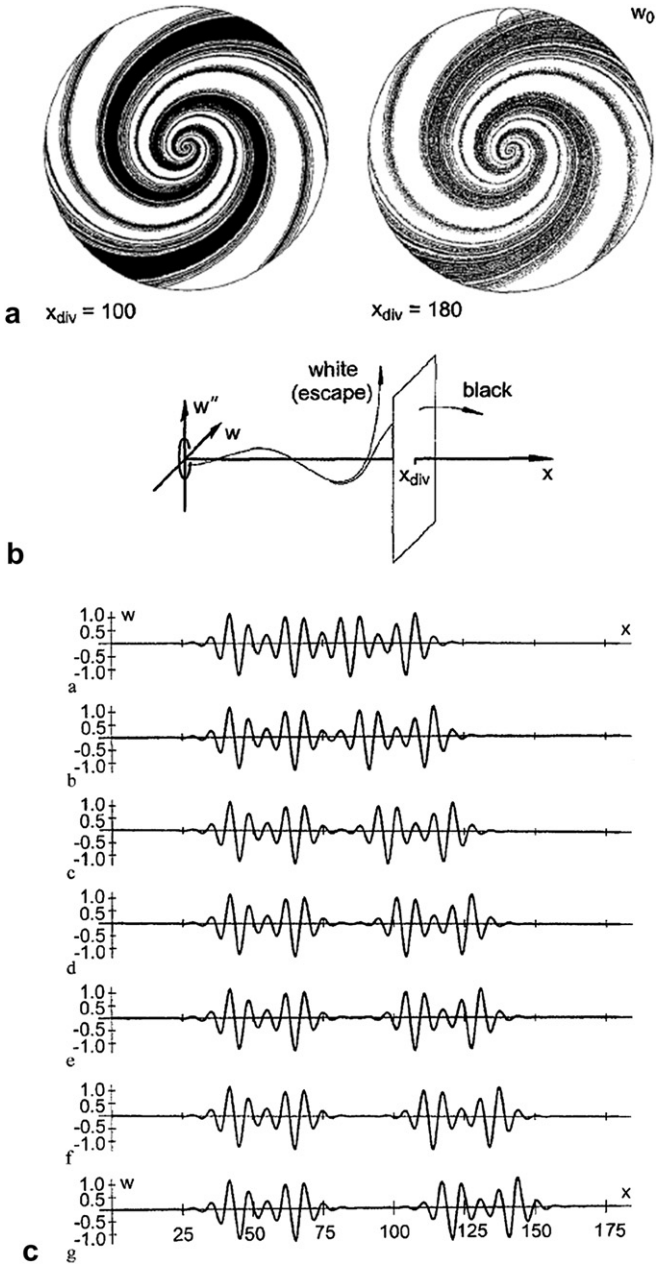

Fig. 40. Localised folding and fractal behaviour arising from buckling of a layer in a softening embedding medium (From Hunt et al., 1996). (a) Fractal phase portraits arising from variations in initial conditions shown in (b). (b) Small variations indicated by the circle at the origin in the initial displacement, w, and initial acceleration, w'', result in localisation (black) or no localisation (white) at a distance x_{div} along the layer. (c) Plots of displacement, w, against distance along the layer, x, for various initial values of w and w'' (see Hunt et al., 1996, for details).

If one remembers that as an example, for a limb dip as low as 30°, $w'^2 \approx (\sin 30^\circ)^2 = 0.25$ one sees that the classical Biot formulation is restricted to quite small limb dips. Biot (1937) derived a linear form of $F(w)$ that is also dependent on the wave-number of the deflection of the folding layer. This is the relationship adopted by most workers in structural geology since Biot. It is mathematically convenient since it means that the folding problem can be considered as a large number of non-interacting waves and the issue becomes one of selecting the fastest growing wavelength. The solutions are strictly periodic and only one wavelength survives to become the dominant wavelength as shown analytically by Muhlhaus et al. (1994, 1998).

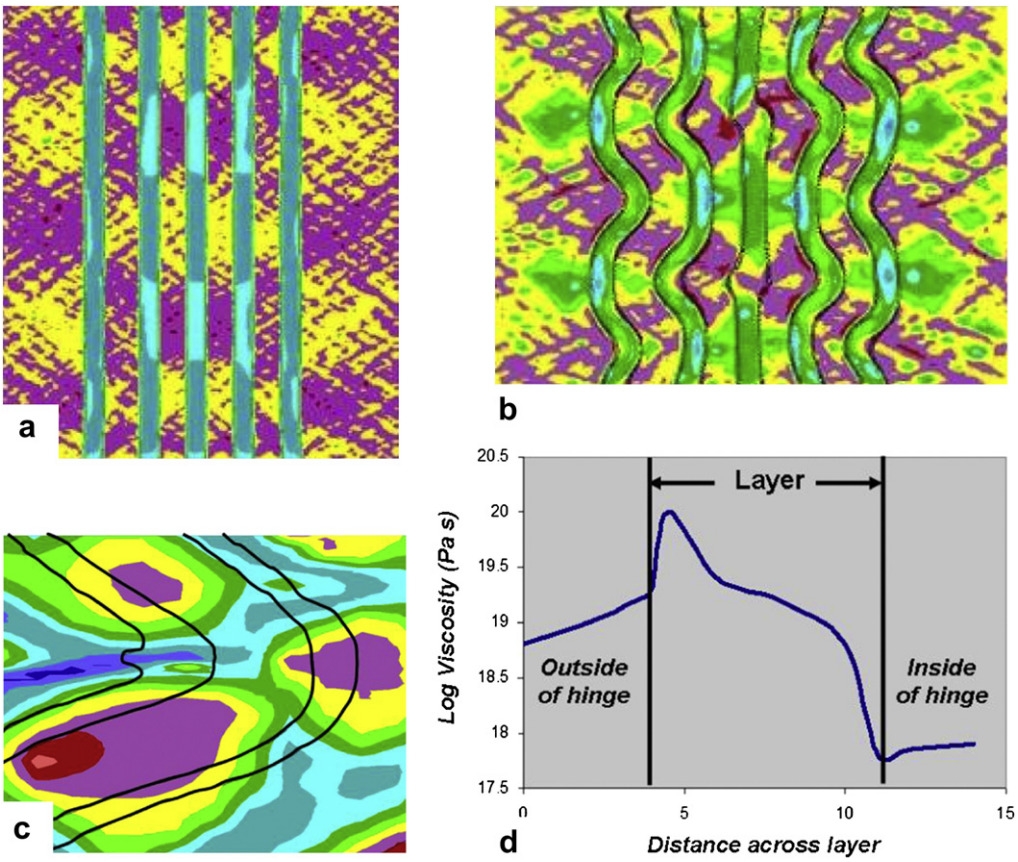

Fig. 41. Development of multi-layer folds in visco-elastic, strain-rate softening materials; $N = 1$. Elastic moduli are the same in all materials. Viscosity of layers initially 10^{20} Pa s; viscosity of embedding material initially 10^{19} Pa s. The materials are also strain hardening. (a) 12% shortening parallel to the layering. Plot of log (current viscosity, Pa s). Red is 18, light blue is 19; contour interval is 2. (b) Same as (a) but with 30% shortening. Red is 17, light blue is 22; contour interval is 1. (c) Zoom into fold hinge showing reversed curvature "cusp" in the inside of the hinge arising from high strain-rate axial plane zone. Colours are a plot of log (strain-rate, s^{-1}). Red is −12.5, dark blue is −10.5; contour interval is 0.25. (d) Plot of log (current viscosity, Pa s) across a layer in the hinge of a fold. Overall shortening of model 25%.

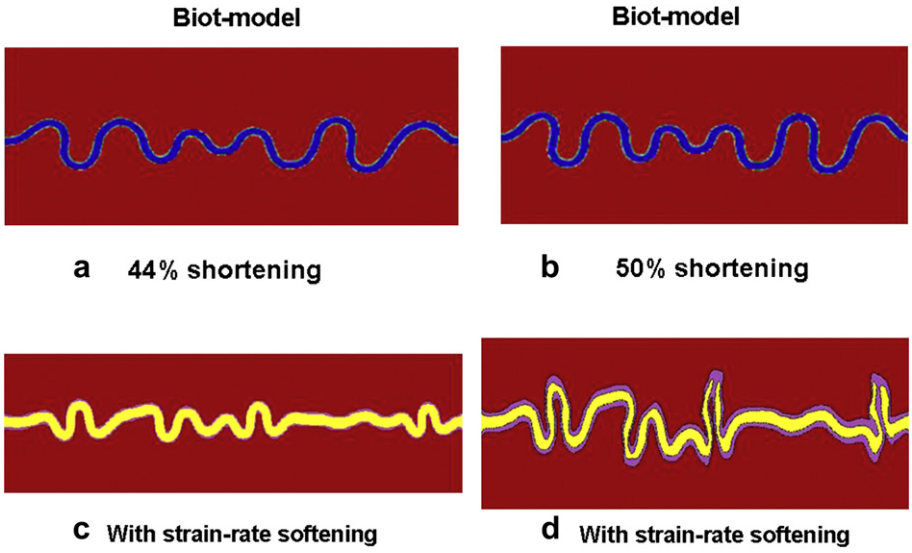

Fig. 42. Development of folds in a single layer for materials without (a, b) and with (c, d) strain-rate softening and with constant velocity boundary conditions. The initial viscosity ratio in both cases is 200. By 44% shortening the model without strain-rate softening has developed a more or less periodic train of folds whereas the model with strain-rate softening has developed localised folds with no dominant wavelength. An extra 6% of shortening makes very little difference to the model with no strain-rate softening because by now the deformation is essentially homogeneous shortening with very little fold amplification. The model with strain-rate softening shows rapid tightening and amplification of the fold profiles. (After Hobbs et al., 2010b.)

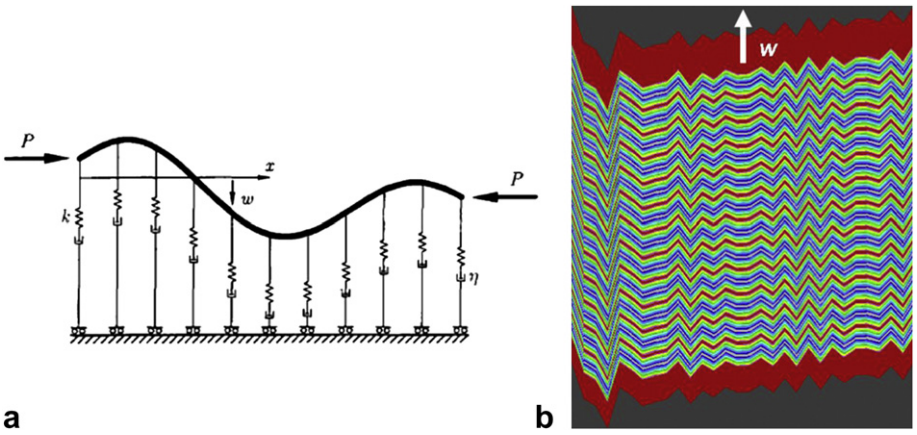

Fig. 43. Structure within the embedding material for folding. (a) An example of one form of rheological response of the embedding material to vertical displacement, *w*, of the layer (after Whiting and Hunt, 1997). (b) An example of localised displacement packets (microlithons) resulting from localised folding. The boundaries of the microlithons are parallel to the displacement vector of the layer, *w*.

A number of non-linear forms of F have been proposed (Whiting and Hunt, 1997) of which the form $F(w) = w - w^2$ has been widely studied. This represents an embedding material that softens as it deforms and the result is localisation of fold packets rather than the Biot periodic solution. Thus a homogeneous embedding material in which metamorphic reactions produce a weaker material will lead to localised folding in embedded layers. However the deformation in the embedded layer is also localised so that structures such as are shown in Fig. 43(b) result. These structures resemble crenulations or microlithons that are associated with crenulation cleavage in natural rocks but no metamorphic differentiation is developed for the situation presented. The axial planes of the crenulations are parallel to the displacement vector $\boldsymbol{w}$. The general form of the localised deformation is (Whiting and Hunt, 1997):

$$w = \exp(\alpha x)[A\cos\beta x + B\sin\beta x] + \exp(-\alpha x)[C\cos\beta x + D\sin\beta x] \tag{86}$$

where α, β, A, B, C, D are constants.

A non-linear form of the reaction-diffusion equation is the Swift–Hohenberg Equation (Cross and Hohenberg, 1993):

$$\frac{\partial w}{\partial t} = \alpha\frac{\partial^4 w}{\partial x^4} + \beta\frac{\partial^2 w}{\partial x^2} + F(w) \tag{87}$$

where α and β are constants, different to the ones in Eq. (86) and F is generally a non-linear function of w. The stationary form of this equation, that is for $\frac{\partial w}{\partial t} = 0$, is identical in form to Eq. (85). These equations result in a range of spatial distributions of mineral compositions; the book by Peletier and Troy (2001) is devoted to solutions of the stationary form of Eq. (87). If we take the redox system as described by the Brusselator discussed by Fisher and Lasaga (1981) then layered metamorphic differentiation develops with a periodic spacing, λ, as discussed by Fisher and Lasaga (1981). In Fig. 44 we show an initially layered system in which a Brusselator reaction system develops with a wavelength, λ. This is reflected in a periodic spatial distribution of mechanical properties which in turn is reflected in the distribution of the reaction forces against the layers within the embedding material as shown in Fig. 44(a). The result is a periodic form of the interaction between the layer and the embedding medium so that Eq. (85) becomes

$$Q\frac{\partial^4 w}{\partial x^4} + P\frac{\partial^2 w}{\partial x^2} + F(w)\left(1 + \sin mx\right) = 0 \tag{88}$$

where m is an integer and is defined by Fisher and Lasaga (1981). We know of no analytical solution to Eq. (88) but numerical simulations are shown in Fig. 44 for deforming Maxwell materials as in Fig. 44(a). For illustrative purposes the metamorphic layering grows across the central layer in Fig. 44. As shown in Fig. 44(b–d), the folding process results in shear displacements parallel to the metamorphic layering. The geometry now resembles crenulated metamorphic layering with, importantly, shearing displacements parallel to the axial planes of the folds. Thus the coupling of metamorphic reactions to the folding process, both governed by reaction-diffusion equations of identical form, develops crenulated differentiated axial plane structures in localised fold systems with shear displacements parallel to the axial planes and parallel to $\boldsymbol{w}$. Such features are hallmarks of deformed metamorphic rocks. The situation modelled in Fig. 44 presents a situation where the metamorphic layering grows faster than the folds develop. Other scenarios where the layering grows at the same rate or slower than the fold grows would be of interest. A more detailed discussion of these models is given in Hobbs and Ord (2010a).

5.5. Boudinage

Boudinage development in power-law materials with no strain-rate softening has been studied by Smith (1975, 1977, 1979) and by Schmalholz et al. (2008). The result is that high rate insensitivity ($N \geq 5$) and viscosity ratios greater than 20 are required to produce boudinage. If strain-rate softening is introduced, boudinage forms readily, even in Newtonian materials as shown in Fig. 45. Moreover the boudins that form with strain-rate softening are localised with no dominant wavelength.

5.6. Overview of Section 5

At the scale of about 1–100 m at tectonic strain-rates of 10^{-12} s^{-1}, or slower, deforming-reacting systems are likely to be isothermal for finite deformations. The dissipation produced by mechanical processes is available to increase the rate of chemical reactions or indeed other processes operating at this scale such as fracturing or grain-size reduction. The dissipation arising from mineral reactions (expressed by Eq. 23c) is also available to influence deformation-rates and this leads to strain-rate softening especially in rate sensitive materials with low values of N. Shear zones form readily in such materials independently of whether the material also undergoes strain softening or hardening. Layered strain-rate softening materials are unstable during deformation and undergo folding in shortening deformations parallel to the layering even in viscous materials with small ($\approx$5) viscosity ratios between layers and the

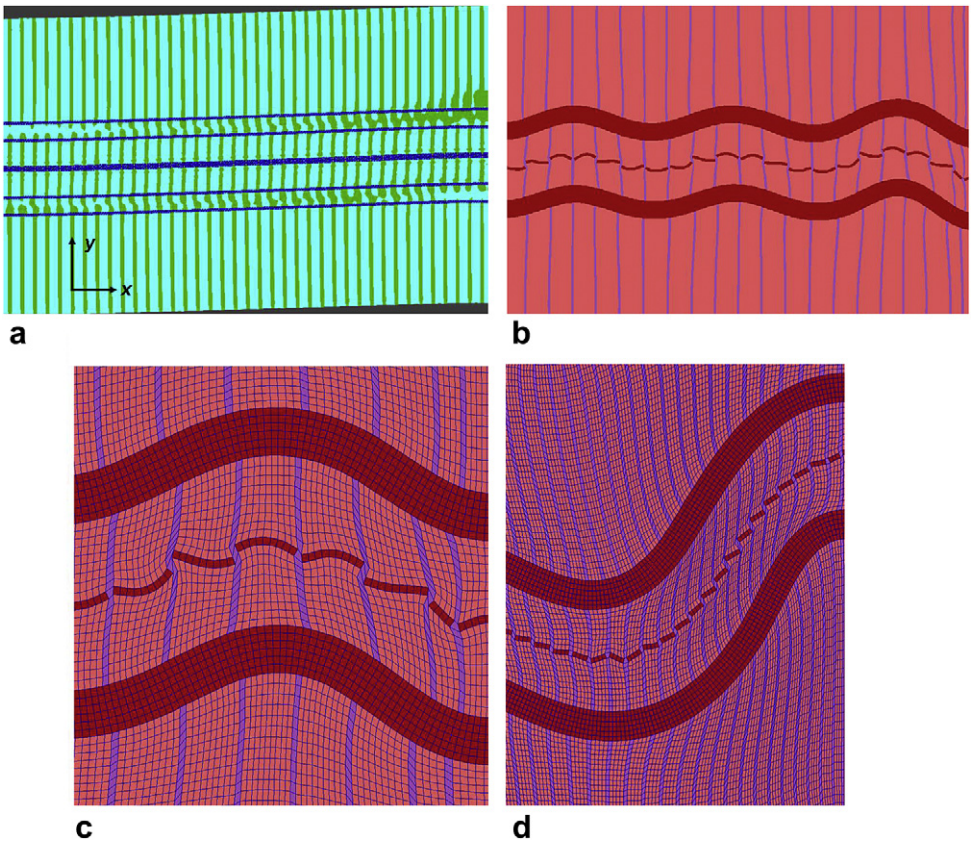

Fig. 44. The influence of growing metamorphic layering (initially vertical in all models) on the folding process. The materials are represented as Maxwell materials with elastic modulus uniform at 10^{10} Pa. The viscosity of the embedding material varies sinusoidally from 5×10^{17} Pa s. to 10^{17} Pa s. within the metamorphic layers as they grow. The initially horizontal layers in the figures have a constant viscosity of 10^{21} Pa s. The strain-rates are approximately 10^{-12} s^{-1} with constant velocity boundary conditions. (a) Distribution of the y-component of the normal stress, σ_{yy}; this represents the reaction of the embedding material to the folding deflections. Horizontal shortening is 10% with a dextral shear through 5°. (b) Model shortened 30% coaxially. The blue vertical layers are growing by metamorphic differentiation according to the Brusselator model of Fisher and Lasaga (1981). (c) Zoom into part of (b). (d) Model shortened 40% horizontally and sheared dextrally through 30°.

embedding materials. The resulting folds are localised in character which means they are not characterised by a dominant wavelength. The mechanism of formation of these folds is different to the Biot mechanism where all fold wavelengths grow independently of each other and one wavelength ultimately dominates to produce a strictly sinusoidal fold system. In materials that exhibit strain-rate softening the mechanism is one of localisation of deformation arising from strain-rate heterogeneities that nucleate along layers undergoing initial deflections. Non-sinusoidal, localised fold systems develop. If the deformation comprises extension parallel to the layers then boudinage develops even in low viscosity contrast (≈ 5) configurations and for values of N as low as 1. This contrasts with boudinage development in layered materials that show no strain-rate softening where viscosity contrasts >20 and values of $N \geq 5$ are necessary to produce boudinage. Again the boudins are localised with no dominant wavelength.

In thinly layered sequences, geometrical softening (as in the case of single slip in crystal plasticity; Section 4.10) leads to non-convexity in the Helmholtz energy of the system and the consequent formation of kink or chevron folds in order to minimise the Helmholtz energy of the system. Softening in one form or another is the essential ingredient in developing localised folding or boudinage (Tvergaard and Needleman, 1980). At peak stress the system undergoes periodic folding as would be predicted from the Biot theory. However at a critical softening the system bifurcates and localised folding and boudinage develop. This is a critical phenomenon associated with the Helmholtz energy function passing from convex to non-convex at a critical strain.

The mechanical response of the embedding material in a layered model is fundamental in controlling the geometrical characteristics of folds and also in defining the types of axial plane structures that develop. If the reaction forces within the embedding material arising from buckling displacements of a layer are a linear function of the displacement then the folding response is sinusoidal as predicted by the Biot theory. An overall softening response of the mechanical properties results in localised folding with the formation of microlithons aligned parallel to the axial plane. If compositional layering develops from metamorphic differentiation early in the folding history and parallel to the developing axial plane then shear strains develop parallel to the axial planes so that the structure resembles differentiated crenulation cleavage.

The literature devoted to intermediate length scales has so far concentrated on mechanical–chemical coupling. The coupling to damage (fracturing and joint system formation) is clearly a fruitful future area of study particularly if linked to fluid flow and mineral reactions to produce vein systems. There has been some progress in these areas by Ord and Hobbs (2010) and Karrech et al. (2011) but we leave discussion, although brief, to Section 6.

6. The regional scale

At the scale of about 1–10 km and tectonic strain-rates of say 10^{-12} s^{-1} heat that is generated by deformation diffuses out of the system in 10^{12}–10^{14} s; these time scales are to be compared with the time scale of 10^{11} s needed to reach 10% strain. Thus a volume of rock larger than 1 km cube and undergoing large deformations will

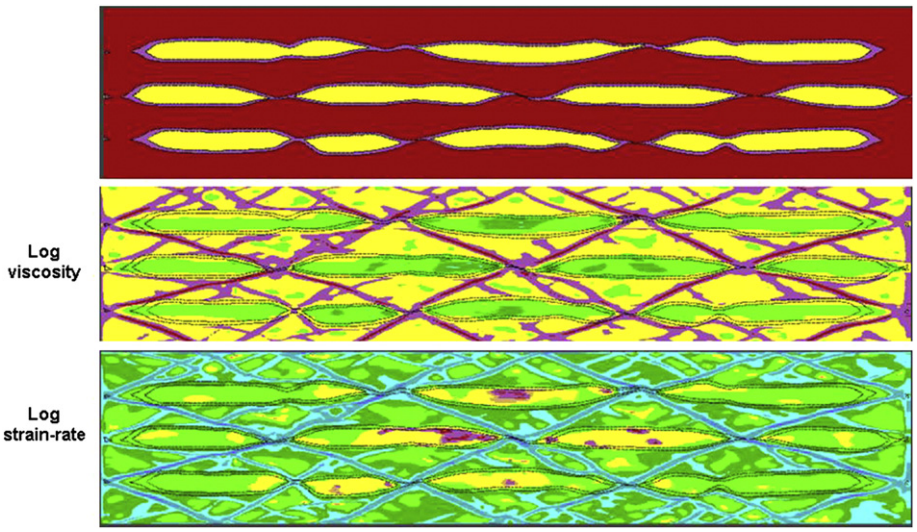

Fig. 45. Boudinage in Newtonian materials with strain-rate softening. Pure shearing deformation. Extension is 70%. (a) Geometry. (b) Logarithm of viscosity , and of strain-rate (c). In the viscosity plot, dark green is 10^{22} Pa s, yellow is 10^{20} Pa s, purple is 10^{18} Pa s. In the strain-rate plot, red is 10^{-14} s^{-1}, blue is 10^{-10} s^{-1}. After Hobbs et al. (2010a).

increase in temperature if heat is generated during deformation. The Clausius–Duhem relation (1) becomes

$$T\dot{s} = \Phi = \Phi^{mechanical} + \Phi^{chemical} + \Phi^{thermal} \geq 0 \qquad (89)$$

This means that the dissipation arising from deformation can be used to increase chemical reaction rates at this scale. In addition, heat generated by the deformation or by chemical reactions can increase the strain-rate. The $V_o \mu_K \dot{m}_K$ term in Eq. (26) is not important at this scale which means that we do not expect metamorphic differentiation at this scale that arises from reaction-diffusion processes. Veveakis et al. (2010) have analysed a situation similar to the one proposed here except that they are concerned with faster strain-rates (associated with seismic events and landslides) and so their results apply to a much smaller spatial scale. As indicated in Table 6 the scale of importance of these effects depends on the strain-rate. Below we develop the argument for length scales larger than 1 km in scale at tectonic strain-rates. We are concerned therefore with situations that dominate the regional crustal scale and play a fundamental role in the mantle of the Earth (Yuen and Schubert, 1979; Regenauer-Lieb and Yuen, 2003).

6.1. Thermal–mechanical feedback including thermal expansion

Thermal–mechanical feedback is by far the most extensively studied (Cherukuri and Shawki, 1995a, b; Yuen and Schubert, 1979; Regenauer-Lieb and Yuen, 2003, 2004) and best understood process of all the coupled processes expressed in Eq. (1). The Arrhenius dependence of strain-rate on temperature expressed by Eq. (54) means that heat generated by deformation at the regional scale and slow strain-rates increases the strain-rate which in turn produces more heat. This feedback process however does not lead to thermal runaway as suggested by many authors so long as the strain-rate has an Arrhenius dependence on temperature (Veveakis et al., 2010, Appendix A). However the increased strain-rates do result in greatly elevated temperatures and Veveakis et al. (2010) propose that other processes such as endothermic chemical reactions (including grain-size reduction, fracturing, melting and prograde mineral reactions) are initiated or accelerated before these elevated temperatures are attained thus limiting the temperature increase and stabilising the system.

The modelling of Regenauer-Lieb and Yuen (2003,2004), Regenauer-Lieb et al. (2006, 2008) and of Hobbs et al. (2008, 2009) shows that localisation of deformation readily results from thermal–mechanical feedback (Fig. 46a,b). Regenauer-Lieb et al. (2008) have modelled the development of shear zones on the scale of the crust and some results are shown in Fig. 46(a,b). The conventional view of the "brittle-ductile" transition being the strongest part of the crust is modified by the observation that this part dissipates energy at a greater rate than the rest of the crust and hence weakens more than the rest of the crust by thermal feedback. Hence the "brittle-ductile" transition becomes the weakest part of the crust. The deforming crust largely unloads to an elastic state during the development of the shear zones so that the force supported by the crust is more related to the elasticity of the crust rather than the plastic/viscous properties. The concept of a "Christmas Tree" structure (Goetze and Evans, 1979) for the crust needs to be reconsidered in the light of thermal–mechanical feedback.

In addition, folding develops in layered viscous materials in exactly the same way as is described for chemical–mechanical coupling at the microscale (Section 4.12) and the outcrop scale (Section 5.3). Thermal feedback results in the effective viscosity decreasing with the square of the strain-rate (Eq. 68; Fleitout and Froidevaux, 1980). This strain-rate softening results in localised fold systems as in Section 5.3 with the effective viscosity decreasing in the inner arc of incipient buckles and increasing in the outer arc (Fig. 46c). The thermal–mechanical feedback response is sensitive to local heterogeneities so that initial mechanical or geometrical heterogeneities result in localised folding rather than the sinusoidal fold systems expected of the Biot (1965) theory although as we have seen earlier it is possible that the Biot mechanism is responsible for the initiation of folds. As indicated earlier in this paper, folds that develop by this mechanism can form with small (≈ 5) viscosity ratios between the layers and the embedding material. Boudinage (Fig. 46d) also develops readily by this mechanism even in Newtonian viscous materials and small (≈ 5) viscosity contrasts whereas boudins do not form without thermal–mechanical feedback unless the viscosity ratio is larger (≈ 20) and N is larger than 5.

The constitutive relation used by Regenauer-Lieb and Yuen (2003) and by Hobbs et al. (2008, 2009) involves a dependence of the strain-rate on the pressure through the thermal expansion. In the

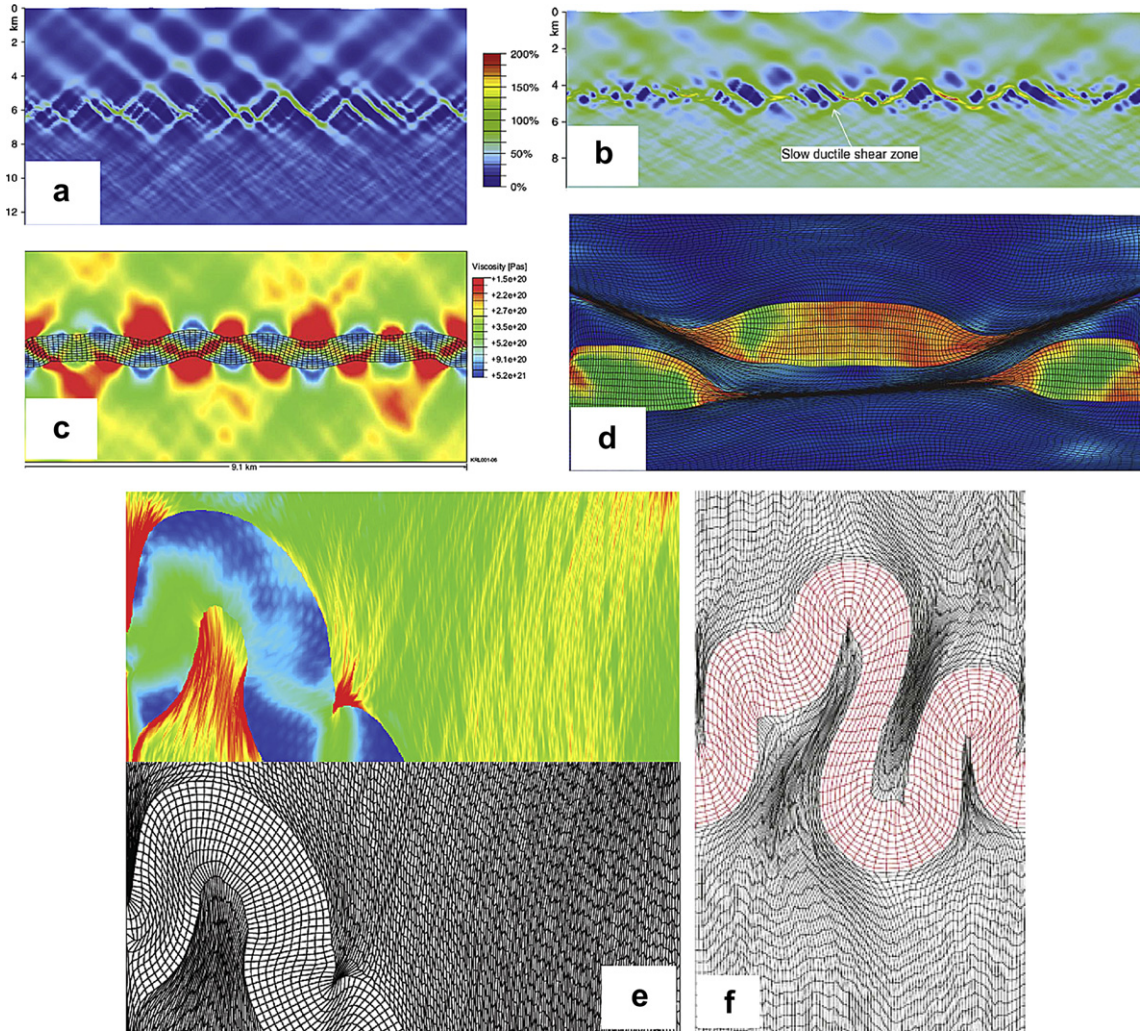

Fig. 46. Structures developed through thermal–mechanical feedback. (a) Shear zones developed at the crustal scale (Regenauer-Lieb et al., 2008). (b) "Slow" ductile shear zone (Regenauer-Lieb et al., 2008). (c) Early stage in the development of localised folds by thermal–mechanical feedback. High viscosities are developed at the outer side of fold hinges and low viscosities develop on the inner sides of the hinges (Hobbs et al., 2008) (d) Boudinage developed in feldspar rich layers embedded in quartz-rich material (Hobbs et al., 2009). (e) and (f) Crenulations developed as axial plane foliations (Hobbs et al., 2008). The upper figure in (e) shows the distribution of strain-rate.

models, heterogeneity in the spatial distribution of the thermal expansion is included as would arise from fluctuations in mineralogical composition. The inclusion of thermal expansion turns out to be very important. The dissipation that arises during thermal expansion against the pressure induces localisation at the scale of the thermal expansion heterogeneities which is much smaller than the scale of the layering. This results in the development of axial plane structures which have some affinities with crenulation cleavages (Fig. 46e,f). Such structures are not an artefact of the computational process; Needleman (1988) and Wang et al. (1997) have shown that localisation arising from strain-rate softening is not mesh dependent as is the case for localisation in rate-independent materials. The results shown in Fig. 46e,f suggest that some axial plane foliations may develop from localisation controlled by feedback processes nucleated at heterogeneities at a scale finer than the layering and this effect may be important at all scales.

6.2. Melting. The development of granitoid systems

Two recurrent and related themes appear in discussions of crustal melting and the emplacement of granitoids. These are: (i) episodicity of melt production and emplacement (Sandiford et al., 1991, 1992; Stüwe et al., 1993; Brown and Solar, 1998a, b; Stüwe, 2007; Brown, 2004, 2010) and (ii) self-organised criticality (SOC) as a characteristic feature of the melting/transport/emplacement system (Brown and Solar, 1998a, b; Petford and Koenders, 1998; Bons and van Milligen, 2001; Brown, 2010; Bonamici and Duebendorfer, 2010). We indicate below that both characteristics of melt systems in the crust are to be expected from thermodynamic considerations although perhaps one should be self-criticising in the use of the term *self-organised criticality*.

SOC is proposed as a characteristic property of computer models that behave as though they undergo a classical phase change (Sornette, 2000; Ben-Zion, 2008). In keeping with classical phase changes in physical and chemical systems, the macroscopic behaviour of the system is characterised by a range of scale invariant properties at and near a critical point which marks the phase boundary. Such properties have fractal (or at least power-law) characteristics in both space and time that result from fluctuations in properties at all scales. The steady state of SOC behaviour results from a slow but steady forcing which results in unsteady, irregular behaviour with extended periods of quiescence punctuated by events, both large and small, again with a fractal nature. This behaviour for SOC is not sensitive to the rate of forcing

and the basic concept behind SOC is that systems undergo criticality with little regard for the details of the forcing mechanism; the system anthropomorphically "self-organises". The fractal characteristics of the system include the resultant geometry, correlation lengths, cluster sizes and the life-times and sizes of events (Bak et al., 1988). Ben-Zion (2008) points out that SOC behaviour is not as rich as is observed in nature at least for seismicity of the crust and that almost all of the concepts inherent in SOC already exist in classical notions of criticality without call for a new name. In fact he prefers that SOC should be an acronym for *Standard Old Criticality* and we agree.

Classical criticality (Sornette, 2000) refers to systems that undergo a phase change at a critical point and include first order transitions where there is a discontinuity in some properties at the transition (critical point) and second order transitions where the behaviour is smooth at the critical point. At that point, for both first and second order transitions, the Helmholtz energy changes from convex to non-convex and this is the hallmark of criticality. We have seen from Section 4.10 that this implies, in deforming systems, the switch from homogeneous deformations that minimise the convex Helmholtz energy to the development of an array of inhomogeneous deformations in order to minimise the non-convex Helmholtz energy. This array forms by a self-similar branching process with the details of the branching process organised to guarantee compatibility with the imposed deformation gradient as far as this is geometrically possible. However, because such an array can never completely match the imposed deformation gradient without gaps, further self-similar refinement is required until the long range stresses are minimised. These processes of refinement produce fractal geometries and so this is a mechanism for producing the fractal geometries observed at a critical point in a deforming system. Although these concepts were developed for elastic systems, they have now been extended to plastic (dissipative) systems and in particular, to systems that undergo fracture (Francfort and Marigo, 1998; Del Piero and Truskinovsky, 2001). Fig. 47(a,c) shows the dependence of the Helmholtz energy on the deformation gradient for a brittle material and Fig. 47(b,d) the resultant stress–strain curves. These models are motivated by both the ubiquitous weakening and the discontinuous stress drops commonly observed in experimental deformation of brittle materials. A thermodynamic approach to damage evolution (based on Eq. 20) has been developed by Lyakhovsky et al. (1997) and

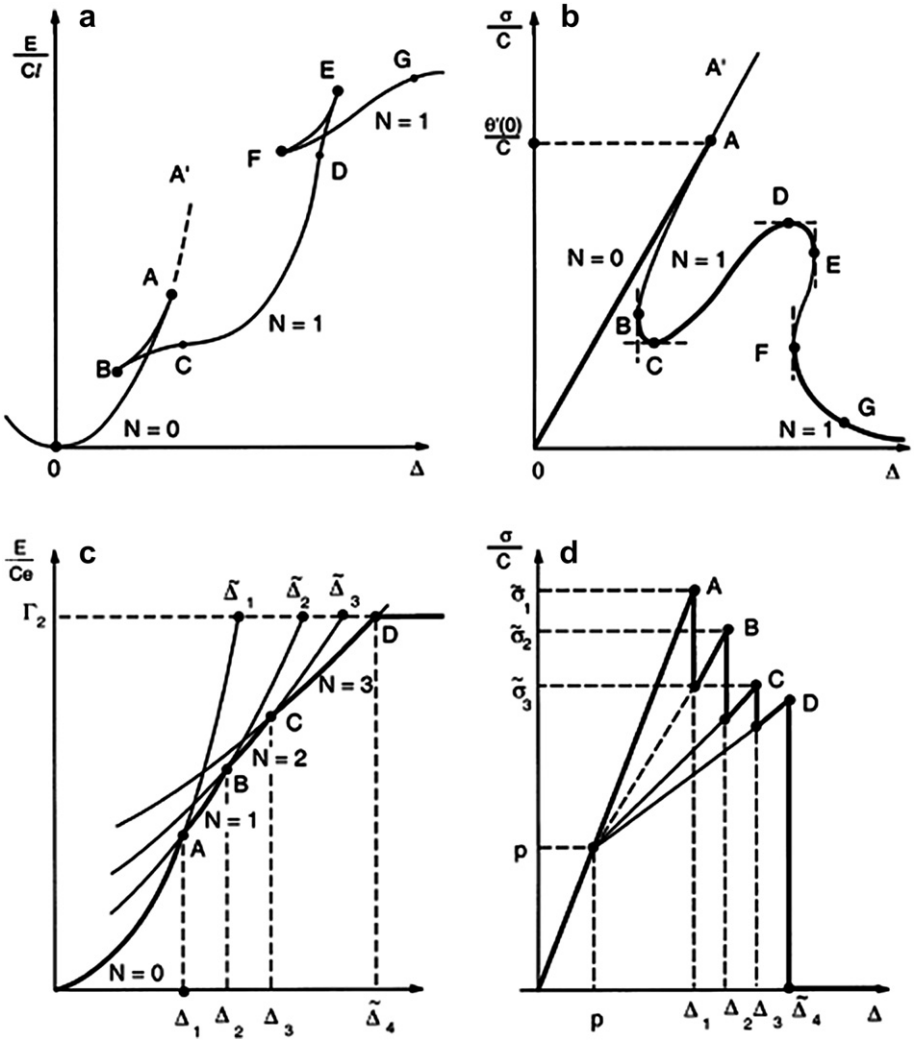

Fig. 47. Helmholtz energy and stress–strain curves for brittle materials. Figs. (a), (c) show the dependence of the Helmholtz energy on the deformation gradient for a brittle material and Fig. 42(b), (d) the resultant stress–strain curve. These models are motivated by both the ubiquitous weakening and the discontinuous stress drops commonly observed in experimental deformation of brittle materials. Fractal geometries (or at least power-law scaling relations) develop for many features in order to minimise the Helmholtz energy of a damaged crust and episodicity develops as the system is deformed through successive non-convex portions of the Helmholtz function. An example is the sequence A → B → C → D in Fig. 42(c,d). See Del Piero and Truskinovsky (2001) for details.

Lyakhovsky and Ben-Zion (2008) where it is shown that the Helmholtz energy becomes non-convex at a critical level of damage; this critical point can be associated with localisation of deformation. The implications for seismic behaviour of such a loss in convexity are discussed by Ben-Zion (2008); we adopt his concept of the crust as a system close to criticality in the classical sense. Fractal geometries (or at least power-law scaling relations) develop for many features in order to minimise the Helmholtz energy of a damaged crust and episodicity develops as the system is deformed through successive non-convex portions of the Helmholtz function. An example is the sequence A → B → C → D in Fig. 47.

Spatial fractal geometries of granitoid systems have been documented by Bons and Elburg (2001) at the regional scale and by Tanner (1999), Marchildon and Brown (2003) and Bonamici and Duebendorfer (2010) at the outcrop scale.

The development of a melt system within the crust is envisaged as follows. The model is based on the analysis of Hobbs and Ord (2010b) which in turn is based on discussions by Phillips (1991). This model proposes that the rate of melt production at the top of the anatectic zone is controlled by the mineralogical composition of the anatectic zone coupled with the rate at which isotherms move through the anatectic zone. This melt production rate governs the melt flux at the top of the anatectic zone which acts as a control valve for the complete melt transport-emplacement system and also controls the evolution of melt pressure throughout the entire system. The crustal melt system differs from most hydrological systems where the permeability is commonly an independent variable and the fluid flux is the dependent variable. In the crustal melt system the melt flux at the anatectic front is fixed by the chemical composition and rate of isotherm migration and the mechanics of the system demands that the permeability evolves in order to accommodate this flux. In general the permeability of the lower crust is low and the pressure at the anatectic front ultimately becomes super-lithostatic resulting in melt-induced fracture (Phillips, 1991). We envisage this event to be a critical point for the system where, by analogy with the arguments of Ben-Zion (2008), the crust undergoes a phase transition and the Helmholtz energy of the crust switches from convex to non-convex due to damage accumulation (Lyakhovsky and Ben-Zion, 2008). The subsequent deformation of the crust in order to accommodate the continued flux of melt develops a fractal system of fractures formed by self-similar refinement (Fig. 48a) with episodicity governed by successive passages through discontinuities in the free energy function with increasing strain. It seems relevant that the model suggested by Brown (2010) for the crustal plumbing system (Fig. 48b) also approximates a self-similar refining network. Such networks are widely developed in fracture systems (Hull, 1999) and are similar to the stochastic networks developed to model seismic events (Kagan, 1982; Libicki and Ben-Zion, 2005).

6.3. Thermal–mechanical–chemical reaction feedback and regional tectonics

Many authors have suggested that orogenic systems are self-organised systems whereby the many processes that operate during orogenesis either compete with one another or reinforce each other to produce the structures and distribution of metamorphic rocks and melts that we observe in mountain belts. Foremost here are papers by Hodges (1998) and Brown (2010). At the regional scale (that is larger than about 1 km), the only processes that contribute to entropy production are (if we neglect regional scale infiltration of fluids) deformation, chemical reactions (including melting and crystallisation) and heat flow (Eq. 89). Of these, deformation is exothermic together with most retrograde metamorphic reactions and crystallisation of melts (Haack and Zimmermann, 1996; Connolly and Thompson, 1989). Most prograde metamorphic reactions including melting are endothermic.

The Clausius–Duhem relation for regional scale thermal –mechanical coupling can be expressed as

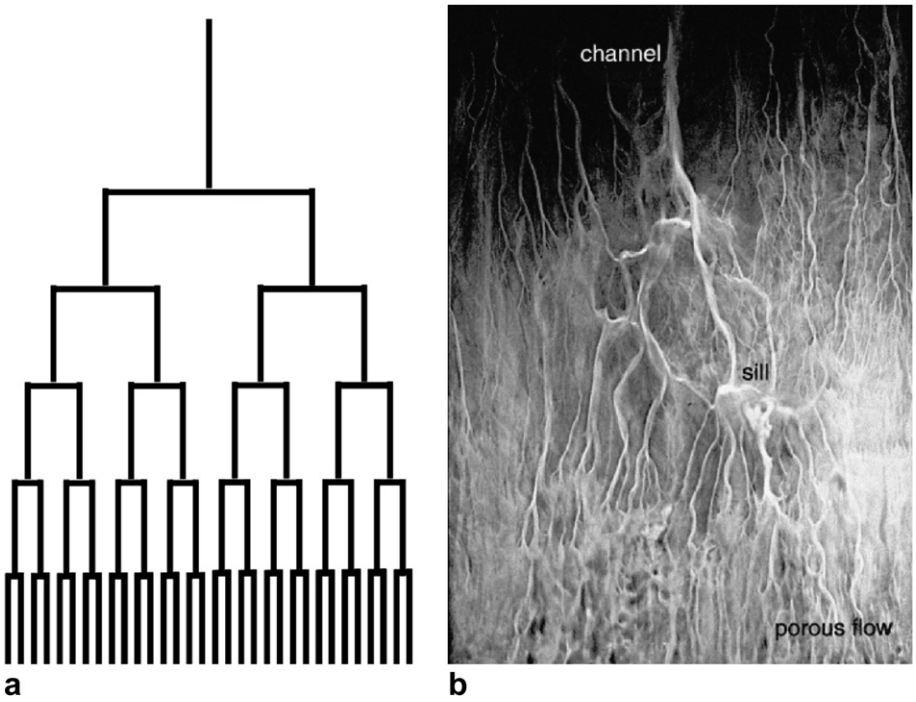

Fig. 48. The deformation of the crust in order to accommodate the continued flux of melt develops a fractal system of fractures formed by self-similar refinement (Fig. 47a) with episodicity governed by successive passages through discontinuities in the free energy function with increasing strain. It seems relevant that the model suggested by Brown (2010) for the crustal plumbing system (Fig. 47b) also approximates a self-similar refining network.

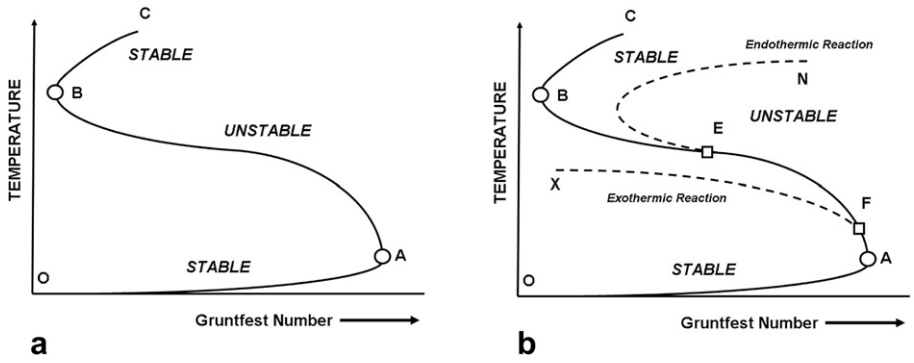

Fig. 49. Solution to the Bratu equation for thermal–mechanical feedback and with coupled chemical reactions. (a) The dissipation is given by $\sigma_{ij}\dot{\varepsilon}_{ij}^{dissipative}$. Stable branches are OA and BC; unstable branch is AB. (b) The addition of endothermic (branch EN) and exothermic (branch FX) to the stability fields shown in (a). Endothermic mineral reaction nucleates at E and produces stability. Exothermic mineral reaction nucleates at F and produces further instability.

$$\frac{dT}{dt} = \kappa^{thermal}\frac{\partial^2 T}{\partial x^2} + \frac{\mathcal{A}}{\rho c_p}\sigma^{N+1}\exp\left[-\frac{\mathcal{Q}}{RT}\right] \tag{90}$$

which is a form of reaction-diffusion equation known as the Bratu equation (Fowler, 1997; Veveakis et al. 2010). The solution to this equation is shown in Fig. 49(a) and consists of three branches (Law, 2006, Chapter 8). The branches OA and BC in Fig. 49(a) represent stable deformation with no localisation whereas the branch AB is unstable and represents localisation of deformation. The stable branch OA is dominated by low temperature, high stress, low strain-rate deformation processes where the heat generated by deformation is not large enough to cause significant weakening via the exponential term in Eq. (90). On the contrary the stable branch BC is dominated by high temperature, low stress, high strain-rate processes where the resultant heat is conducted away by the diffusive term at the same rate it is generated. The AB branch represents temperature conditions where weakening from the exponential term offsets the conduction of heat so the thermal–mechanical instabilities can initiate. As the ambient temperature increases, the point A shrinks to the left of the diagram and eventually the S-curve of Fig. 49(b) becomes a "stretched" S-curve shown in Fig. 29(c). Thus, as the ambient temperature of the crust increases the likelihood of localisation by thermal–mechanical feedback decreases.

The effect of coupling mineral reactions to the thermal–mechanical coupling is to stabilise or destabilise the deformation at a particular temperature depending on whether the reaction is endothermic or exothermic as shown in Fig. 49(b). In Fig. 49(b) an exothermic reaction is initiated at a temperature corresponding to F and this destabilises the deformation along the branch FX. At a higher temperature, corresponding to E, an endothermic reaction is initiated and that stabilises the deformation along the branch EN. Hence endothermic reactions, which commonly correspond to pro-grade mineral reactions, including devolatilisation, and anatexis, stabilise the deforming system whereas exothermic reactions, which commonly correspond to retrograde hydrating reactions and melt crystallisation destabilise the system. The proposal by authors such as Brown (2010) that melt accumulation in the anatectic zone results in wholesale weakening and subsequent collapse of orogenic belts could be an expression of criticality arising from the Helmholtz energy of the crust losing convexity and instability initiating as a result. As yet there is no synthesis of processes such as damage and melt accumulation that can result in criticality (and hence instability) and the initiation of endothermic pro-grade mineral reactions (including melting) that can stabilise the system. It would appear that the ways in which these competing processes evolve and interact in an orogenic system control the detailed geometry of individual systems.

6.4. Overview of Section 6

Thermal–mechanical coupling at the regional scale produces shear zones, folding and boudinage at the regional scale in a large class of materials that otherwise would not produce these structures. Crustal scale shear zones develop preferentially in the strongest parts of the crust where the mechanical dissipation is highest. This means that the "brittle-ductile" transition which is commonly taken to be the strongest part of the crust evolves to become weaker than in classical models. During localisation the crust unloads to an elastic state so that the elastic properties of the crust control the "strength" of the crust (the forces it will support) rather than the plastic/viscous properties. Both folding and boudinage are localised in character rather than sinusoidal and form in layered materials with small viscosity contrasts and values of N smaller than develop in materials with no thermal–mechanical feedback. Axial plane foliations nucleate at heterogeneous sites of dissipation smaller than the thickness scale defined by the layering; these foliations are crenulation-like in character.

During deformation and metamorphism (including anatexis) the crust behaves in a critical manner in the sense that it undergoes classical phase transitions and these can be of an intermittent character. One explanation for this behaviour is the development of a non-convex Helmholtz energy function for the crust associated with the development of critical levels of damage. These phase transitions are expressed as the formation of power-law spatial distributions of fractures. Such distributions arise from self-similar refinement of inhomogeneous deformations to accommodate the imposed regional deformation gradient. These fractal systems presumably act as conduits for melt transport and lead to the fractal geometry of melt transport systems and pluton distributions. The progressive development of damage and the associated evolution of the Helmholtz energy with time are proposed as an explanation for episodic melt emplacement in the crust.

7. Concluding remarks

Structural geology is concerned with the processes that operate during the deformation and metamorphic evolution of the lithosphere of the Earth and hence differs in a fundamental way to a common approach in metamorphic petrology that is concerned only with equilibrium mineral assemblages. The theory of Equilibrium Chemical Thermodynamics has been remarkably successful especially in the field of metamorphic petrology over the past 30 years

in enabling the construction of phase diagrams for general bulk rock compositions. An additional success of the equilibrium theory is that it enables the calculation of a large number of physical quantities such as thermal expansion and specific heat from a bare minimum of relations. It would of course be advantageous if similar rules of behaviour could be established for systems not at equilibrium. To date the progress in this regard has been slow and undoubtedly is still very much in progress. For over 20 years the subject was dominated by the minimum entropy production "principle" (Prigogine, 1955; Biot, 1958) and it was not until the 1960s that Ziegler's maximum entropy production "principle" appeared (Ziegler, 1963 and references therein) in apparent contradiction to the views of Prigogine and Biot. Ziegler showed that the Biot principle and others deriving from Onsager are identical to the maximum entropy production rate principle. It was not until 1987 (Hunt et al. 1987) that severe doubts were cast on Prigogine's principle for chemical systems and only in the last 5 years (Ross and Vlad, 2005) that any clarity has emerged. It turns out that only for thermodynamically "linear systems" defined as systems where the thermodynamic flux is a linear function of the thermodynamic force does a non-equilibrium extremum in the entropy production exist. For most systems, and this includes the classical examples of thermal conduction, mass diffusion and chemical reactions an extremum in entropy production does not exist and recourse has to be made to tracking the entropy production rate which is conveniently expressed in the most general manner as the Clausius–Duhem relation. This relation, combined with the first law of thermodynamics, enables the Energy Equation to be written which expresses the temperature change in a non-equilibrium system arising from all of the dissipative processes. The fact that some dissipative processes dominate at different length scales then enables some simplifications to be made but also establishes a fundamental scale invariant characteristic of deformed rocks, namely, that *the deformation of rocks is scale dependent but different processes dominate at different scales to result in geometrically similar structures*.

The Clausius–Duhem relation ultimately leads to a system of coupled reaction-diffusion equations or reaction-diffusion-deformation equations which for various ranges of parameters can become unstable and produce patterns in deformed rocks which comprise the range of structures that we are familiar with in deformed rocks: various microstructures, crystallographic preferred orientations, foliations, mineral lineations and the various combinations of the two expressed as S–L tectonites, folds and boudinage at all scales, and the overall structure of orogenic belts. An important conclusion at the microscale is that catalysis is a fundamental aspect of metamorphic reactions that enables reactions to be coupled together (perhaps involving coupling to deformation and fluid infiltration) to produce metamorphic differentiation patterns.

An important outcome of this review is that it highlights the role of criticality in the development of structures in deformed rocks. The term criticality is used in its classical sense (and not in the sense of self-organised criticality) of the behaviour of the system being associated with a critical parameter that marks the emergence of a phase transition where the Helmholtz energy passes from convex to non-convex (Ben-Zion, 2008). Such a transition exists for a diverse array of processes including metamorphic differentiation, the formation of subgrains and the development of CPO through rotation recrystallisation, the transition from periodic to localised fold and boudinage systems, the localisation of deformation within shear zones to form thin layers of ultracataclasites, ultramylonites and pseudotachylites and the evolution of damage at all scales including the crustal scale. All of the structures formed by these processes have fractal characteristics as is the case with classical phase transitions. There is no need to invoke the concept of self-organised criticality. The overarching concept involves the evolution of deforming-reacting systems towards minimising the Helmholtz energy which, commonly at the critical point, becomes non-convex due to some strain or strain-rate softening process which may be geometrical (rotation of planar fabrics), physical (damage accumulation that degrades the strength) or chemical (the production of new weak phases or thermal weakening arising from chemical dissipation) in character. In some instances this minimisation process seems to involve the evolution of geometries towards those characterised by minimal surfaces.

Intimately bound up with this tendency to minimise non-convex Helmholtz energy functions is the development of multiple non-equilibrium stationary states. Again, these arise through geometrical softening, deforming networked chemical reactions, fluid infiltration into networked chemical reactions and both thermal–mechanical feedback and damage accumulation at the crustal scale.

Epilogue

We have elected to devote relatively little space to the topics of deformation and its effect on metamorphic phase diagrams, diffusion (including pressure solution), preferred orientation development in the sense of Kamb (1959), damage and grain-size reduction, and the evolution of crustal scale orogenic systems. There have been important advances in some of these areas (the influence of deformation on metamorphic phase diagrams, diffusion and pressure solution: Wheeler, 2010; Shimizu, 1992, 1997, 2001; Paterson, 1995; damage: Lyakhovsky et al. 1997; Lyakhovsky and Ben-Zion, 2008; Karrech et al., 2011; grain-size reduction: Shimizu, 1998, 2008; Ricard and Bercovici, 2009 and references therein; Austin and Evans, 2007) but such advances have not yet been built into a fully coupled thermodynamic framework. Interestingly, some of these areas are those considered by Paterson (1973). In particular a major advance has been to develop theories of fracture that involve non-convex Helmholtz energies (Del Piero and Truskinovsky, 2001). The classical theories of fracture proposed by Griffith (1920) and Barenblatt (1962) assume a convex Helmholtz energy together with concave surface energies and have been very successful in explaining aspects of fracture development. The new non-convex theories explain the development of more complicated fracture arrays but to date these approaches have not formed a basis for understanding the fracture patterns so widespread in naturally deformed rocks. Another approach to this subject, which treats cracks as defects and formulates their interactions in terms of coupled reaction-diffusion equations, is by Ord and Hobbs (2010).

There is much to be learnt about systems not at equilibrium. Deformed metamorphic rocks offer a natural laboratory to test new hypotheses at all scales but such an approach will require a set of eyes adapted to read the non-equilibrium messages written in the rocks. We look forward to an exciting future as the possibilities are fleshed out.

Acknowledgements

We would like to thank Mervyn Paterson, Ron Vernon, John Christie, Hans Muhlhaus and Giles Hunt for many discussions that have led to this paper. Bob Wintsch offered helpful comments during the preparation of the paper and supplied Fig. 6b, and we thank Professor Yang for the supply of Fig. 19a. Tom Blenkinsop and Bob Wintsch are thanked for critical and helpful reviews.

References

Aifantis, E.C., 1986. On the dynamical origin of dislocation patterns. Mater. Sci. Eng. 81, 563–574.
Aifantis, E.C., 1987. The physics of plastic deformation. Int. J. Plast. 3, 211–247.

Aksimentiev, A., Fialkowski, M., Holyst, R., 2002. Morphology of surfaces in mesoscopic polymers, surfactants, electrons, or reaction-diffusion systems: methods, simulations, and measurements. Adv. Chem. Phys. 121, 141–239.
Alber, M., Glimm, T., Hentschel, H.G.E., Kazmierczak, B., Newman, S.A., 2005. Stability of *n*-dimensional patterns in a generalized Turing system: implications for biological pattern formation. Nonlinearity 18, 125–138.
Antman, S.S., 1983. The influence of elasticity on analysis: modern developments. Bull. Am. Math. Soc. 9, 267–291.
Andronov, A.A., Vitt, A.A., Khaikin, S.E., 1966. Theory of Oscillations. Pergamon, New York.
Austin, N.J., Evans, B., 2007. Paleowattmeters: a scaling relation for dynamically recrystallized grain size. Geology 35, 343–346.
Bak, P., Tang, C., Wiesenfeld, K., 1988. Self-organized criticality. Phys. Rev. A 38, 364–374.
Ball, J.M., 1977. Convexity conditions and existence theorems in nonlinear elasticity. Arch. Ration. Mech. Anal. 63, 337–403.
Ball, J.M., James, R.D., 1987. Fine phase mixtures as minimizers of energy. Arch. Ration. Mech. Anal. 100, 13–52.
Ball, J.M., 1998. The calculus of variations and material science. Q. Appl. Math. 61, 719–740.
Barenblatt, G.I., 1962. The mathematical theory of equilibrium cracks in brittle fracture. Adv. Appl. Mech. 7, 55–129.
Bell, T., 1981. Foliation development – the contribution, geometry and significance of progressive, bulk, inhomogeneous shortening. Tectonophysics 75, 273–296.
Bell, T.H., Bruce, M.D., 2006. The internal inclusion trail geometries preserved within a first phase of porphyroblast growth. J. Struct. Geol. 28, 236–252.
Bell, T.H., Bruce, M.D., 2007. Progressive deformation partitioning and deformation history; evidence from millipede structures. J. Struct. Geol. 29, 18–35.
Ben-Zion, Y., 2008. Collective behavior of earthquakes and faults: continuum-discrete transitions, progressive evolutionary changes and different dynamic regimes. Rev. Geophys. 46, 70. RG4006.
Bhattacharya, K., 2003. Microstructure of Martensite: Why it Forms and How it Gives Rise to the Shape-Memory Effect. Oxford University Press, p. 288.
Biot, M.A., 1937. Bending of an infinite beam on an elastic foundation. J. Appl. Mech. 59, A1–A7.
Biot, M.A., 1954. Theory of stress-strain relations in anisotropic viscoelasticity and relaxation phenomena. J. Appl. Phys. 25, 1385–1391.
Biot, M.A., 1955. Variational principles in irreversible thermodynamics with application to viscoelasticity. Phys. Rev. 97, 1463–1469.
Biot, M.A., 1958. Linear Thermodynamics and the Mechanics of Solids. Proceedings Third U.S. National Congress of Applied Mechanics, Brown University, Providence, R.I.. ASME, New York, pp. 1–18.
Biot, M.A., Ode, H., Roever, W.L., 1961. Experimental verification of the folding of stratified viscoelastic media. Geol. Soc. Am. Bull. 72, 1621–1630.
Biot, M.A., 1965. Mechanics of Incremental Deformations. John Wiley, New York. p. 504.
Biot, M.A., 1978. Variational irreversible thermodynamics of physical–chemical solids with finite deformation. Int. J. Solid. Struct. 14, 881–903.
Biot, M.A., 1984. New variational-Lagrangian irreversible thermodynamics with application to viscous flow, reaction-diffusion, and solid mechanics. Adv. Appl. Mech. 24, 1–91.
Bishop, J.F.W., Hill, R., 1951. A theory of the plastic distortion of a polycrystalline aggregate under combined stresses. Phil. Mag. 42, 414–427.
Bonamici, C.E., Duebendorfer, E.M., 2010. Scale-invariance and self-organized criticality in migmatites of the southern Hualapai Mountains, Arizona. J. Struct. Geol. 32 (8), 1114–1124.
Bons, P.D., Elburg, M.A., 2001. Fractal size distribution of plutons: an example from the Lachlan fold belt, Australia. In: Chappell, B., Fleming, P. (Eds.), S-type Granites and Related Rocks A collection of abstracts for a symposium held to mark the 70th birthday of Professor Allan White, 11–12 January 2001. BMR Record 2001/2, 21–22.
Bons, P.D., van Milligen, B.P., 2001. New experiment to model self-organized critical transport and accumulation of melt and hydrocarbons from their source rocks. Geology 29, 919–922.
Boyce, W.E., DiPrima, R.C., 2005. Elementary Differential Equations and Boundary Value Problems. John Wiley, New Jersey, p. 789.
Brown, M., Solar, G.S., 1998a. Shear zone systems and melts: feedback relations and self-organization in orogenic belts. J. Struct. Geol. 20, 211–227.
Brown, M., Solar, G.S., 1998b. Granite ascent and emplacement during contractional deformation in convergent orogens. J. Struct. Geol. 20, 1365–1393.
Brown, M.A., Brown, M., Carlson, W.D., Denison, C., 1999. Topology of syntectonic melt flow networks in the deep crust: inferences from three-dimensional images of leucosome geometry in migmatites. Am. Mineral. 84, 1793–1818.
Brown, M., 2004. Melt extraction from lower continental crust. Earth Environ. Sci. Trans. R. Soc. Edinb. 95, 35–48.
Brown, M., 2010. The spatial and temporal patterning of the deep crust and implications for the process of melt extraction. Philos. Transact. A Math. Phys. Eng. Sci. 368, 11–51.
Budd, C.J., Hunt, G.W., Kuske, R., 2001. Asymptotics of cellular buckling close to the Maxwell load. Proc. Math. Phys. Eng. Sci. 457, 2935–2964.
Burg, J.-P., Gerya, T.P., 2005. The role of viscous heating in Barrovian metamorphism of collisional orogens: thermomechanical models and application to the Lepontine Dome in the Central Alps. J. Metamorph. Geol. 23, 75–95.
Callen, H.B., 1960. Thermodynamics: An Introduction to the Physical Theories of Equilibrium Thermostatics and Irreversible Thermodynamics. John Wiley and Sons, New York, London, p. 376.
Carmichael, D.M., 1969. On the mechanism of prograde metamorphic reactions in quartz-bearing pelitic rocks. Contrib. Mineral. Petrol. 20, 244–267.
Carslaw, H.S., Jaeger, J.C., 1959. Conduction of Heat in Solids, second ed. OxfordUniversity Press, London, p. 510.
Carstensen, C., Hackl, K., Mielke, A., 2002. Non-convex potentials and microstructures in finite-strain plasticity. Proc. Math. Phys. Eng. Sci. 458, 299–317.
Champneys, A.R., Hunt, G.W., Thompson, J.M.T., 1997. Localization and solitary waves in solid mechanics. Philos. Transact. A Math. Phys. Eng. Sci. 355, 2077–2081.
Cheng, C., Zhang, N., 1999. Buckling and Multiple Equilibrium States of Viscoelastic Rectangular Plates, vol. 3. J. Shanghai University, pp. 192–198.
Chernoff, C.B., Carlson, W.D., 1997. Disequilibrium for Ca during growth of pelitic garnet. J. Metamorph. Geol. 15, 421–438.
Cherukuri, H.P., Shawki, T.G., 1995a. An energy-based localization theory: I. Basic framework. Int. J. Plast. 11, 15–40.
Cherukuri, H.P., Shawki, T.G., 1995b. An energy-based localization theory: II. Effects of the diffusion, inertia, and dissipation numbers. J. Plast. 11, 41–64.
Clarke, B.L., 1976. Stability of the bromate–cerium–malonic acid network. I. Theoretical formulation. J. Chem. Phys. 64, 4165–4178.
Clarke, B.L., 1980. Stability of complex reaction networks. Adv. Chem. Phys. 43, 1–215.
Coleman, B.D., Noll, W., 1963. The thermodynamics of elastic materials with heat conduction and viscosity. Arch. Ration. Mech. Anal. 13, 167–178.
Coleman, B.D., Gurtin, M.E., 1967. Thermodynamics with internal state variables. J. Chem. Phys. 47, 597–613.
Collins, I.F., Houlsby, G.T., 1997. Application of thermomechanical principles to the modelling of geotechnical materials. Proc. R. Soc. Lond. A 453, 1975–2001.
Collins, I.F., Hilder, T., 2002. A theoretical framework for constructing elastic/plastic constitutive models of triaxial tests. Int. J. Numer. Anal. Meth. Geomech. 26, 1313–1347.
Connolly, J.A.D., Thompson, A.B., 1989. Fluid and enthalpy production during regional metamorphism. Contrib. Mineral. Petrol. 102, 347–366.
Coussy, O., 1995. Mechanics of Porous Continua. Wiley, Chichester, UK, p. 472.
Coussy, O., Ulm, F.-J., 1996. Creep and plasticity due to chemo-mechanical couplings. Arch. Appl. Mech. 66, 523–535.
Coussy, O., 2004. Poromechanics. Wiley, Chichester, UK, p. 298.
Coussy, O., 2010. Mechanics and Physics of Porous Solids. Wiley, Chichester, UK. p. 281.
Cross, M.C., Hohenberg, P.C., 1993. Pattern formation out of equilibrium. Rev. Mod. Phys. 65, 851–1123.
Curie, P., 1894. Sur la symétrie dans les phénomènes physiques, symétrie d'un champ électrique et d'un champ magnétique. J. Physique 3, 393–415.
Curie, P., 1908. Oeuvres de Pierre Curie. Gauthier-Villars, Paris.
De Groot, S.R., 1952. Thermodynamics of Irreversible Processes. North-Holland Publishing Co., Amsterdam.
De Groot, S.R., Mazur, P., 1962. Non-Equilibrium Thermodynamics. North-Holland Publishing Co., Amsterdam.
Detournay, E., Cheng, A.H.-D., 1993. Fundamentals of poroelasticity. In: Hudson, J.A., Fairhurst, C. (Eds.), Comprehensive Rock Engineering, vol. 2. Pergamon Press, Oxford, pp. 113–171.
Del Piero, G., Truskinovsky, L., 2001. Macro- and micro-cracking in one-dimensional elasticity. Int. J. Solid. Struct. 38, 1135–1148.
Dewars, T., Ortoleva, P.J., 1989. Self-organisation of mineralization patterns in metamorphic rocks through mechanochemical coupling. J. Phys. Chem. 93, 2842–2848.
Dewars, T., Ortoleva, P.J., 1990. Geochemical self-organization III: a mechanochemical model of metamorphic differentiation. Am. J. Sci. 290, 473–521.
De Wit, A., Dewel, G., Borckmans, P., Walgraef, D., 1992. 3-dimensional dissipative structures in reaction diffusion-systems. Physica D 61, 289–296.
De Wit, A., Lima, D., Dewel, G., Borckmans, P., 1996. Spatiotemporal dynamics near a codimensional-two point. Phys. Rev. E 54, 261–271.
De Wit, A., Borckmans, P., Dewel, G., 1997. Twist grain boundaries in three-dimensional lamellar Turing structures. Proc. Natl. Acad. Sci. U S A 94, 12765–12768.
Epstein, I.R., Pojman, J.A., 1998. An Introduction to Nonlinear Chemical Dynamics. Oxford, New York, p. 392.
Ericksen, J.L., 1980. Some phase-transitions in crystals. Arch. Ration. Mech. Anal. 73, 99–124.
Ericksen, J.L., 1998. Introduction to the Thermodynamics of Solids. Revised Edition. Springer-Verlag, New York.
Eringen, A.C., 1962. Nonlinear Theory of Continuous Media. McGraw-Hill, New York, p. 477.
Estrin, Y., Kubin, L.P., 1991. Plastic instabilities: phenomenology and theory. Mater. Sci. Eng. A137, 125–134.
Everall, P.R., Hunt, G.W., 1999. Arnold tongue predictions of secondary buckling in thin elastic plates. J. Mech. Phys. Solids 47, 2187–2206.
Faria, S.H., 2006a. Creep and recrystallization of large polycrystalline masses. I. General continuum theory. Proc. R. Soc. A 462, 1493–1514.
Faria, S.H., Kremer, G.M., Hutter, K., 2006b. Creep and recrystallization of large polycrystalline masses. II. Constitutive theory for crystalline media with transversely isotropic grains. Proc. R. Soc. A 462, 1699–1720.
Faria, S.H., 2006c. Creep and recrystallization of large polycrystalline masses. III. Continuum theory of ice sheets. Proc. R. Soc. A 462, 2797–2816.
Fisher, G.W., Lasaga, A.C., 1981. Irreversible thermodynamics in petrology. Mineral. Soc. 8, 171–210. Am. Rev. Mineral.

Fleitout, L., Froidevaux, C., 1980. Thermal and mechanical evolution of shear zones. J. Struct. Geol. 2, 159–164.
Fletcher, R.C., 1974. Wavelength selection in the folding of a single layer with power-law rheology. Am. J. Sci. 274, 1029–1043.
Fletcher, R.C., Sherwin, J.A., 1978. Arc lengths of single layer folds: a discussion of the comparison between theory and observation. Am. J. Sci. 278, 1085–1098.
Fletcher, R.C., 1982. Coupling of diffusional mass-transport and deformation in a tight rock. Tectonophysics 83, 275–291.
Fowler, A.C., 1997. Mathematical Models in the Applied Sciences. CambridgeUniversity Press, pp. 179–199.
Francfort, G.A., Marigo, J.-J., 1998. Revisiting brittle fracture as an energy minimization problem. J. Mech. Phys. Solids 46, 1319–1342.
Frehner, M., Schmalholz, S.M., 2006. Numerical simulations of parasitic folding in multilayers. J. Struct. Geol. 28, 1647–1657.
Fressengeas, C., Molinari, A., 1987. Instability and localization of plastic flow in shear at high strain rates. J. Mech. Phys. Solids 35, 185–211.
Fung, Y.C., 1965. Foundations of Solid Mechanics. Prentice-Hall Inc, Englewood Cliffs, New Jersey.
Johnson, A.M., Fletcher, R.C., 1994a. Folding of viscous layers. Columbia.
Gabrielli, R., 2009. A new counter-example to Kelvin's conjecture on minimal surfaces. Phil. Mag. Lett. 89, 483–491.
Gibbs, J.W., 1906. Collected Works of J. Willard Gibbs, vol. 1. Yale University Press, New Haven, p. 434.
Glimm, T., Hentschel, H.G.E., 2008. On isoconcentration surfaces of three-dimensional Turing patterns. Int. J. Bifurcat. Chaos 18, 391–406.
Goetze, C., Evans, B., 1979. Stress and temperature in the bending lithosphere as constrained by experimental rock mechanics. Geophys. J. R. Astr. Soc. 59, 463–478.
Griffith, A.A., 1920. The phenomenon of rupture and flow in solids. Phil. Trans. R. Soc. Lond. A 221, 163–198.
Gross, K.A., 1965. X-ray line broadening and stored energy in deformed and annealed calcite. Phil. Mag. 12, 801–813.
Guckenheimer, J., Holmes, P., 1986. Nonlinear Oscillations, Dynamical Systems and Bifurcations of Vector Fields. Springer-Verlag, New York, p. 459.
Haack, U.K., Zimmermann, H.D., 1996. Retrograde mineral reactions: a heat source in the continental crust? Geol. Rundsch. 85, 130–137.
Hahner, P., Bay, K., Zaiser, M., 1998. Fractal dislocation patterning during plastic deformation. Phys. Rev. Lett. 81, 2470–2473.
Heilbronner, R., Tullis, J., 2006. Evolution of c axis pole figures and grain size during dynamic recrystallization: Results from experimentally sheared quartzite. J. Geophys. Res. 111, B10202.
Hobbs, B.E., 1966. Microfabrics of tectonites from the Wyangala Dam area, New South Wales, Australia. Geol. Soc. Am. Bull. 77, 685–706.
Hobbs, B.E., 1968. Recrystallization of single crystals of quartz. Tectonophysics 6, 353–401.
Hobbs, B.E., Mühlhaus, H.B., Ord, A., 1990. Instability, softening and localization of deformation. In: Knipe, R.J., Rutter, E.H. (Eds.), Deformation Mechanisms, Rheology and Tectonics. Geol. Soc. Spec. Pub., vol. 54. The Geological Society, London, pp. 143–165.
Hobbs, B., Regenauer-Lieb, K., Ord, A., 2007. Thermodynamics of folding in the middle to lower crust. Geology 35, 175–178.
Hobbs, B.E., Regenauer-Lieb, K., Ord, A., 2008. Folding with thermal–mechanical feedback. J. Struct. Geol. 30, 1572–1592.
Hobbs, B.E., Regenauer-Lieb, K., Ord, A., 2009. Folding with thermal–mechanical feedback: a reply. J. Struct. Geol. 31, 752–755.
Hobbs, B.E., Ord, A., 2010a. The Development of Microstructure Within Deforming-Reactive Systems Accepted for publication in Special Issue of Geological Society of London Special Publications.
Hobbs, B.E., Ord, A., 2010b. The mechanics of granitoid systems and maximum entropy production rates. Phil. Trans. R. Soc. A 368, 53–93.
Hobbs, B.E., Ord, A., Spalla, I., Gosso, G., Zucalli, M., 2010a. The interaction of deformation and metamorphic reactions. In: Spalla, M.I., Marotta, A.M., Gosso, G. (Eds.), Advances in Interpretation of Geological Processes: Refinement of Multi-scale Data and Integration in Numerical Modelling. Geological Society, London, Special Publications, vol. 332, pp. 189–223.
Hobbs, B.E., Regenauer-Lieb, K., Ord, A., 2010b. Folding with thermal–mechanical feedback: another reply. J. Struct. Geol. 32, 131–134.
Hodges, K.V., 1998. The thermodynamics of Himalayan orogenesis. In: Treloar, P.J., O'Brien, P.J. (Eds.), What Drives Metamorphism and Metamorphic Reactions. Geological Society, London, Special Publications, vol. 138, pp. 7–22.
Holyst, R., 2005. Some features of soft matter systems. Soft Matter 1, 329–333.
Houlsby, G.T., Puzrin, A.M., 1999. An Approach to Plasticity Based on Generalised Thermodynamics, Proc. Int. Symp. Hypoelasticity, Horton, Greece, pp. 233–245.
Houlsby, G.T., Puzrin, A.M., 2006a. Principles of Hyperplasticity. Springer-Verlag. Londonp. 351.
Houlsby, G.T., Puzrin, A.M., 2006b. Thermodynamics of porous continuaSpringer Proc. Phys.. Modern Trends in Geomechanics 106, 39–60.
Hudleston, P.J., 1973a. An analysis of 'single-layer' folds developed experimentally in viscous media. Tectonophysics 16, 189–214.
Hudleston, P.J., 1973b. The analysis and interpretation of minor folds developed in the Moine rocks of Monar, Scotland. Tectonophysics 17, 89–132.
Hudleston, P.J., Treagus, S.H., 2010. Information from folds: a review. J. Struct. Geol. 32, 2042–2071.
Hull, D., 1999. Fractography. Cambridge University Press, p. 366.
Hunt, G.W., Bolt, H.M., Thompson, J.M.T., 1989. Structural localization phenomena and the dynamical phase-space analogy. Proc. R. Soc. Lond. Math Phys Eng Sci 425, 245–267.
Hunt, G.W., Wadee, M.K., 1991. Comparative Lagrangian formulations for localised buckling. Proc. R. Soc. A 434, 485–502.
Hunt, G., Muhlhaus, H., Hobbs, B., Ord, A., 1996. Localized folding of viscoelastic layers. Geol. Rundsch. 85, 58–64.
Hunt, G.W., Lawther, R., Costa, P.R.E., 1997a. Finite element modelling of spatially chaotic structures. Int. J. Numer. Meth. Eng. 40, 2237–2256.
Hunt, G.W., Muhlhaus, H.–B., Whiting, I.M., 1997b. Folding processes and solitary waves in structural geology. Phil. Trans. R. Soc. 355, 2197–2213.
Hunt, G.W., Everall, P.R., 1999. Arnold tongues and mode jumping in the supercritical post-buckling of an archetypal elastic structure. Proc. R. Soc. Lond. A 455, 125–140.
Hunt, G.W., Peletier, M.A., Wadee, M.A., 2000. The Maxwell stability criterion in pseudo-energy models of kink banding. J. Struct. Geol. 22, 669–681.
Hunt, G.W., Wadee, M.A., Ord, A., 2001. Length scale interactions in the folding of sandwich structures. Tectonophysics 335, 111–120.
Hunt, G.W., Edmunds, R., Budd, C.J., Cosgrove, J.W., 2006. Serial parallel folding with friction: a primitive model using cubic B-splines. J. Struct. Geol. 28, 444–455.
Hunt, K.L.C., Hunt, P.M., Ross, J., 1987. Dissipation in steady states of chemical systems and deviations from minimum entropy production. Physica A 147, 48–60.
Hunt, K.L.C., Hunt, P.M., Ross, J., 1988. Deviations from minimum entropy production at steady states of reacting chemical systems arbitrarily close to equilibrium. Physica A 154, 207–211.
Jeng, F.S., Lin, M.L., Lai, Y.C., Teng, M.H., 2002. Influence of strain rate on buckle folding of an elasto-viscous single layer. J. Struct. Geol. 24, 501–516.
Jeng, F.S., Huang, K.P., 2008. Buckling folds of a single layer embedded in matrix – Theoretical solutions and characteristics. J. Struct. Geol. 30, 633–648.
Johnson, A.M., Fletcher, R.C., 1994. Folding of Viscous Layers. Columbia University Press, New York, p. 461.
Jou, D., Casas-Vazquez, G., Lebon, 1993. Extended Irreversible Thermodynamics. Springer, Berlin.
Jou, D., Casas-Vazquez, J., Criado-Sancho, M., 2001. Thermodynamics of Fluids Under Flow. Springer, Berlin.
Kagan, Y.Y., 1982. Stochastic model of earthquake fault geometry. Geophys. J. R. Astr. Soc. 71, 659–691.
Kamb, B., 1959. Theory of preferred crystal orientation developed by crystallisation under stress. J. Geol. 67, 153–170.
Kamb, W.B., 1961. The thermodynamic theory of non-hydrostatically stressed solids. J. Geophys. Res. 66, 259–271.
Kameyama, M., 2003. Comparison between thermal viscous coupling and frictional sliding. Tectonophysics 376, 185–197.
Karrech, A., Regenauer-Lieb, K., Poulet, T., 2011. Continuum damage mechanics for the lithosphere. Jour. Geophys. Res. 116. doi:10.1029/2010JB007501.
Kerr, A.D., 1964. Elastic and viscoelastic foundation models. J. Appl. Mech. 31, 491–498.
Kestin, J., Rice, J.R., 1970. Paradoxes in the application of thermodynamics to strained solids. In: Stuart, E.B., Brainard, A.J., Gal-Or, B. (Eds.), A Critical Review of Thermodynamics. Mono Book Corp., Baltimore, pp. 275–298.
Ketcham, R.A., Carlson, W.D., 2001. Acquisition, optimization and interpretation of X-ray computed tomographic imagery: applications to the geosciences. Comput. Geosci. 27, 381–400.
Kondepudi, D.K., 1988. Remarks on the validity of the theorem of minimum entropy production. Physica A 154, 204–206.
Kondepudi, D., Prigogine, I., 1998. Modern Thermodynamics. John Wiley, Chichester, p. 486.
Korzhinskii, D.S., 1959. Physiochemical Basis of the Analysis of the Paragenesis of Minerals. Consultants Bureau, New York, p. 142.
Kruhl, J.H., Nega, M., 1996. The fractal shape of sutured quartz boundaries: application as a geothermometer. Geol. Rundsch. 85, 34–43.
Larche, F.C., Cahn, J.W., 1985. The interactions of composition and stress in crystalline solids. Acta Metall. 33, 331–357.
Lavenda, B.H., 1978. Thermodynamics of Irreversible Processes. MacMillan Press. p. 182.
Law, C.K., 2006. Combustion Physics. Cambridge University Press, Cambridge. p. 722.
Lehner, F.K., 1995. A model for intergranular pressure solution in open systems. Tectonophysics 245, 153–170.
Leppanen, T., Karttunen, M., Barrio, R.A., Kaski, K., 2004. Turing systems as models of complex pattern formation. Braz. J. Phys. 34, 368–372.
Libicki, E., Ben-Zion, Y., 2005. Stochastic branching models of fault surfaces and estimated fractal dimension. Pure Appl. Geophys. 162, 1077–1111.
Lind, P.G., Baram, R.M., Herrmann, H.J., 2008. Obtaining the size distribution of fault gouges with polydisperse bearings. Phys. Rev. E 77, 021304.
Lister, G.S., Paterson, M.S., Hobbs, B.E., 1978. The simulation of fabric development in plastic deformation and its application to quartzite: the model. Tectonophysics 45, 107–158.
Lister, G.S., Hobbs, B.E., 1980. The simulation of fabric development during plastic deformation and its application to quartzite: the influence of deformation history. J. Struct. Geol. 2, 355–370.
Lopez-Barron, C.R., Macosko, C.W., 2009. Characterizing interface shape evolution in immiscible polymer blends via 3D image analysis. Langmuir 25, 9392–9404.
Lyakhovsky, V., Ben-Zion, Y., Agnon, A., 1997. Distributed damage, faulting, and friction. J. Geophys. Res. 102, 27635–27649.

Lyakhovsky, V., Ben-Zion, Y., 2008. Scaling relations of earthquakes, aseismic deformation and evolving fault structures in a damage rheology model. Geophys. J. Int. 172, 651–662.
Mandlebrot, B.B., 1977. The Fractal Geometry of Nature. Freeman, New York, p. 468.
Mancktelow, N.S., 2002. Finite-element modelling of shear zone development in viscoelastic materials and its implications for localization of partial melting. J. Struct. Geol. 24, 1045–1053.
Marchildon, N., Brown, M., 2003. Spatial distribution of melt-bearing structures in anatectic rocks from Southern Brittany, France: implications for melt transfer at grain- to orogen-scale. Tectonophysics 364, 215–235.
Martyushev, L.M., Selezvev, V.D., 2006. Maximum entropy production principle in physics, chemistry and biology. Phys. Rep. 426, 1–45.
Maugin, G.A., 1999. The Thermomechanics of Non-linear Irreversible Behaviours. World Science.
McLellan, A.G., 1980. The Classical Thermodynamics of Deformable Materials. Cambridge University Press, Cambridge, p. 338.
Mecke, K.R., 1996. Morphological characterization of patterns in reaction-diffusion systems. Phys. Rev. E 53, 4794–4800.
Mecke, K.R., 1997. Morphology of spatial patterns-porous media, spinodal decomposition and dissipative structures. Acta Phys. Pol. B28, 1747–1782.
Mesarovic, S.D., 1995. Dynamic strain aging and plastic instabilities. J. Mech. Phys. Solids 43, 671–700.
Meth, C.E., Carlson, W.D., 2005. Diffusion-controlled synkinematic growth of garnet from a heterogeneous precursor at Passo Del Sole, Switzerland. Can. Mineral. 43, 157–182.
Miehe, C., Lambrecht, M., 2003. A two-scale finite element relaxation analysis of shear bands in non-convex inelastic solids: small-strain theory for standard dissipative materials. Comput. Meth. Appl. Mech. Eng. 192, 473–508.
Miehe, C., Lambrecht, M., Gurses, E., 2004. Analysis of material instabilities in inelastic solids by incremental energy minimisation and relaxation methods: evolving deformation microstructures in finite plasticity. J. Mech. Phys. Solids 52 5725–2769.
Muhlhaus, H.-B., Hobbs, B.E., Ord, A., 1994. The role of axial constraints on the evolution of folds in single layers. In: Siriwardane, Zaman (Eds.), Computer Methods and Advances in Geomechanics. Balkema, Rotterdam, pp. 223–231.
Mühlhaus, H.-B., Sakaguchi, H., Hobbs, B.E., 1998. Evolution of three-dimensional folds for a non-Newtonian plate in a viscous medium. Proc. R. Soc. A 454, 3121–3143.
Murray, J.D., 1989. Mathematical Biology. Springer-Verlag, Berlin, p. 767.
Needleman, A., 1988. Material rate dependence and mesh sensitivity in localisation problems. Comput. Meth. Appl. Mech. Eng. 67, 69–85.
Nguyen, Q.S., 2000. Stability and Nonlinear Solid Mechanics. Wiley, Chichester, UK, p. 398.
Nye, J.F., 1957. Physical Properties of Crystals. Oxford Press, p. 322.
Onsager, L., 1931a. Reciprocal relations in irreversible processes I. Phys. Rev. 37, 405–426.
Onsager, L., 1931b. Reciprocal relations in irreversible processes II. Phys. Rev. 38, 2265–2279.
Ord, A., Vardoulakis, I., Kajewski, R., 1991. Shear band formation in Gosford Sandstone. Int. J. Rock Mech. Min. Sci. Geomech. Abstr. 28, 397–409.
Ord, A., Hobbs, B.E., 2010. Fracture pattern formation in frictional, cohesive, granular media. Phil. Trans. R. Soc. A 368, 95–118.
Ord, A., Hobbs, B.E., 2011. Microfabrics as energy minimisers: rotation recrystallisation as an example. J. Struct. Geol. 33 (3), 220–243.
Ortiz, M., Repetto, E.A., 1999. Nonconvex energy minimization and dislocation structures in ductile single crystals. J. Mech. Phys. Solids 47, 397–462.
Ortoleva, P., Ross, J., 1973. Phase waves in oscillatory chemical reactions. J. Chem. Phys. 58, 5673–6580.
Ortoleva, P.J., Ross, J., 1974. On a variety of wave phenomena in chemical reactions. J. Chem. Phys. 59, 5090–5107.
Ortoleva, P.J., Merino, E., Strickholm, P., 1982. Kinetics of metamorphic layering in anisotropically stressed rock. Am. J. Sci. 282, 617–643.
Ortoleva, P., Auchmuty, G., Chadam, J., Hettmer, J., Merino, E., Moore, C.H., Ripley, E., 1986. Redox front propagation and banding modalities. Physica D 19, 334–354.
Ortoleva, P., Merino, E., Moore, C., Chadam, J., 1987a. Geochemical self-organization I; reaction-transport feedbacks and modeling approach. Am. J. Sci. 287, 979–1007.
Ortoleva, P., Chadam, J., Merino, E., Sen, A., 1987b. Geochemical self-organization II; the reactive-infiltration instability. Am. J. Sci. 287, 1008–1040.
Ortoleva, P.J., 1989. Nonequilibrium reaction-diffusion structures in rigid and viscoelastic media: knots and unstable noninertial flows. Modelisation mathematique et analyse numerique 23, 507–517.
Ortoleva, P.J., 1994. Geochemical Self-organization. Oxford University Press, p. 411.
Ottinger, H.C., 2005. Beyond Equilibrium Thermodynamics. Wiley, p. 648.
Paterson, M.S., 1969. The ductility of rocks. In: Argon, A.S. (Ed.), Physics of Strength and Plasticity. The MIT Press, pp. 377–392. The Orowan 65th Anniversary Volume.
Paterson, M.S., 1973. Nonhydrostatic thermodynamics and its geological applications. Rev. Geophys. 11, 355–389.
Paterson, M.S., 1995. A theory for granular flow accommodated by material transfer via an intergranular fluid. Tectonophysics 245, 135–151.
Peletier, L.A., Troy, W.C., 2001. Spatial Patterns: Higher Order Models in Physics and Mechanics. Progress in NonLinear Differential Equations and Their Applications, vol. 45. Birkhauser, USA, p. 320.
Petford, N., Koenders, M.A., 1998. Self-organisation and fracture connectivity in rapidly heated continental crust. J. Struct. Geol. 20, 1425–1434.
Phillips, O.M., 1991. Flow and Reactions in Permeable Rocks. CambridgeUniversity Press, p. 296.
Pontes, J., Walgraef, D., Aifantis, E.C., 2006. On dislocation patterning: multiple slip effects in the rate equation approach. Int. J. Plast. 22, 1486–1505.
Powell, R., Holland, T.J.B., Worley, B., 1998. Calculating phase diagrams involving solid solutions via non-linear equations, with examples using THERMOCALC. J. Metamorph. Geol. 16, 577–588.
Powell, R., Guiraud, M., White, R.W., 2005. Truth and beauty in metamorphic phase-equilibria: conjugate variables and phase diagrams. Can. Mineral. 43, 21–33.
Prigogine, I., 1955. Introduction to the Thermodynamics of Irreversible Processes. Charles C. Thomas, Springfield, Illinois, p. 115.
Rajagopal, K.R., Srinivasa, A.R., 2004. On thermomechanical restrictions of continua. Proc. R. Soc. Lond. A 460, 631–651.
Ramberg, H., 1961. Contact strain and folding instability of a multilayered body under compression. Geol. Rundsch. 51, 405–439.
Ramberg, H., 1963. Fluid dynamics of viscous buckling applicable to folding of layered rocks. Bull. Am. Assoc. Petrol. Geol. 47, 484–515.
Ramsay, J.G., 1967. Folding and Fracturing of Rocks. McGraw-Hill, New York.
Reddy, S.M., Buchan, C., 2005. Constraining kinematic rotation axes in high-strain zones: a potential microstructural method? In: Gapais, D., Brun, J.P., Cobbold, P.R. (Eds.), Deformation Mechanisms and Tectonics from Minerals to the Lithosphere Geological Society of London, Special Publications, vol. 243, pp. 1–10.
Regenauer-Lieb, K., Yuen, D.A., 2003. Modeling shear zones in geological and planetary sciences: solid- and fluid-thermal–mechanical approaches. Earth Sci. Rev. 63, 295–349.
Regenauer-Lieb, K., Yuen, D., 2004. Positive feedback of interacting ductile faults from coupling of equation of state, rheology and thermal-mechanics. Phys. Earth Planet. In. 142, 113–135.
Regenauer-Lieb, K., Weinberg, R.F., Rosenbaum, G., 2006. The effect of energy feedbacks on continental strength. Nature 44, 67–70.
Regenauer-Lieb, K., Rosenbaum, G., Weinberg, R.F., 2008. Strain localisation and weakening of the lithosphere during extension. Tectonophysics 458, 96–104.
Regenauer-Lieb, K., Hobbs, B., Ord, A., Gaede, O., Vernon, R., 2009. Deformation with coupled chemical diffusion. Phys. Earth Planet. In. 172, 43–54.
Ricard, Y., Bercovici, D., 2009. A continuum theory of grain size evolution and damage. J. Geophys. Res. 114, 30. B01204.
Rice, J.R., 1971. Inelastic constitutive relations for solids: an internal-variable theory and its application to metal plasticity. J. Mech. Phys. Solids 19, 433–455.
Rice, J.R., 1975. Continuum mechanics and thermodynamics of plasticity in relation to microscale deformation mechanisms. In: Argon, Ali (Ed.), Constitutive Equations in Plasticity. MIT Press, pp. 23–79.
Ross, J., Vlad, M.O., 2005. Exact solutions for the entropy production rate of several irreversible processes. J. Phys. Chem. A 109, 10607–10612.
Ross, J., 2008. Springer Series in Chemical Physics. Thermodynamics and Fluctuations far from Equilibrium, vol. 90. Springer, Berlin, p. 209.
Ross, J., Villaverde, A.F., 2010. Thermodynamics and fluctuations far from equilibrium. Entropy 12, 2199–2243.
Rudnicki, J.W., Rice, J.R., 1975. Conditions for the localization of deformation in pressure-sensitive dilatant materials. J. Mech. Phys. Solids 23, 371–394.
Ruina, A., 1983. Slip instability and state variable friction laws. J. Geophys. Res. 88, 10,359–10,370.
Rusinov, V.L., Kudrya, P.F., Laputina, I.P., Kuzmina, O.V., 1994. Periodical metasomatic zonation in pyroxene–wollastonite scarns. Petrology 2, 510–525.
Rusinov, V.L., Zhukov, V.V., 2000. Dynamic model of the infiltration metasomatic zonation. Pure Appl. Geophys. 157, 637–652.
Rusinov, V.L., Bityutskaya, L.A., Bogatikov, E.V., Zhukov, V.V., 2006. Fractal features and morphological differences between periodic infiltration and diffusion metasomatic zonation. Dokl. Earth Sci. 409, 769–773.
Rusinov, V.L., Zhukov, V.V., 2008. Model for the development of rhythmically banded wollastonite–hedenbergite skarns at the Dal'negorsk deposit, Southern Russian Far East. Geochem. Int. 46, 789–799.
Sander, B., 1911. Uber Zusammenhange zwischen Teilbewegung und Gefuge in Gesteinen. Tscher. Miner. Petrog. 30, 281–314.
Sandiford, M., Martin, N., Zhou, S., Fraser, G., 1991. Mechanical consequences of granite emplacement during high-T, low-P metamorphism and the origin of 'anticlockwise' PT paths. Earth Planet. Sci. Lett. 107, 164–172.
Sandiford, M., Foden, J., Zhou, S., Turner, S., 1992. Granite genesis and the mechanics of convergent orogenic belts with application to the southern Adelaide Fold Belt. Trans. R. Soc. Edinb. Earth Sci. 83, 83–93.
Schiller, C., Walgraef, D., 1988. Numerical simulation of persistent slip band formation. Acta Metall. 36, 563–574.
Schmalholz, S.M., Schmid, D.W., Fletcher, R.C., 2008. Evolution of pinch-and swell structures in a power-law layer. J. Struct. Geol. 30, 649–663.
Schmid, D.W., Podladchikov, Y.Y., 2006. Fold amplification rates and dominant wavelength selection in multilayer stacks. Phil. Mag. 86, 3409–3423.
Schmid, D.W., Dabrowski, M., Krotkiewski, M., 2010. Evolution of large amplitude 3D fold patterns: a FEM study. Phys. Earth Planet. In. 171, 400–408.
Schmid, S.M., Casey, M., 1986. Complete fabric analysis of some commonly observed quartz c-axis patterns. In: Hobbs, B.E., Heard, H.C. (Eds.), Mineral and Rock Deformation: Laboratory Studies. The Paterson Volume, vol. 36. American Geophysical Union, pp. 263–286. Geophysical Monograph.

Schmid, S.M., 1994. Textures of geological materials: computer model predictions versus empirical interpretations based on rock deformation experiments and field studies. In: Bunge, H.J., et al. (Eds.), Textures of Geological Materials. DGM Informationsges, Uberursel, Germany, pp. 279–301.
Schreibner, I., Ross, J., 2003. Mechanisms of oscillatory reactions deduced from bifurcation diagrams. J. Phys. Chem. A 107, 9846–9859.
Schumacher, R., Rotzler, K., Maresch, W.V., 1999. Subtle oscillatory zoning in garnet from regional metamorphic phyllites and mica schists, Western Erzgebirge, Germany. Can. Mineral. 37, 381–402.
Sherwin, J., Chapple, W.M., 1968. Wavelength of single layer folds: a comparison between theory and observation. Am. J. Sci. 266, 167–179.
Shimamoto, T., Hara, I., 1976. Geometry and strain of single-layer folds. Tectonophysics 30, 1–34.
Shimizu, I., 1992. Nonhydrostatic and nonequilibrium thermodynamics of deformable materials. J. Geophys. Res. 97, 4587–4597.
Shimizu, I., 1997. The non-equilibrium thermodynamics of intracrystalline diffusion under non-hydrostatic stress. Phil. Mag. A 75, 1221–1235.
Shimizu, I., 1998. Stress and temperature dependence of recrystallized grain size: a subgrain misorientation model. Geophys. Res. Lett. 25, 4237–4240.
Shimizu, I., 2001. Nonequilibrium thermodynamics of nonhydrostatically stressed solids. Chapter 3. In: Teisseyre, R., Majewski, E. (Eds.), Earthquake Thermodynamics and Phase Transformations in the Earth's Interior. Academic Press, New York, pp. 81–102.
Shimizu, I., 2008. Theories and applicability of grain size piezometers: the role of dynamic recrystallization mechanisms. J. Struct. Geol. 30, 899–917.
Shizawa, K., Zbib, H.M., 1999. A thermodynamical theory of gradient elastoplasticity with dislocation density tensor. I: fundamentals. Int. J. Plast. 15, 899–938.
Shizawa, K., Kikuchi, K., Zbib, H.M., 2001. A strain-gradient thermodynamic theory of plasticity based on dislocation density and incompatibility tensors. Mater. Sci. Eng., A309–A310. 416–419.
Smith, R.B., 1975. A unified theory of the onset of folding, boudinage and mullions in non-Newtonian materials. Geol. Soc. Am. Bull. 86, 1601–1609.
Smith, R.B., 1977. Formation of folds, boudinage and mullions in non-Newtonian materials. Geol. Soc. Am. Bull. 88, 312–320.
Smith, R.B., 1979. The folding of a strongly non-Newtonian layer. Am. J. Sci. 279, 272–287.
Sornette, D., 2000. Critical Phenomena in Natural Sciences; Chaos, Fractals, Self Organization and Disorder: Concepts and Tools. Springer-Verlag, Berlin.
Stainier, L., Ortiz, M., 2010. Study and validation of a variational theory of thermo-mechanical coupling in finite visco-plasticity. Int. J. Solid. Struct. 47, 705–715.
Stixrude, L., Lithgow-Bertelloni, C., 2005. Thermodynamics of mantle minerals – I. Physical properties. Geophys. J. Int. 162, 610–632.
Strogatz, S.H., 1994. Nonlinear Dynamics and Chaos: With Applications to Physics, Biology, Chemistry, and Engineering. Addison-Wesley, Reading, MA.
Stüwe, K., Sandiford, M., Powell, R., 1993. Episodic metamorphism and deformation in low-pressure, high-temperature terranes. Geology 21, 829–832.
Stüwe, K., 2007. Geodynamics of the Lithosphere. Springer, p. 504.
Takahashi, M., Nagahama, H., Masuda, T., Fujimura, A., 1998. Fractal analysis of experimentally, dynamically recrystallized quartz grains and its possible application as a strain-rate meter. J. Struct. Geol. 20, 269–275.
Tanner, D.C., 1999. The scale-invariant nature of migmatite from the Oberpfalz, NE Bavaria and its significance for melt transport. Tectonophysics 302, 297–305.
Taylor, G.I., 1938. Plastic strains in metals. J. Inst. Metals 62, 307–324.
Taylor, G.I., Quinney, H., 1934. The latent energy remaining in a metal after cold working. Proc. R. Soc. Lond. A 143, 307–326.
Thompson Jr., J.B., 1959. Local equilibrium in metasomatic processes. In: Abelson, P.H. (Ed.), Researches in Geochemistry. Wiley, New York, pp. 427–457.
Thompson, J.M.T., Hunt, G.W., 1973. A General Theory of Elastic Stability. Wiley, London, UK, p. 322.
Treagus, S.H., Fletcher, R.C., 2009. Controls of folding on different scales in multilayered rocks. J. Struct. Geol. 31, 1340–1349.
Truesdell, C.A., 1966. Six Lectures on Modern Natural Philosophy. Springer-Verlag, Berlin, p. 117.
Truesdell, C.A., 1969. Rational Thermodynamics, second ed. Springer-Verlag, New York.
Truesdell, C., Noll, W., 1965. The non-linear field theories of mechanics. In: S. Flugge (Ed.), Encyclopedia of Physics, vol. 3/3. Springer-Verlag, Berlin, p. 602.
Truskinovsky, L., Zanzotto, G., 1995. Finite-scale microstructures and metastability in one-dimensional elasticity. Meccanica 30, 577–589.
Truskinovsky, L., Zanzotto, G., 1996. Ericksen's bar revisited: energy wiggles. J. Mech. Phys. Solids 44, 1371–1408.
Turing, A.M., 1952. The chemical basis for morphogenesis. Phil. Trans. R. Soc. Lond. B 237, 37–72.
Tvergaard, V., Needleman, A., 1980. On the localization of buckling patterns. J. Appl. Mech. 47, 613–619.
Ulm, F.-J., Coussy, O., 1995. Modeling of thermochemomechanical couplings of concrete at early ages. J. Eng. Mech. 121, 785–794.
Vernon, R.H., 2004. A Practical Guide to Rock Microstructure. Cambridge University Press, Cambridge, p. 594.
Veveakis, E., Alevizos, S., Vardoulakis, I., 2010. Chemical reaction capping of thermal instabilities during shear of frictional faults. J. Mech. Phys. Solids 58, 1175–1194.
Voyiadjis, G.Z., Dorgan, R.J., 2004. Bridging of length scales through gradient theory and diffusion equations of dislocations. Comput. Meth. Appl. Mech. Eng. 193, 1671–1692.
Walgraef, D., Aifantis, E.C., 1985a. On the formation and stability of dislocation patterns – I: one-dimensional considerations. Int. J. Eng. Sci. 23, 1351–1358.
Walgraef, D., Aifantis, E.C., 1985b. On the formation and stability of dislocation patterns – II: two-dimensional considerations. Int. J. Eng. Sci. 23, 1359–1364.
Walgraef, D., Aifantis, E.C., 1985c. On the formation and stability of dislocation patterns – III: three-dimensional considerations. Int. J. Eng. Sci. 23, 1365–1372.
Wang, W.M., Sluys, L.J., De Borst, R., 1997. Viscoplasticity for instabilities due to strain softening and strain-rate softening. Int. J. Numer. Meth. Eng. 40 3839–3664.
Wheeler, J., 2010. Anisotropic rheology during grain boundary diffusion creep and its relation to grain rotation, grain boundary sliding and superplasticity. Phil. Mag. 90, 2841–2864.
Whiting, A.I.M., Hunt, G.W., 1997. Evolution of nonperiodic forms in geological folds. Math. Geol. 29, 705–723.
Whitmeyer, S.J., Wintsch, R.P., 2005. Reaction localisation and softening of texturally hardened mylonites in a reactivated fault zone, central Argentina. J. Metamorph. Geol. 23, 411–424.
Wintsch, R.P., Aleinikoff, J.N., Yi, K., 2005. Foliation development and reaction softening by dissolution and precipitation in the transformation of granodiorite to orthogneiss, Glastonbury Complex, Connecticut, USA. Can. Mineral. 43, 327–347.
Wiggins, S., 2003. Introduction to Applied Nonlinear Dynamical Systems and Chaos. Springer, New York, p. 843.
Yang, P., Rivers, T., 2001. Chromium and manganese zoning in pelitic garnet and kyanite: spiral, overprint, and oscillatory (?) zoning patterns and the role of growth rate. J. Metamorph. Geol. 19, 455–474.
Yang, P., Rivers, T., 2002. The origin of Mn and Y annuli in garnet and the thermal dependence of P in garnet and Y in apatite in calc-pelite and pelite, Gagnon terrane, western Labrador. Geol. Mater. Res. 4, 1–35.
Yuen, D.A., Schubert, G., 1979. On the stability of frictionally heated shear flows in the asthenosphere. Geophys. J. R. Astr. Soc. 57, 189–207.
Zbib, H.M., Rhee, M., Hirth, J.P., 1996. 3-D Simulation of Curved Dislocations: Discretization and Long Range Interactions, Advances in Engineering Plasticity and its Applications: Proceedings of the 3rd Asia-Pacific Symposium on Advances in Engineering Plasticity and its Applications. pp. 15–20.
Ziegler. H., 1963. Some extremum principles in irreversible thermodynamics with application to continuum mechanics. Chapter 2 in: Sneddon, I. N., and Hill, R, Prog. Solid Mech., 4, 91–193.
Ziegler, H., 1983. An Introduction to Thermomechanics, second ed. North-Holland Publishing Company, Amsterdam, p. 356.